Title
Characterizing compound coastal flood risk in urbanized communities: A Multivariate approach

Author
Lucey, Joseph

Publication Date
2023

Peer reviewed|Thesis/dissertation

UNIVERSITY OF CALIFORNIA

Los Angeles

Characterizing compound coastal flood risk in urbanized communities: A Multivariate approach

A dissertation submitted in partial satisfaction
of the requirements for the degree
Doctor of Philosophy in Civil Engineering

by

Joseph Thomas-Daniel Lucey

2023

ABSTRACT OF THE DISSERTATION

Characterizing compound coastal flood risk
in urbanized communities:
A Multivariate approach

by

Joseph Thomas-Daniel Lucey
Doctor of Philosophy in Civil Engineering
University of California, Los Angeles, 2023
Professor Timu Gallien, Chair

Coastal flooding is a growing concern. Compound coastal flooding considers the joint impacts of marine and hydrologic events characterized by multiple flooding pathways (i.e., high offshore water levels, streamflow, energetic waves, precipitation) acting concurrently. Flood risks are commonly assessed using numerical models or statistical methods. Quantifying event uncertainty is critical to accurate flood risk assessment. This work develops a hybrid statistical-hydrodynamic flood modeling methodology to characterize flood mapping uncertainty in highly urbanized, tidally and wave dominated regions. Uncertainties associated with copula selection, sampling method, data record length, utilized rainfall gauge, and event choice along an isoline were considered. Univariate statistics are analyzed for individual sites and events. Conditional and joint probabilities are developed using a range of copulas, sampling methods, and hazard scenarios. Multiple copulas (Nelsen, BB1, BB5, and Roch-Alegre, Fischer-Koch) consistently passed a Cramér-von Mises test and presented similar event pairs, with the exception of the BB5 copula which was often more conservative

(i.e., more severe event pairs). Sampling impacts are considered using annual maximum, annual coinciding, wet season monthly maximum, and wet season monthly coinciding sampling. Generally, annual maximum sampling yielded the largest (most severe) event pairs. However, in some cases wet season monthly coinciding sampling suggested higher marine water levels. Uncertainties associated with record length were quantified by creating subsets with different sizes from long data records ($\sim$100 years). Significant event pair variability was observed when using short data record lengths, although results stabilized at 70-years. Flood risk estimates using local rainfall gauges significantly varied suggesting microclimatologies must be considered in flood risk analysis. Validated Delft3D-FM hydrodynamic models were developed for multiple urbanized coastal communities. Compound events were simulated to quantify flood mapping uncertainties associated with statistical characterization.

The dissertation of Joseph Thomas-Daniel Lucey is approved.

Sanjay Mohanty

Alexander D. Hall

Mekonnen Gebremichael

Timu Gallien, Committee Chair

University of California, Los Angeles

2023

TABLE OF CONTENTS

LIST OF FIGURES

LIST OF TABLES

ACKNOWLEDGMENTS

This work has been supported by the US Coastal Research Program under contract W912HZ-20-200-004, California Department of Parks and Recreation contact number C1670006, the National Science Foundation Graduate Research Fellowship Program grant number DGE-1650604, The National GEM Consortium Fellowship, and the UCLA Cota-Robles Fellowship. The US Coastal Research Program (USCRP) is administered by the US Army Corps of Engineers® (USACE), Department of Defense. The content of the information provided in this publication does not necessarily reflect the position or the policy of the government, and no official endorsement should be inferred. The authors' acknowledge the USACE and USCRP's support of their effort to strengthen coastal academic programs and address coastal community needs in the United States. Any opinions, findings, conclusions or recommendations expressed in this material are those of the author(s) and do not necessarily reflect the views of the agencies supporting the work. Chapter 3 of this work (Lucey and Gallien, 2022) is published in the journal of Natural Hazards and Earth Systems Sciences with the Creative Commons Attribution 4.0 License `https://creativecommons.org/licenses/by/4.0/legalcode`.

VITA

2018 B.S.in Civil Engineering, California State University, Los Angeles, Los Angeles, California.

2018 Gallien, Timu W., Nikos Kalligeris, Marie-Pierre C. Delisle, Bo-Xiang Tang, Joseph T.D. Lucey, and Maria A. Winters. "Coastal flood modeling challenges in defended urban backshores." Geosciences 8.12 (2018): 450

2020 M.S. in Civil & Environmental Engineering, University of California, Los Angeles, Los Angeles, California.

2020 Brandenberg, Scott J., Jonathan P. Stewart, Pengfei Wang, Chukwuebuka C. Nweke, Kenneth Hudson, Christine A. Goulet, Xiaofeng Meng, Craig A. Davis, Sean K. Ahdi, Martin B. Hudson, Andrea Donnellan, Gregory Lyzenga, Marlon Pierce, Jun Wang, Maria A. Winters, Marie-Pierre Delisle, Joseph Lucey, Yeulwoo Kim, Timu W. Gallien, Andrew Lyda, J. Sean Yeung, Omar Issa, Tristan Buckreis, and Zhengxiang Yi. "Ground deformation data from GEER investigations of Ridgecrest earthquake sequence." Seismological Research Letters 91.4 (2020): 2024-2034.

2022 Lucey, Joseph T.D. and Timu W. Gallien, Characterizing multivariate coastal flooding events in a semi-arid region: the implications of copula choice, sampling, and infrastructure, Natural Hazards and Earth System Sciences, 22, 2145–2167, https://doi.org/10.5194/nhess-22-2145-2022, 2022.

2023 Lucey, Joseph T.D. and Timu. W. Gallien, Assessing the effects of uncertainty on coastal flood risks in a tide and wave dominated coast, Journal of Flood Risk Management, in review.

2023 Lucey, Joseph T.D., Bo-Xiang Tang, and Timu W. Gallien, A statistical-modeling hybrid compound flood risk assessment and quantification of uncertainties, Coastal Engineering, in preparation.

CHAPTER 1

Introduction

1.1 Sea Level Rise

Coastal flooding is a significant human hazard (Leonard et al., 2014; Wahl et al., 2015) and is considered a primary health hazard by the U.S. Global Change Research Program (Bell et al., 2016). Coastal migration and utilization continues to increase (Nicholls et al., 2007; Nicholls, 2011). Over 600 million people populate coastal zones (Merkens et al., 2016). Climate change-induced sea level rise will substantially increase flood risk (Church et al., 2013; Horton et al., 2014), and negatively impact coastal populations (Bell et al., 2016). Even relatively modest sea level rise will significantly increase flood frequencies through the US (e.g., Tebaldi et al., 2012; Taherkhani et al., 2020). California is especially vulnerable to the effects of sea level rise as 67% of California's population live along its coastlines and produces over $2 trillion of California's gross domestic product (NOAA, Accessed 2021b). A projected sea level rise of 1.4 m results in an 85% increase to the vulnerable population and an additional 33 million in economic risk caused by the 100-year water level along the California coast (Heberger et al., 2011). Small changes in sea level ($\sim$5 cm) double the odds of the 50-year flooding event (Taherkhani et al., 2020) and the 100-year event is expected to become annual by 2050 (Tebaldi et al., 2012). Regional research has explored flood risks caused by sea level rise and coastal forcing (e.g., Heberger et al., 2011; Hanson et al., 2011; Gallien et al., 2015). However, accurately characterizing future, coastal vulnerability requires considering the joint and potentially nonlinear impacts of compound (marine and hydrologic) events (Gallien et al., 2018).

1.2 Compound Flooding

Compound flooding is a recent and rapidly developing topic (Sebastian, 2022). Flooding may occur from various sources including marine water levels, waves, precipitation, and fluvial flows. Compound flooding considers the combined impacts of multiple flood sources where events are co-occurring or in succession resulting in an amplified or extreme event (Seneviratne et al., 2012; Leonard et al., 2014; Zscheischler et al., 2018). In urban coastal settings multiple flooding pathways (i.e., high marine water levels, wave runup and overtopping, large fluvial flows, and pluvial flooding from precipitation) interact with infrastructure (e.g., sea walls, human-made dunes, and the storm system) potentially exacerbating hazards. Traditionally, literature has focused on river discharge or storm surge dominated multivariate events (Table 1.1). Along the U.S. West Coast wave runup accounts for nearly half of maximum total water levels (Serafin et al., 2017), and Reguero et al. (2019) suggest wave impacts will be amplified in a changing climate. Quantifying multivariate events explicitly accounting for wave impacts is critical to characterizing coastal flooding in wave influenced areas (e.g., Erikson et al., 2018; Gallien et al., 2018; Barnard et al., 2019). Exclusion of one or more significant flood pathways may underestimate flood risks (Moftakhari et al., 2017).

Table 1.1: A non-exhaustive list of multivariate studies which utilized copulas to study the associated variables

Variable Pairs	References
Waves and water level	Masina et al. (2015); Mazas and Hamm (2017); Didier et al. (2019); Radfar et al. (2021)
Waves and storm duration	De Michele et al. (2007); Salvadori et al. (2014, 2015)
Waves and storm surge	Wahl et al. (2012); Paprotny et al. (2018); Chen et al. (2019); Marcos et al. (2019)

Variable Pairs	References
Wave height and period	Kim et al. (2018); Wrang et al. (2021)
River discharge and water level	White (2007); Bray and McCuen (2014); Sadegh et al. (2018); Ganguli and Merz (2019a,b)
River discharge and storm surge	Paprotny et al. (2018); Ganguli et al. (2020)
River discharge and volume	Yue (2001a,b); Shiau (2003); Favre et al. (2004); De Michele et al. (2005); Poulin et al. (2007); Li et al. (2013); Salvadori et al. (2013); Requena et al. (2013); Aghakouchak (2014)
River discharge, rainfall, and water level	Bray and McCuen (2014); Jeong et al. (2014)
Multiple river discharges	Salvadori and De Michele (2010)
Rainfall and tide	Lian et al. (2013)*, Xu et al. (2014)*, Tu et al. (2018)*, Xu et al. (2019)*, Bevacqua et al. (2020), Yang et al. (2020)*
Rainfall and water levels	Jane et al. (2020)
Rainfall and storm surge	Wahl et al. (2015); Paprotny et al. (2018); Bevacqua et al. (2019)
Rainfall intensity and depth	Yue (2000a,b, 2002); De Michele and Salvadori (2003)
Rainfall and groundwater	Anandalekshmi et al. (2019)
Rainfall and runoff	Zhang and Singh (2012); Hao and Singh (2020)
Rainfall and river discharge	Zhong et al. (2020)
Rainfall and temperature	Zhang et al. (2017)
Rainfall and duration	Salvadori and De Michele (2007)

Variable Pairs	References
Combinations of rainfall intensity, depth, and duration	Zheng et al. (2014)
Combinations of river discharge, volume, and duration	Karmakar and Simonovic (2009); Reddy and Ganguli (2012); Ganguli and Reddy (2013); Gräler et al. (2013); Mitková and Halmová (2014)
Combinations of water level, wave height and period, and storm duration	Corbella and Stretch (2012)
Combinations of sea level, precipitation, wave height, and storm surge	Hawkes (2008)

*Note these studies use the term tide measurement but actually represent observed water level measurements.

1.3 Characterizing Flooding Hazards

From a flood risk perspective there are multiple methods to characterize events. A univariate approach is often used where a single variable (e.g., water level) is considered. For example, FEMA recommends characterizing multivariate events by developing univariate water level and discharge statistics and then adopting a smooth, blended result for transitional areas (FEMA, 2011, 2016c). This can lead to underestimating flood risk because of the interplay between two flood pathways (i.e., a high tail water forces fluvial flooding upstream). Conditional probabilities represent an alternative where the multivariate flood risk can be evaluated given available information on a primary variable (e.g., water level) to determine the exceedance probability of a secondary variable (e.g., precipitation) (Shiau, 2003; Karmakar and Simonovic, 2009; Zhang and Singh, 2012; Li et al., 2013; Mitková and Halmová,

2014; Serinaldi, 2015, 2016; Anandalekshmi et al., 2019). A third method uses copulas to analyze the dependence of multiple flood drivers and develop joint statistics.

Multivariate studies typically employ copulas to evaluate dependencies between flood drivers and develop multivariate statistics. Numerous studies have used a copula based approach to study floods from various combinations of variables (Table 1.1). Compound flood risks can be described and quantified from previous copula studies (Salvadori, 2004; Salvadori and De Michele, 2004, 2007; Salvadori et al., 2011, 2013, 2016), and estimated flood risk varies depending upon the copula selection (Sadegh et al., 2018; Couasnon et al., 2020; Lucey and Gallien, 2022). A select group of copulas (Clayton, Frank, Gumbel, Student t, and Gaussian) are often used in multivariate inland and coastal hydrology risk assessments, however alternative copulas may better characterize coastal applications (Jane et al., 2020; Lucey and Gallien, 2022). Additionally, hazard scenarios provide various perspectives on critical multivariate events (Salvadori et al., 2016), but current studies are often limited to select hazard scenarios (Table 1 in Salvadori et al. (2016)).

1.4 Hydrodynamic Flood Modeling

Numerical models of varying complexity have been widely used to investigate compound flooding events (Table 1.2). Reduced complexity models (i.e., diffusive wave) are limited to slowly-varying flows and cannot resolve sub- and supercritical flow transitions (Neal et al., 2012). In urban environments where flow transitions are common inertial terms improve predictions (Sanders, 2017). The full two-dimensional nonlinear shallow water models have proven to provide excellent velocity and depth estimates (e.g. Mignot et al., 2006; Gallegos et al., 2009; Gallien, 2016). Particular attention should be paid to the numerical implementation and its suitability for rapidly variable flows. Godunov-based finite volume schemes and discontinuous Galerkin finite element methods admit supercritical flows from abrupt elevation changes inherent to urban environments such as sea walls, streets, and curbs with-

out case specific parameter tuning. Finite volume schemes are the most widely used 2D nonlinear shallow water solution method (Teng et al., 2017). Numerous Godunov-type finite volume codes have been successfully implemented in coastal embayment modeling (Arega and Sanders, 2004; Cea et al., 2006; Sanders et al., 2008; Gallien et al., 2011), urban flood simulations (Mignot et al., 2006; Villaneueva and Wright, 2006; Sanders et al., 2008; Schubert et al., 2008; Gallegos et al., 2009; Schubert and Sanders, 2012) and compound modeling (e.g., Gallien, 2016; Herdman et al., 2018; Shen et al., 2019; Muñoz et al., 2020; Nederhoff et al., 2021).

More recently, a hybrid approach combining multivariate statistical and numerical modeling have been adopted. Copulas are developed to investigate dependence structures between variables after numerical modeling (Bevacqua et al., 2019, 2020; Couasnon et al., 2020; Ganguli et al., 2020; Santos et al., 2021; Tanim and Goharian, 2021; Xu et al., 2022), and have been used to characterize multivariate return periods for flood modeling (Sebastian et al., 2017; Couasnon et al., 2018; Didier et al., 2019; Moftakhari et al., 2019). Xu et al. (2022) uses copulas after modeling tropical cyclone events to establish pairs of peak water levels and precipitation for an area without water level observations. Moftakhari et al. (2019) established copulas for coastal-riverine compound flooding then models pairs to compare to the suggested FEMA coastal-riverine compound flooding guidelines (FEMA, 2015). Hybrid approaches simulating multivariate events present an attractive option for quantifying flood mapping uncertainties associated with statistical characterization.

1.5 Uncertainty

Previous studies have explored multiple sources of uncertainty and their influences on numerical models or events estimates (Table 1.3). Studies have observed significant variability in event estimates depending on the sampling methods (Mazas and Hamm, 2017; Lucey and Gallien, 2023). Two sampling methods commonly used are peaks over threshold (Jarušková

Table 1.2: Numerical models used in recent coastal flood applications

Model	References
Delft3D	Cañizares and Irish (2008); Irish and Cañizares (2009); Horstman et al. (2013); Symonds et al. (2016); Martyr-Koller et al. (2017); Van Thanh et al. (2017); Kumbier et al. (2018); Herdman et al. (2018); Ganguli et al. (2020); Paprotny et al. (2020); Muñoz et al. (2020); Nederhoff et al. (2021); Xu et al. (2022)
LISFLOOD-FP	Bates et al. (2005); Purvis et al. (2008)
TUFLOW	Shen et al. (2019)
Delft-FLS	(Brown et al., 2007)
TOMAWAC	Dawson et al. (2009)
TRIM-2D	Knowles (2010)
MIKE21	Martinelli et al. (2010)
BreZo	Gallien et al. (2011, 2014); Gallien (2016); Moftakhari et al. (2019)
SELFE	Chen and Liu (2014)
SLOSH	Thompson and Frazier (2014)
AdH	Savant et al. (2019a,b)

and Hanek, 2006), which partitions events above a predetermined threshold as the events of concern, and block maxima (Engeland et al., 2004), which selects the maximum event per "block" of time (yearly, seasonal, semiannual, etc.). Many studies utilize 12-month block maxima sampling, the annual maximum sampling method (Baratti et al., 2012; Bezak et al., 2014; Wahl et al., 2015), and is specifically recommended by FEMA (2016c) for evaluating coastal hazards. Alternatively, studies utilize a "coinciding" type sampling to define events where the primary variable is sampled with a maximum type sampling and other variables are sampled where they co-occur with the primary variable (Lian et al., 2013; Xu et al., 2014; Sadegh et al., 2018; Tu et al., 2018; Lucey and Gallien, 2022). Sampling methods may be the most influential for extreme value studies (Mazas and Hamm, 2017), yet there is limited understanding of data sampling impacts on flood risk estimates (Mazas and Hamm, 2017; Sadegh et al., 2017; Lucey and Gallien, 2022).

Multiple data sources within a geographic area may exist and the choice of observations may influence flood risk estimates. Previous studies have shown model inputs (e.g., gauge measurements, DEMs, distributions) pose a significant source of uncertainty on results (Coveney and Fotheringham, 2011; Bates et al., 2014; Sampson et al., 2014; Saint-Geours et al., 2015). Recent studies have also emphasized record length impacts on estimates (Genest et al., 2009; Su and Tung, 2013; Tong et al., 2015; Sadegh et al., 2017; Dodangeh et al., 2019). Genest et al. (2009) observes the significance of goodness-of-fit tests significantly increase with sample size given that copula dependency structure is better defined with larger samples. Sadegh et al. (2017) showed short data records result in large event estimate uncertainties regardless of the fitted distribution's goodness of fit. Tong et al. (2015) found various return periods of annual maximum flood magnitudes were overestimated when using shorter data records. While observations and record length impart uncertainties in studies, there is no suggested minimum record length for characterizing coastal flooding events.

Numerical models have their sources of uncertainties as well. Teng et al. (2017) identifies model structure, inputs, parameters, validation data quality, landscape cover, and nonsta-

tionarity as key sources of uncertainty within flood models. Coasatal flood modeling is well established in the literature (e.g., Table 1.2). The challenge of accurate modeling lies in resolving infrastructure (e.g., storm drainage systems, seawalls, berms), including wave impacts, and quantifying event uncertainty (Gallien et al., 2018). While studies continue to identify and quantify sources of uncertainty (Table 1.3), it is unknown how compound event statistical characterization affects flood mapping applications, particularly in infrastructure-rich urban applications.

1.6 Proposed Work

This research proposes to evaluate and quantify multivariate coastal flood risk uncertainty in highly urbanized regions. Three studies are proposed which evaluate univariate and multivariate flood risks in highly urbanized regions while exploring the effects of sampling methods, flood defense structures, data selection, record length, distribution choice, and event choice on risk assessments. The first study (Chapter 3) explores events considering observed water levels (OWL) and precipitation at urbanized coastal communities in a semi-arid region. A unique structural scenario, considering a drainage system and sea wall, is explored and the effects of data sampling and distribution choice are evaluated. The second study (Chapter 4) expands by accounting for wave impacts and quantifying uncertainties induced by sampling methods, record length, distribution choice, and precipitation gauge source. Wave measurements are combined with observed water levels into total water levels (TWL, discussed in Methods) resulting in three univariate (observed and total water levels, and precipitation) and two bivariate (observed water level-precipitation and total water level-precipitation) flood hazards under consideration. Lastly, various multivariate flood events are hydrodynamically modeled in an infrastructure-rich test site to consider the uncertainty impacts in modeled flooding outcomes (Chapter 5).

Table 1.3: List of sources of uncertainties and studies which quantify their impacts

Uncertainty Source	References
Sampling methods	Engeland et al. (2004); Jarušková and Hanek (2006); Mazas and Hamm (2017); Sadegh et al. (2017); Lucey and Gallien (2022, 2023)
Distribution choice	Jane et al. (2020); Lucey and Gallien (2022, 2023)
Data availability	(Genest et al., 2009; Su and Tung, 2013; Tong et al., 2015; Sadegh et al., 2017; Dodangeh et al., 2019; Lucey and Gallien, 2023)
Observation source	Lucey and Gallien (2023)
Microclimatology	Lucey and Gallien (2023)
Distribution parameters	Wahl et al. (2012); Sadegh et al. (2017, 2018)
Numerical model inputs	Brown et al. (2007); Coveney and Fotheringham (2011); Bates et al. (2014); Sampson et al. (2014); Saint-Geours et al. (2015)
Reveiw on numerical modeling uncertainty	Teng et al. (2017)

CHAPTER 2

Methods

2.1 Univariate, bivariate, & conditonal distributions

Potential flooding events are determined with three different probability definitions: univariate, conditional, and bivariate. Assuming X and Y are random variables, x and y are observations of these variables, and F_X and F_Y represent the variables' respective cumulative distribution functions (CDF). Formulations for univariate ($F_X(x), F_Y(y)$) and bivariate joint ($F_{XY}(x, y)$) CDFs follow DeGroot and Schervish (2014) (Eq. (2.1) and (2.2)). Conditionals ($F_{X|Y\geq y}(x|Y \geq y)$, $F_{X|Y\leq y}(x|Y \leq y)$, and $F_{X|Y=y}(x|Y = y)$) are developed from Shiau (2003) (Eq. (2.3)) and Serinaldi (2015) (Eq. (2.4) and (2.5)). Conditionals 1 (C1), 2 (C2), and 3 (C3) represent Eq. (2.3), (2.4), and (2.5) going forward. Univariate statistics are developed using the appropriate continuous random variable distribution while conditional and bivariate CDFs are determined using copulas.

Copulas are functions that associate random variables' univariate CDFs to their joint CDF (e.g., F_X and F_Y to $F_{X,Y}(x, y)$) according to Sklar's theorem (Sklar, 1959; Salvadori, 2004). There is no requirement for the univariate distributions to be the same. This is particularly advantageous since the optimal univariate distributions may be used for each variable. Bivariate probabilities for different hazard scenarios, which represent various multivariate events, and conditional probabilities can be calculated using fitted copula functions.

$$F_X(x) = Pr(X \leq x) \tag{2.1}$$

$$F_{X,Y}(x,y) = Pr(X \leq x \; and \; Y \leq y) \tag{2.2}$$

$$F_{X|Y\geq y}(x|Y \geq y) = Pr(X > x|Y \geq y) = \frac{F_X(x) - F_{XY}(xy)}{1 - F_Y(y)} \tag{2.3}$$

$$F_{X|Y\leq y}(x|Y \leq y) = Pr(X > x|Y \leq y) = 1 - \frac{F_{X,Y}(x,y)}{F_Y(y)} \tag{2.4}$$

$$F_{X|Y=y}(x|Y = y) = Pr(X > x|Y = y) = 1 - \frac{\partial F_{XY}(xy)}{\partial y} \tag{2.5}$$

2.2 Hazard scenarios

Notation and definitions from Salvadori et al. (2016), unless otherwise stated, are used to define the upper set (S) and scenario types. Salvadori et al. (2016) and Serinaldi (2015) present figures of each scenario's probability space. Further discussion of hazard scenarios and copulas assume a bivariate situation.

2.2.1 "OR"

"OR" scenario events have one or both random variables exceed a specified threshold. That is, what is the probability of a water level or precipitation event exceeding a given value? Standard univariate CDFs make up the associated copula.

$$\alpha_x^{\vee} = \mathbf{P}(\mathbf{X} \in S_x^{\vee}) = 1 - \mathbf{C}(\mathbf{F}_1(x_1), ..., \mathbf{F}_d(x_d)) \tag{2.6}$$

2.2.2 "AND"

"AND" scenario events have both random varibles exceed a specified threshold. In this case the fundamental question is "what is the probability of a particular water level and

precipitation rate exceeding specified values?". The survival copula ($\hat{\mathbf{C}}(u, v)$) is comprised of univariate survival CDFs ($\bar{\mathbf{F}}(x) = 1 - \mathbf{F}(x)$) and the provided equation can be found in Serinaldi (2015) and Salvadori and De Michele (2004).

$$\alpha_x^{\wedge} = \mathbf{P}(\mathbf{X} \in S_x^{\wedge}) = \hat{\mathbf{C}}(\bar{\mathbf{F}}_1(x_1), ..., \bar{\mathbf{F}}_d(x_d)) \tag{2.7}$$

$$\hat{\mathbf{C}}(u, v) = 1 - u - v + C(u, v) \tag{2.8}$$

2.2.3 "Kendall"

The "Kendall" (K) scenario highlights an infinite set of OR events that separate the subcritical (i.e, "safe") and supercritical (i.e.,"dangerous") statistical regions. In the OR scenario, events along an isoline (t) share a common probability, but define separate regions. Events along a Kendall t represent the same super critical region (Serinaldi, 2015) and provide a "safety lower bound" (Salvadori et al., 2011). Essentially the Kendall scenario considers the minimum OR events of concern. $\mathbf{K}$(t) is estimated by a method outlined in Salvadori et al. (2011).

$$\mathbf{K}(t) = \mathbf{P}(\mathbf{F}(X_1, ..., X_d) \leq t) = \mathbf{P}(\mathbf{C}(F_1(X_1), ..., F_d(X_d)) \leq t) \tag{2.9}$$

$$\alpha_t^{\mathbf{K}} = \mathbf{P}(\mathbf{X} \in S_t^{\mathbf{K}}) = 1 - \mathbf{K}(t) \tag{2.10}$$

2.2.4 "Survival Kendall"

"Survival Kendall" (SK) scenario highlights an infinite set of AND events which also separate safe and dangerous statistical spaces. AND events along a t also share a common probability, but define separate regions. Events along an SK t represent the same super critical region,

but provide an "(upper) bounded safe region" (Salvadori et al., 2013). The Survival Kendall specifically considers the largest AND events of concern and is estimated by the method outlined in Salvadori et al. (2013).

$$\hat{\mathbf{K}}(t) = \mathbf{P}(\overline{\mathbf{F}}(X_1, ..., X_d) \leq t) = \mathbf{P}(\hat{\mathbf{C}}(\bar{F}_1(X_1), ..., \bar{F}_d(X_d)) \leq t) \tag{2.11}$$

$$\alpha_t^{\check{\mathbf{K}}} = \mathbf{P}(\mathbf{X} \in S_t^{\check{\mathbf{K}}}) = 1 - \check{\mathbf{K}}(t) = \hat{\mathbf{K}}(t) \tag{2.12}$$

2.2.5 "Structural"

The "Structural" scenario considers the probability of an output from a structural function, $\Psi(\mathbf{X})$, exceeding a design load or capacity (z) (Salvadori et al., 2016). For example, De Michele et al. (2005) and Volpi and Fiori (2014) used a structural function to evaluate a dam spillway while Salvadori et al. (2015) considers the preliminary design of rubble mound breakwater. In this work, the structural failure function focuses on the question "what is the probability of a water level forcing tide valve closure and subsequent flooding during a precipitation event?".

$$\alpha_z^{\Psi} = \mathbf{P}(\mathbf{X} \in S_z^{\Psi}) = \mathbf{P}(\Psi(\mathbf{X}) > z) \tag{2.13}$$

2.3 MvCAT

Sadegh et al. (2017) developed a publicly available MATLAB toolbox called The Multivariate Copula Analysis Toolbox (MvCAT) where users can fit multiple copula functions for characterizing bivariate events. Additional information about MvCAT and its updated version (MhAST) can be found in Sadegh et al. (2017, 2018). The MvCAT framework was expanded in Lucey and Gallien (2022), and is used to determine all uni- and multivariate statistics. Copulas without continuous PDF functions or complex derivatives (Cuadras-Auge, Raftery,

Shih-Louis, Linear-Spearman, Fischer-Hinzmann, Marshal-Olkin, Gaussian, and Student t) were removed from the studies. However, all copulas were considered when creating isolines to assess the uncertainty in the flood metrics for events of the same return period (i.e., along the same isoline).

2.4 Return periods

Return period (T) is a statistical description of event severity and is commonly used in hydrologic studies (e.g., De Michele et al., 2005, 2007; FEMA, 2011; Wahl et al., 2012; USACE, 2013; Salvadori et al., 2014; Wahl et al., 2015; Salvadori et al., 2015). A return period is the inverse of an event's probability of exceedance presented as F in Eq. (2.14) (Tu et al., 2018). N is the utilized record length, n is the number of considered events within N, and N_e is the average number of events per unit of time (monthly, yearly, etc.) in Eq. (2.15). $N_e = 1$ when using annual samplings (Tu et al., 2018) and will vary when using the wet season monthly samplings depending on the average number of events sampled per year.

$$T = 1/(N_e * F) \tag{2.14}$$

$$N_e = n/N \tag{2.15}$$

2.5 Goodness of fit metrics

Multiple goodness of fit metrics and correlations serve to quantify the quality of distribution fits and dependencies between variables. Marginal fits are selected by Bayesian Information Criterion (BIC; Eq. (2.19)) and must pass the Chi-square goodness-of-fit test at standard significance levels ($\alpha = 0.05$), unless otherwise stated. Copulas are selected by BIC and must pass the Cramér-von Mises test (Genest et al., 2009; Couasnon et al., 2018; Sadegh

et al., 2018; Ward et al., 2018). Likelihood ($\mathcal{L} \in [0, \infty)$) measures how well a distribution's estimated parameters fit the sample data with larger values suggesting a better fit. Log-likelihood ($\ell \in (-\infty, \infty)$) is the log transformation of Eq. (2.16) used to calculate BIC. BIC ($BIC \in (-\infty, \infty)$) is similar to the likelihood, but penalizes for the number of estimated parameters (D) and the data's sample size (n). Smaller BIC values represent a better fit. Equations and definitions can be found in Sadegh et al. (2017). Correlation measurements include Pearson's linear correlation, Kendall's tau, and Spearman's rho coefficients.

$$\mathcal{L}(\boldsymbol{\theta}|\tilde{\mathbf{Y}}) = \prod_{i=1}^{n} \frac{1}{\sqrt{2\pi\tilde{\sigma}^2}} exp\{-\frac{1}{2}\tilde{\sigma}^2[\tilde{y}_i - y_i(\boldsymbol{\theta})]^2\} \tag{2.16}$$

$$\tilde{\sigma}^2 = \frac{\sum_{i=1}^{n}[\tilde{y}_i - y_i(\boldsymbol{\theta})]^2}{n} \tag{2.17}$$

$$\ell(\boldsymbol{\theta}|\tilde{\mathbf{Y}}) = -\frac{n}{2}\ln(2\pi) - \frac{n}{2}\ln\tilde{\sigma}^2 - \frac{1}{2}\tilde{\sigma}^2\sum_{i=1}^{n}[\tilde{y}_i - y_i(\boldsymbol{\theta})]^2 \tag{2.18}$$

$$BIC = Dln(n) - 2\ell \tag{2.19}$$

CHAPTER 3

Characterizing multivariate coastal flooding events from precipitation and high marine water levels

3.1 Background

Coastal flooding studies primarily focus on locations defined by storm-surge-dominated oceanographic conditions with warm and humid (Wahl et al., 2012; Lian et al., 2013; Xu et al., 2014; Masina et al., 2015; Wahl et al., 2015; Mazas and Hamm, 2017; Paprotny et al., 2018; Tu et al., 2018; Bevacqua et al., 2019; Didier et al., 2019; Xu et al., 2019; Yang et al., 2020) climatic conditions (i.e. Köppen-Geiger system, Beck et al., 2018). In contrast, along the southern California coast typical tidal variability is 1.7 to 2.2 m (Flick, 2016) and storm surge rarely exceeds approximately 20 cm (Flick, 1998). Notably, during the wet season (October to March), when precipitation typically occurs, spring tide ranges are relatively large ($\sim$ 2.6 m). Critically, few studies consider areas where coastal flooding events are dominated by large tides and either precipitation or wave events (Masina et al., 2015; Mazas and Hamm, 2017; Didier et al., 2019; Jane et al., 2020). This study explores univariate and multivariate flooding events in a semi-arid, tidally dominated, highly urbanized region. Here, the dependency between observed water levels and precipitation, impacts of sampling methods and distribution fitting, and the resulting flood values are explored.

3.2 Site description & data

This study considers observed water level and precipitation influences for coastal multivariate events at Santa Monica (SM), Sunset Beach (S), and LA Jolla (SD) areas in Los Angeles, Huntington Beach, and San Diego, California (Fig. 4.1); three semi-arid, tidally dominated sites in the United States. All are low-lying estuarine or bay-backed highly urbanized beach communities requiring extensive coastal management to mitigate flooding events. For example, sea walls and artificial berms in Sunset Beach protect infrastructure from high embayment water levels, wave runup, and overtopping along the open coast. The storm drain network is managed to prevent back flooding during high tides. Notably, Gallien et al. (2014) suggested when tide valves are closed, the storm drain network cannot reduce pluvial flooding caused by alternative flooding pathways (e.g., precipitation or wave overtopping). Pacific Coast Highway (PCH) is heavily utilized and is a primary transportation corridor along the southern California coastline. All locations are densely urbanized and highly impacted by flooding.

Observed water levels from the Los Angeles (Station ID: 9410660), La Jolla (Station ID: 9410230), and Santa Monica (Station ID: 9410840) tide gauges are available on NOAA's Tides and Currents for daily high-low, hourly, or six minute intervals (NOAA, Accessed 2019c). Verified hourly water levels (m NAVD88) had the longest record length at all three stations and provided an additional 31-years of observations overlapping precipitation data for Los Angeles and La Jolla, and 6-years for Santa Monica. The resulting observations windows are November 22, 1973 to December 19, 2013 for Santa Monica, July 1, 1948 to December 1, 2012 for Sunset and July 1, 1948 to December 19, 2013 for San Diego (Table 3.1).

It is worth noting, that within the body of multivariate flooding literature, the terms tide and water level may be interchanged (e.g., Lian et al., 2013; Xu et al., 2014; Tu et al., 2018; Xu et al., 2019; Yang et al., 2020). This is a key distinction since compound event

dependencies may change depending on water level selection. Recent efforts have been made to standardize language where tide represents only the astronomical changes in water levels and storm surge specifically excludes astronomical variability and consists only of the inverse barometric effects along with wind and wave setup (Gregory et al., 2019). In this study, the term observed water level (OWL) is adopted. OWL is the water level measured at the NOAA tide gauges which includes all tidal, storm, and climatic effects.

The U.S. Hourly Precipitation Data dataset provided by NOAA's National Centers for Environmental Information (NOAA, Accessed 2019b) at the Signal Hill (COOP:048230), Los Angeles International Airport (COOP:045114), and San Diego International Airport (COOP:047740) stations is used as the precipitation inputs. Observations do not contain trace amounts (< 0.25 mm) and are provided as cumulative precipitation (mm) per event. Precipitation measurements were converted to a mmday^{-1} rate by dividing the total event precipitation by the event duration to match the hourly OWL measurements. The final precipitation input is a 24-hour cumulative precipitation record made from the hourly observations. All data was transformed to UTC for analysis.

Multivariate flood probabilities are determined with combinations of sampling methods: Annual Maximum (AM), Annual Coinciding (AC), Wet Season Monthly Maximum (WMM), and Wet Season Monthly Coinciding (WMC). AM sampling pairs the single largest precipitation and OWL observations within a given year (without regard to co-occurrence), where AC sampling pairs the single largest precipitation observation within a given year to the largest OWL observation within its 24-hour accumulation period. Each sampling method samples from a unique probability space and therefore will provide varying perspectives for a return period. A summary of each sites' associated gauges, observation windows, and number of pairs is provided in Table 3.1. Southern California's wet season is defined between October to March and provides a majority of the total annual rainfall (Cayan and Roads, 1984; Conil and Hall, 2006). It is likely for extreme multivariate events to occur during this period. Maximum sampling pairs the single largest precipitation and OWL observa-

Table 3.1: Water level and precipitation observations at Santa Monica (SM), Sunset (S), and San Diego (SD) using annual maximum (AM), annual coinciding (AC), wet season monthly maximum (WMM), and wet season monthly coinciding (WMC) samplings

Site	Tide Gauge	Precip. Gauge	Observation Window	AM Pairs	AC Pairs	WMM Pairs	WMC Pairs
SM	9410840	045114	November 22, 1973 to December 19, 2013	40	38	193	191
S	9410660	048230	July 1, 1948 to December 1, 2012	63	63	257	258
SD	9410230	047740	July 1, 1948 to December, 19 2013	65	60	328	329

tions within each year or wet season month. A multivariate event created with the largest observed precipitation and OWL within a year or wet season month can result in an event with severe flooding potential. Although strictly speaking maximum parings (annual or wet season) do not technically represent an observed multivariate event, they would represent a severe event and are consistent with the blended approach recommended by FEMA (2016c). Coinciding sampling pairs the single largest precipitation observation within each year or wet season month to the largest OWL observation within its 24-hour accumulation period, providing more realistic pairs compared to maximum sampling.

Distributions are fit with existing precipitation observations greater than zero consistent with previous studies (Swift Jr and Schreuder, 1981; Hanson and Vogel, 2008). Months with no OWL measurements were excluded. In the case of coinciding sampling, pairs that had three or more OWL measurements missing within the 24-hour window were manually reviewed and removed if their tidal peak was clearly missing. Specifically for WMM sampling, months with more than half their observations missing were also reviewed and removed if the tidal peak was missing. The resulting data pairs are shown in Fig. 3.2.

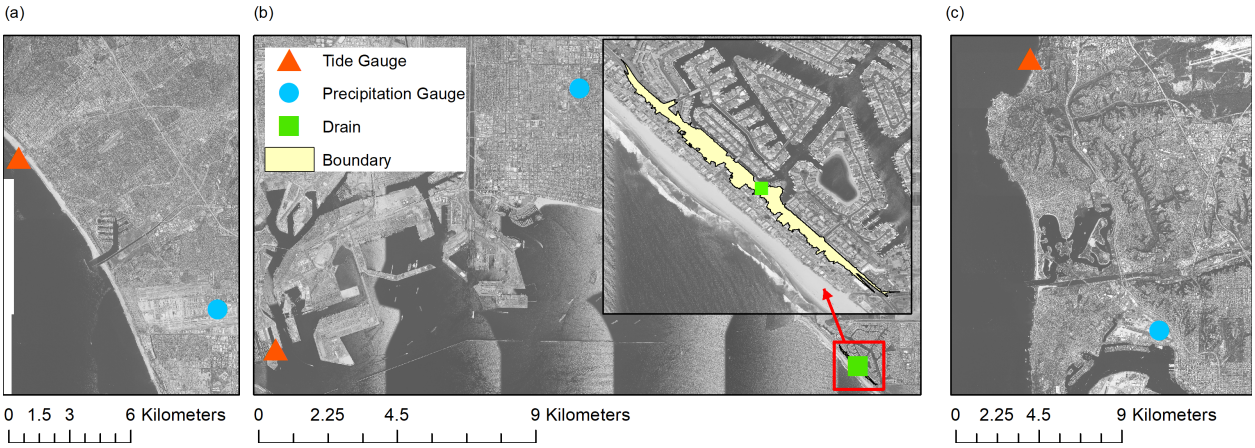

Figure 3.1: Map displaying (a) Santa Monica, (b) Sunset, and (c) San Diego sites along with locations of tide gauges (triangle) and precipitation stations (circle). The road drain (square) and boundary (yellow) at Sunset (∼2 km^2) is for the Structural scenario. Aerial imagery from NOAA (Accessed 2020).

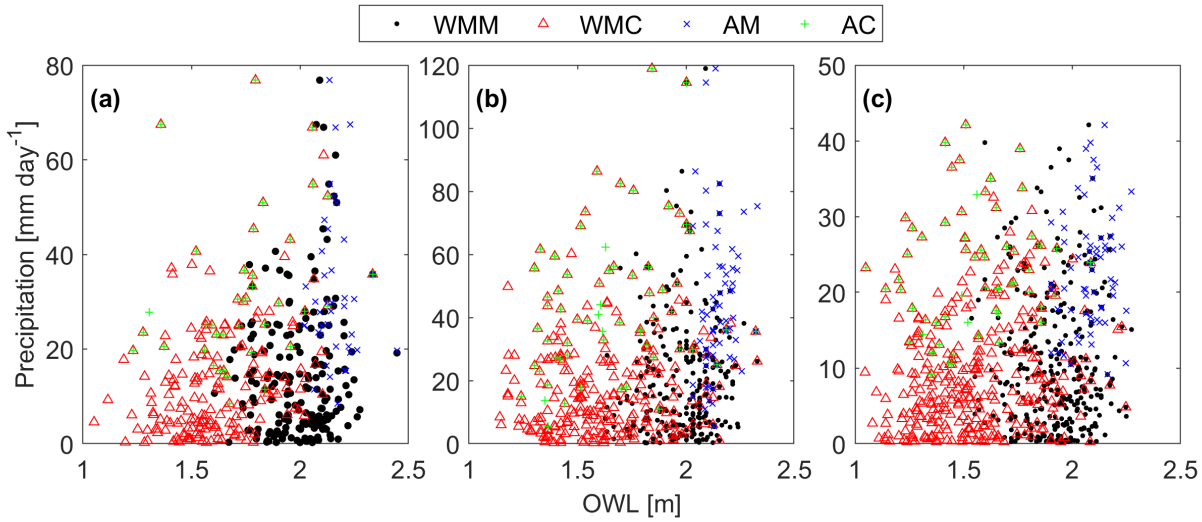

Figure 3.2: Data pairs for each sampling method. annual maximum (AM, cross), annual coinciding (AC, plus), wet season monthly maximum (WMM, dot), and wet season monthly coinciding (WMC, triangle) at (a) Santa Monica, (b) Sunset, and (c) San Diego

3.3 Results

Univariate, conditional, and bivariate probabilities were developed using four sampling methods (AM, AC, WMM, and WMC) and seventeen different copulas. Two marginal distributions do not pass the chi square test at the standard 0.05 level of significance (San Diego AM OWL and Santa Monica WMM OWL). These distributions pass at reduced significance levels of 0.01. Four copulas almost always passed (Nelsen, BB1, BB5, and Roch-Alegre) the Cramér-von Mises test and are used for analysis. It is noted the Roch-Alegre (Roch.) did not pass at Sunset for WMM sampling, and the BB1 and BB5 did not pass at San Diego for WMC sampling. Additionally, Santa Monica's AM data is slightly negatively correlated (> -0.06). Copula and sampling effects differ significantly at low (i.e., low return period) and high (i.e., severe return period) probabilities of non-exceedance. In the case of annual sampling, non-exceedance (exceedance) probabilities are 0.9 (0.1) and 0.99 (0.01) for the 10- and 100-year events, respectively. In wet season sampling, return period exceedance probabilities vary depending on sampling type and location due to the average number of event observations per year (N_e from Eq. (2.15)). For example, San Diego WMC sampling has 329 observations within the 65 year record (i.e., $N_e = 5.06$). Therefore, the exceedance probabilities (F in Eq. (2.14)) associated to a 10- and 100-year event are 0.0198 and 0.0020 (non-exceedance probabilities at 0.9802 and 0.9980), respectively. Table 3.2 presents wet season (WMM and WMC) exceedance probabilities for all sites.

Table 3.2: Santa Monica, Sunset, and San Diego exceedance probabilities at the 10- and 100-year return periods for wet season monthly maximum (WMM) and wet season monthly coinciding (WMC) samplings.

	Santa Monica		Sunset		San Diego	
	10-year	100-year	10-year	100-year	10-year	100-year
WMM	0.0207	0.0021	0.0245	0.0025	0.0198	0.0020
WMC	0.0209	0.0021	0.0244	0.0024	0.0198	0.0020

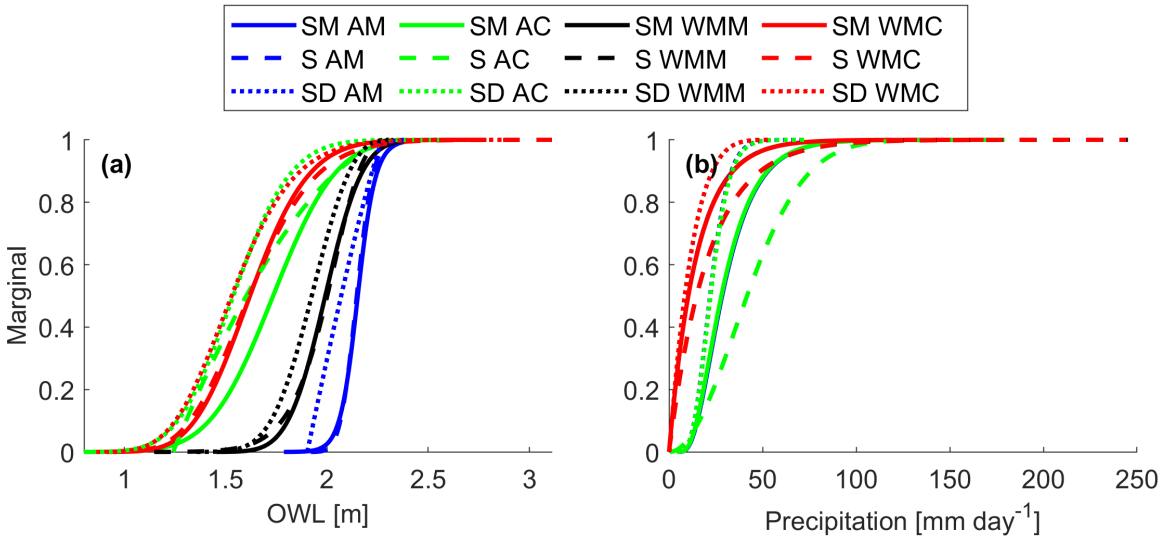

Figure 3.3: (a) OWL and (b) precipitation marginals for Santa Monica (SM, solid lines), Sunset (S, dashed lines), and San Diego (SD, dotted lines) using annual maximum (AM, blue), annual coinciding (AC, green), wet season monthly maximum (WMM, black), and wet season monthly coinciding (WMC, red) samplings.

3.3.1 Marginals

The selected marginal distributions (Fig. 3.3, Table 7.1) were tested and/or suggested fits in previous studies. Rainfall has been widely fit with an Exponential distribution (refer to Table 2 in Salvadori and De Michele (2007)), but more recently been fit using a variety of distributions including Gamma (Husak et al., 2007), Rayleigh (Pakoksung and Takagi, 2017; Esberto, 2018), Generalized Pareto or Birnbaum-Saunders (Ayantobo et al., 2021). In the case of annual precipitation (coinciding or maximum sampling) Santa Monica was well described by a Birnbaum-Sanders, Rayleigh best described Sunset data, and a Gamma was the best fit for San Diego data. Similarly, wet season precipitation data (maximum or coinciding sampling) was best described by the Exponential distribution for Santa Monica and Sunset while the Generalized Pareto best represented San Diego.

Historically, water levels have been described using a number of distributions including Normal (Hawkes et al., 2002), Generalized Pareto (Mazas and Hamm, 2017), Log Logistic and Nakagami (Sadegh et al., 2018), Birnbaum-Saunders (Sadegh et al., 2018; Didier et al., 2019; Jane et al., 2020), along with Gamma, Weibull, and Inverse Gaussian (Jane et al., 2020). Observed water levels did not exhibit site specific patterns and were described by a range of distributions (Table 7.1).

3.3.2 Copulas

San Diego wet season monthly coinciding conditional CDFs display individual copulas effects (Fig. 3.4). The Nelsen, Roch., and BB1 copulas consistently suggest similar OWL (Fig. 3.4a, e) and precipitation values (Fig. 3.4b, f) while, in this example, the BB5 suggests higher OWL and precipitation values (solid black line, Fig. 3.4a, b, e, f). C1's 100-year pair in Table 3.5 displays an example of the BB5's conservative nature. Copula choice has nearly no effect on the Conditional 2 scenario (Fig. 3.4c, d). Most probable OWL and precipitation values in Tables 3.4 and 3.5 further display the aforementioned behaviors. These conditional

Table 3.3: Best fitting univariate distributions for each location and sampling method (annual maximum (AM), annual coinciding (AC), wet season monthly maximum (WMM), wet season monthly coinciding (WMC)).

Dataset	Variable	Santa Monica	Sunset	San Diego
AM	OWL	L	BS	GP
	Precip	BS	R	G
AC	OWL	N	GP	NA
	Precip	BS	R	G
WMM	OWL	N	W	GEV
	Precip	E	E	GP
WMC	OWL	G	IG	IG
	Precip	E	E	GP

BS - Birnbaum-Saunders; GP - Generalized Pareto; E - Exponential
R - Rayleigh; N - Normal; L - Log logistic; G - Gamma
W - Weibull; IG - Inverse Gaussian; NA - Nakagami

patterns generally persist at all locations with an additional note that the Nelsen can suggest lower OWL values and the BB5 can provide similar results to the Roch. and BB1 copulas.

Figures 3.5 and 3.6 show the 10- and 100-year return periods, respectively, for the four focused copulas using wet season monthly coinciding sampling at San Diego. Clearly the BB5 presents conservative results suggesting higher OWL and precipitation pairs in the AND and SK scenarios (Fig. 3.5a, c and 3.6a, c), while the BB1, Nelsen, and Roch-Alegre copulas present similar OWL and precipitation values. The OR and Kendall scenarios suggest quite similar isolines between copulas, suggesting similar values, but the BB5 suggests less severe OWL and larger precipitation values according to the densest location along its isoline (Fig. 3.5b, d, and 3.6b, d). Tables 3.4 and 3.5 further display the bivariate patterns. Again, these bivariate patterns generally persist at all locations with the additional notes: the Nelsen

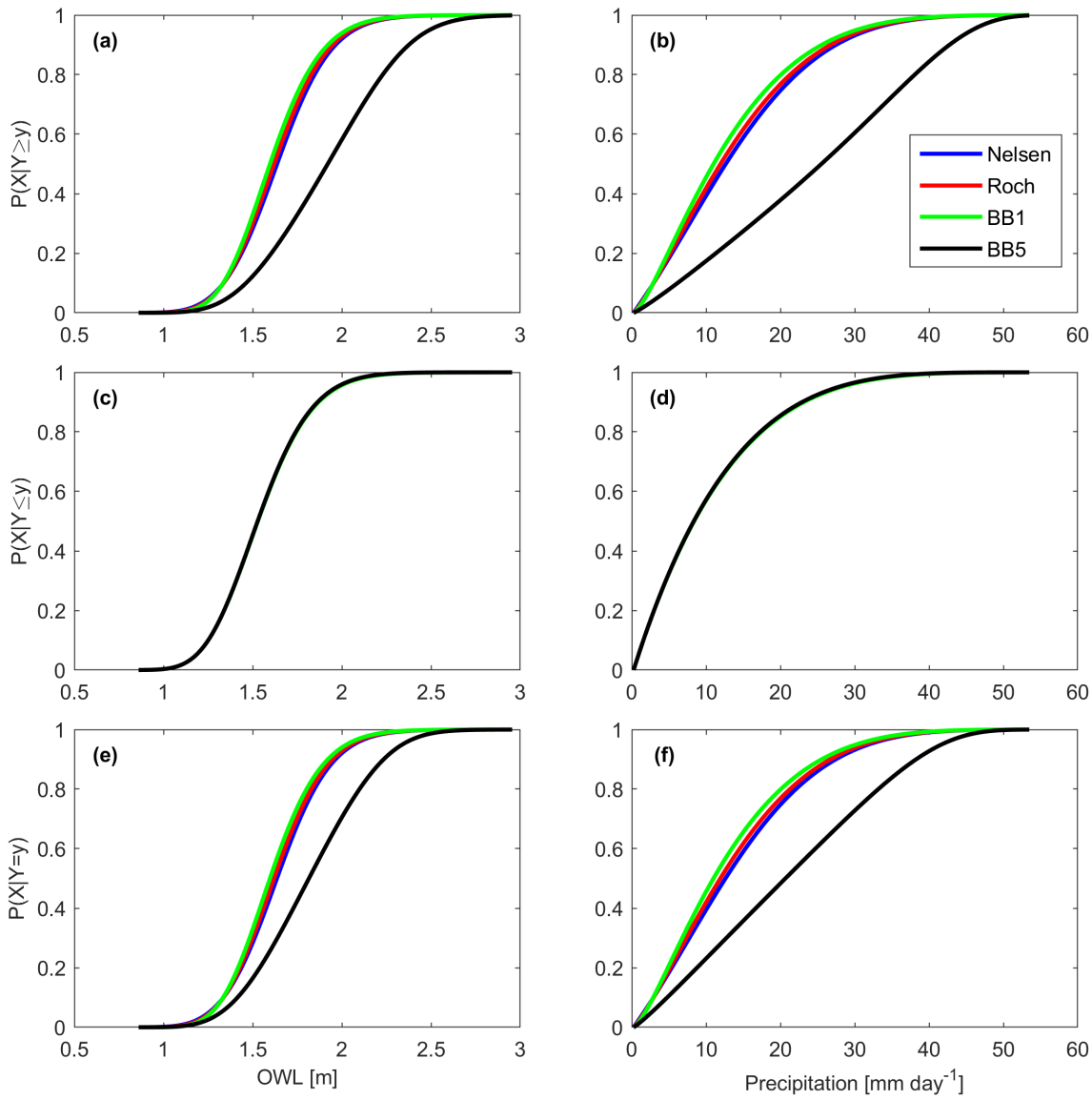

Figure 3.4: San Diego wet season monthly coinciding OWL (left column) and precipitation (right column) (a), (b) C1, (c), (d) C2, and (e), (f) C3 CDFs using the Nelsen (blue), Roch-Alegre (Roch), BB1 (green), and BB5 (black) copulas. OWL/ Precipitation conditionals are conditioned on the occurrence of a 25-year precipitation/ OWL event.

may suggest lower OWL values in the AND and SK scenarios, the BB5 typically has similar results to the Roch. and BB1 copulas in the AND and SK scenarios, and the BB5 typically agreed with the other copula results outside of San Diego for the OR and K scenarios.

Table 3.4: San Diego 10-year marginal (M), conditional (C), and bivariate OWL (m) and precipitation ($mmday^{-1}$) values using wet season monthly coinciding sampling. Conditionals are conditioned on a 25-year event occurring.

	Nelsen		Roch.		BB1		BB5	
	OWL	Precip	OWL	Precip	OWL	Precip	OWL	Precip
M	2.11	33.64	2.11	33.64	2.11	33.64	2.21	33.64
C1	2.19	36.79	2.18	36.27	2.16	35.41	2.62	48.65
C2	2.11	33.61	2.11	33.61	2.11	33.62	2.09	33.02
C3	2.19	36.76	2.18	36.24	2.15	35.37	2.46	44.92
AND	1.85	22.49	1.85	22.15	1.84	21.65	1.91	24.99
OR	2.20	37.06	2.17	38.29	2.20	37.06	2.12	43.47
K	2.22	37.67	2.22	37.67	2.05	32.52	2.14	44.11
SK	2.15	35.13	2.15	35.11	2.15	35.04	2.21	37.88

3.3.3 Sampling

San Diego conditional CDFs using the BB1 copula clearly present sampling effects (i.e. maximum versus coinciding and annual versus wet season months). It should be noted, that each sampling method represents a unique probability space and accordingly results in alternative realizations of a given return period. Coinciding samplings exhibit similar OWL CDFs (green and red lines, Fig. 3.7a, c, e), whereas wet season samplings exhibit similar precipitation CDFs (red and black lines Fig. 3.7b, d, f). OWL values can be larger for maximum samplings at lower non-exceedance probabilities (i.e lower return periods) (Fig. 3.7a, c, e blue and black lines, Table 3.6). However, the extended tail from WMC

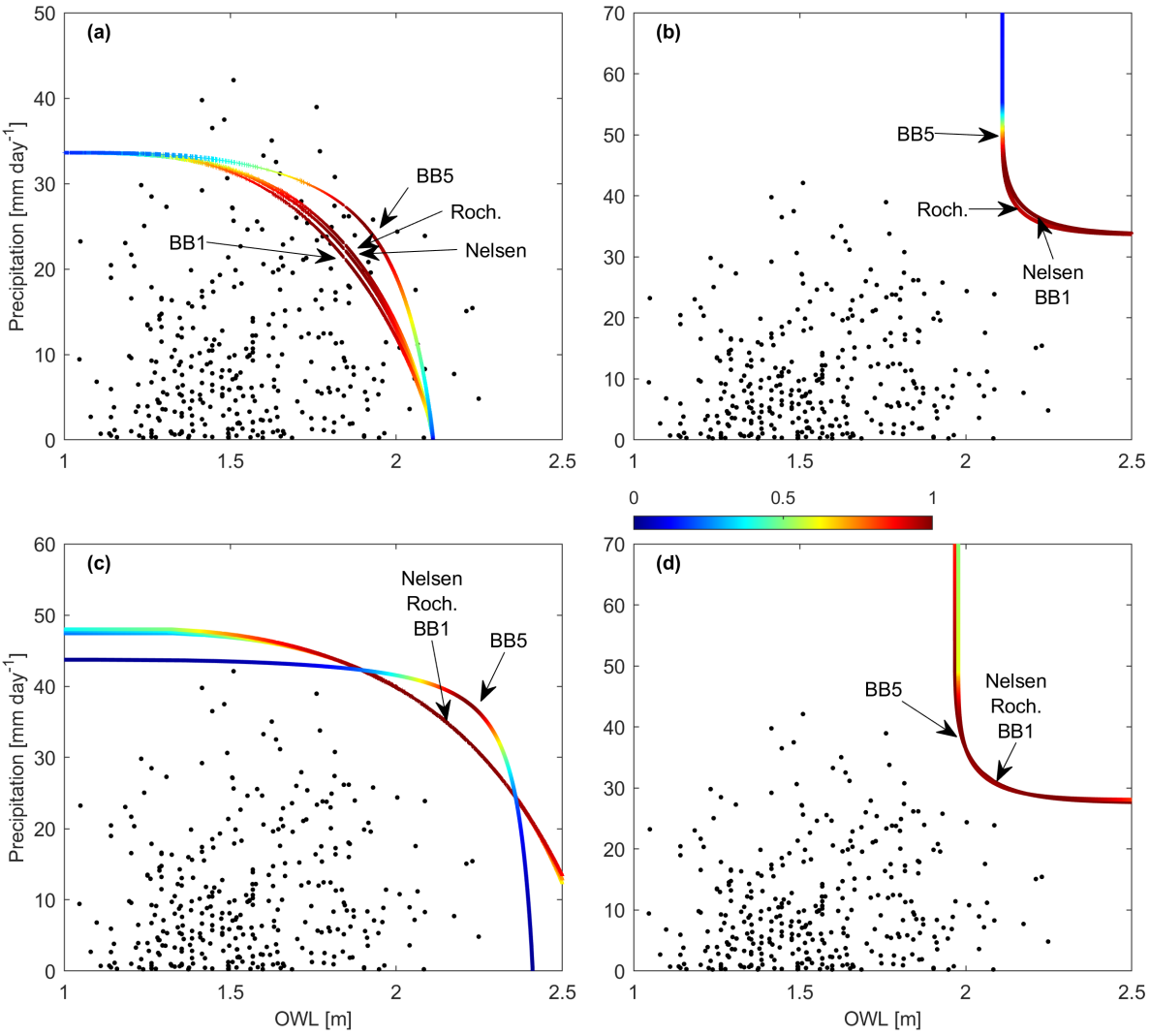

Figure 3.5: San Diego wet season monthly coinciding (a) AND, (b) OR, (c) SK, and (d) K hazard scenarios with the Nelsen, Roch-Alegre (Roch), BB1, and BB5 10-year isolines. Copula labels point to the mostly likely value on their respective isolines.

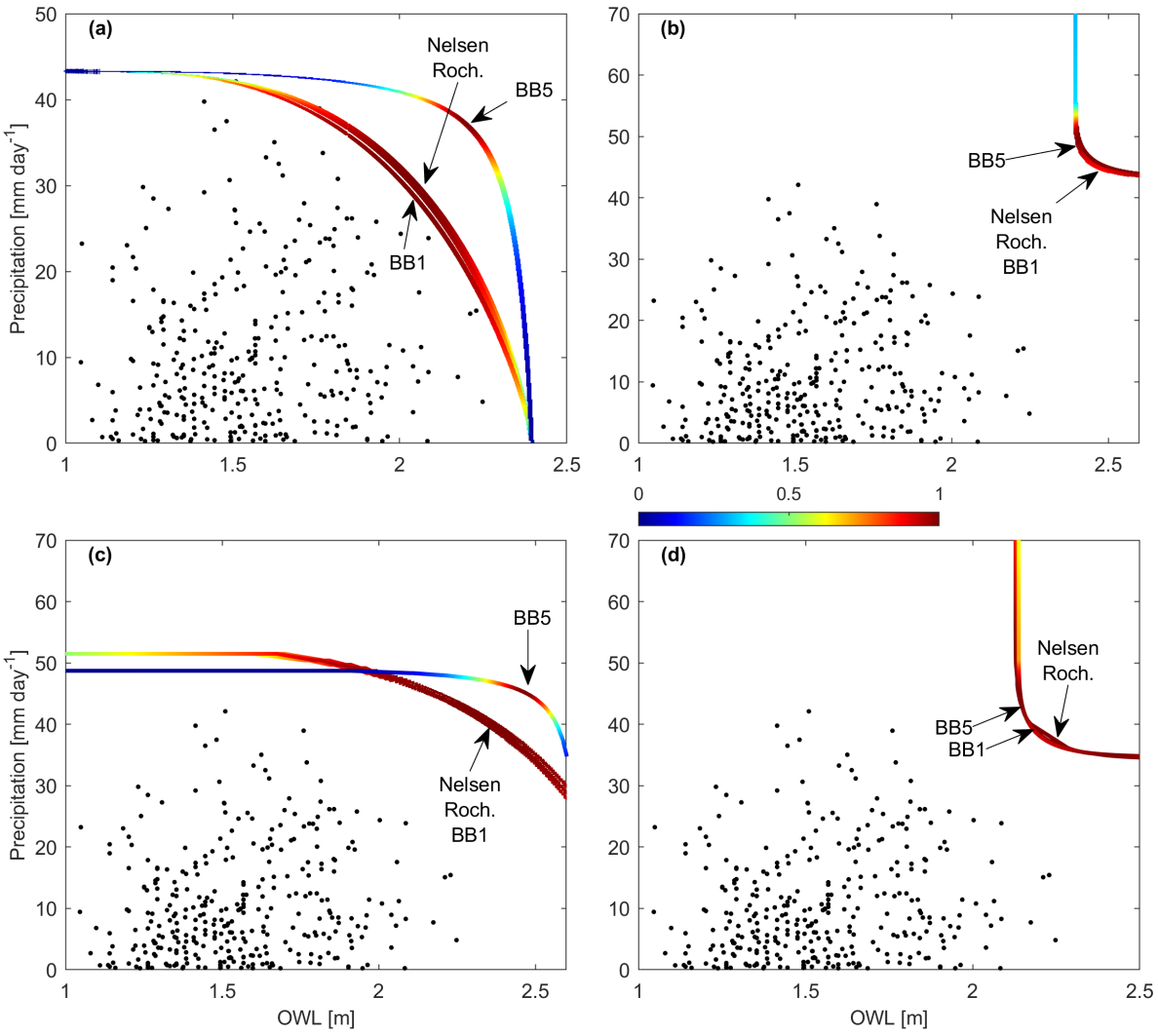

Figure 3.6: San Diego wet season monthly coinciding (a) AND, (b) OR, (c) SK, and (d) K hazard scenarios with the Nelsen, Roch-Alegre (Roch), BB1, and BB5 100-year isolines. Copula labels point to the mostly likely value on their respective isolines.

Table 3.5: San Diego 100-year marginal (M), conditional (C), and bivariate OWL (m) and precipitation ($mmday^{-1}$) values using wet season monthly coinciding sampling. Conditionals are conditioned on a 25-year event occurring.

	Nelsen		Roch.		BB1		BB5	
	OWL	Precip	OWL	Precip	OWL	Precip	OWL	Precip
M	2.40	43.34	2.40	43.34	2.40	43.34	2.40	43.34
C1	2.47	45.26	2.46	44.95	2.44	44.48	2.89	52.72
C2	2.40	43.32	2.40	43.32	2.40	43.34	2.35	42.11
C3	2.47	45.26	2.46	44.92	2.44	44.42	2.68	49.72
AND	2.04	30.77	2.03	30.45	2.02	29.93	2.20	37.42
OR	2.47	45.53	2.48	45.39	2.47	45.53	2.40	49.17
K	2.22	31.79	2.22	31.79	2.17	40.13	2.14	38.59
SK	2.31	40.97	2.33	41.53	2.32	41.26	2.46	45.25

sampling produces larger OWL at higher return periods (red line Fig. 3.7a, c, e; Table 3.7). Annual coinciding sampling displays significantly lower OWL values at low (Table 3.6) and high (Table 3.7) return periods. Only minimal differences between annual and wet season precipitation exist at the 10- and 100-year return periods (maximum difference of 1.06 and 4.56 $mmday^{-1}$ respectively; Tables 3.6 and 3.7). Annual (wet season) precipitation CDFs appear similar as OWL measurements are chosen subsequent to precipitation observations (Fig. 3.7b, d, f).

Figures 3.8 and 3.9 present the 10- and 100-year return periods using the BB1 copula for all samplings (AM, AC, WMM, and WMC). For the AND and K scenarios, AM sampling results in the largest OWL compared to the other sampling methods (Fig. 3.8a, d and 3.9a, d, Tables 3.6 and 3.7). Additionally for the AND and K scenarios (Fig. 3.8a, d and 3.9a, d), maximum samplings (AM and WMM) provide more conservative OWLs compared to WMC OWL values (Tables 3.6 and 3.7). When comparing maximum samplings (AM

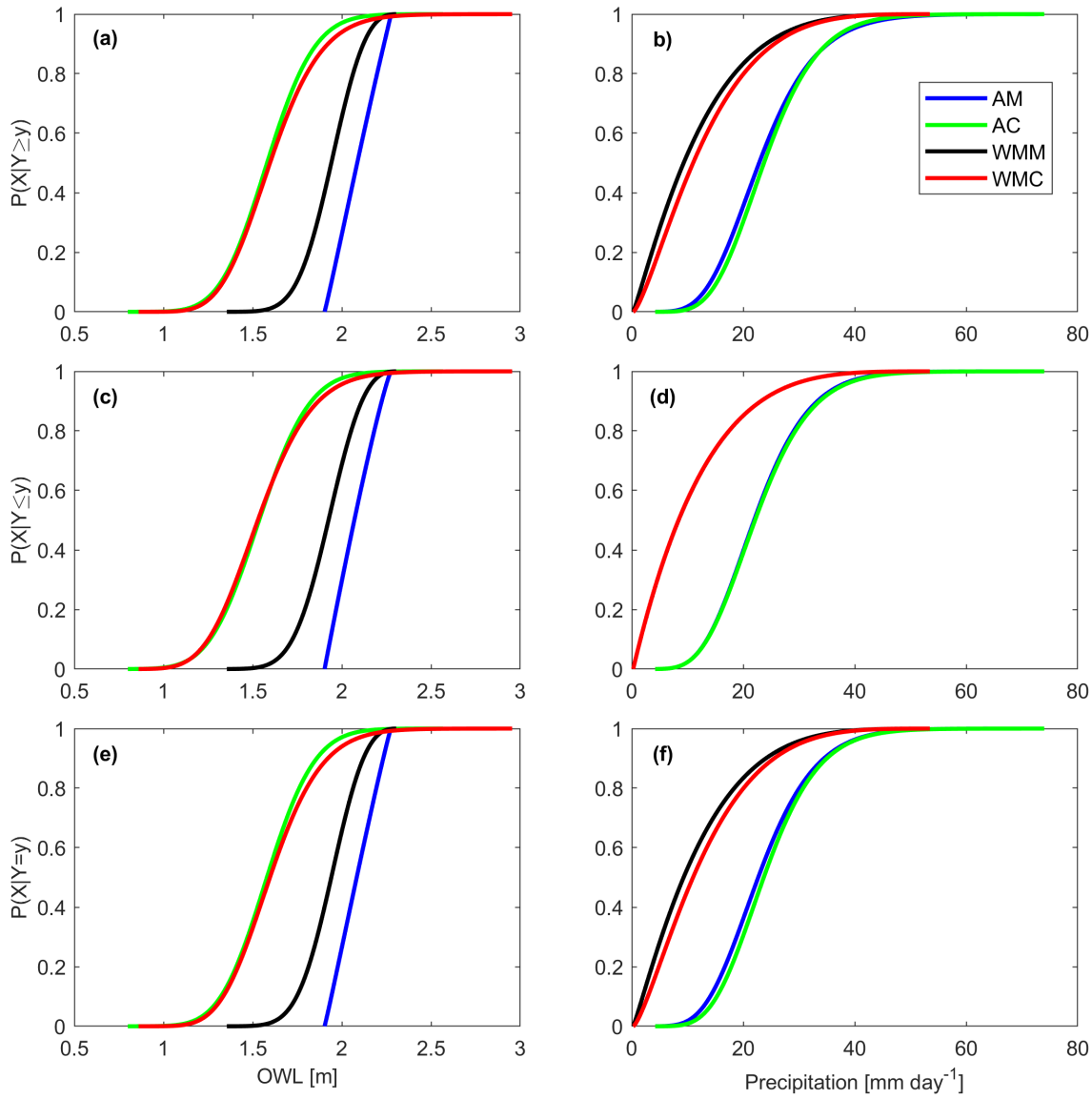

Figure 3.7: San Diego OWL (left column) and precipitation (right column) (a), (b) C1, (c), (d) C2, and (e), (f) C3 CDFs for annual maximum (AM, blue), annual coinciding (AC, green), wet season monthly maximum (WMM, black), and wet season monthly coinciding (WMC, red) samplings using the BB1 copula. OWL/ Precipitation conditionals are conditioned on the occurrence of a 25-year precipitation/ OWL event.

and WMM) to WMC sampling in the OR and SK scenarios, maximum samplings generally provide larger OWL values at lower return periods (Fig. 3.8b, c; Table 3.6), but smaller or similar OWL at larger return periods (Fig. 3.9b, c; Table 3.7). AC sampling generally results in the smallest OWL levels at all hazard scenarios. These behaviors persist across all locations. Given wet season monthly coinciding sampling results in larger OWL values for the marginal, conditional, OR, and Kendall scenarios, this suggests maximum type sampling may not accurately reflect OWL at extreme return periods.

Table 3.6 and 3.7 shows the most probable 10- and 100-year marginal and multivariate event values. AM OWL exceed AC OWL across all probability types and sites, which is expected given the (nonphysical) paring of the two largest individual OWL and precipitation events without regard to co-occurrence. For example, in the 10-year return period annual maximum OWLs are at least 30 cm higher than AC (Table 3.6). In the 100-year return period annual maximum OWLs exceed annual coinciding OWLs by at least 17 cm (Table 3.7). Precipitation is generally consistent across sampling types with only minor variations observed. AM and WMM sampling generally produced similar OWL results at both the 10- and 100-year return periods with maximum difference of 6 cm across all conditionals and copulas.

3.3.4 Structural failure

A structural scenario is presented to consider flood severity along the Pacific Coast Highway (PCH) in Sunset Beach. PCH road elevation ranges from 1.7-2.4 m NAVD88 (Fig. 3.10), below typical spring tide (∼2.13 m) and more extreme (∼2.3 m) water levels (NOAA, Accessed 2019a), requiring tide valves along PCH for flood prevention. Tide valve closures prevent back-flooding from high bay water levels coming up through subsurface storm drains that (normally) discharge to the bay. Additionally, closed tide valves enable precipitation pooling since water cannot be drained to the bay. Severe pooling may result in a critical highway closure, which can further damage property and inhibit emergency service operations.

Table 3.6: San Diego 10-year marginal (M), conditional (C), and bivariate OWL (m) and precipitation ($mmday^{-1}$) values using the BB1 with annual maximum (AM), annual coinciding (AC), wet season monthly maximum (WMM), and wet season monthly coinciding (WMC) samplings. Conditionals are conditioned on a 25-year event occurring.

	AM		AC		WMM		WMC	
	OWL	Precip	OWL	Precip	OWL	Precip	OWL	Precip
M	2.22	33.38	1.83	33.76	2.20	33.61	2.11	33.64
C1	2.24	35.20	1.86	35.03	2.21	34.39	2.16	35.41
C2	2.22	33.31	1.83	33.70	2.20	33.60	2.11	33.62
C3	2.23	34.50	1.86	34.99	2.21	34.31	2.15	35.37
AND	2.14	26.13	1.66	26.79	2.09	20.89	1.84	21.65
OR	2.25	37.03	1.91	37.71	2.22	38.48	2.20	37.06
K	2.24	36.02	1.89	36.44	2.18	32.10	2.05	32.52
SK	2.25	38.45	1.94	38.70	2.21	35.06	2.15	35.04

Areal precipitation flooding extent and depth can be estimated for water levels exceeding tide valve closure elevation. A water level equal to or greater than 1.68 m NAVD88 forces valve closures and frames the structural failure as a Conditional 1 type event. The local watershed is convex and drains an area of 94,897 m^2. Water pools in the low elevation areas along PCH (Fig. 3.10). When pluvial water levels exceed the sea wall elevation, water overflows the sea wall and exits to the harbor. The maximum pool storage is 11,342 m^3. The percent of flooding is then calculated with Eq. (3.1) as the structural function.

Structural scenario precipitation and percent flooding (Ψ) values utilizing the Nelsen, Roch-Alegre, and BB1 copulas are shown in Table 3.8. Rows and columns separate the utilized sampling methods and return periods of interest, respectively. Fig. 3.11 shows Ψ as a function of precipitation for the Nelsen, Roch-Alegre, and BB1 copulas along with the 5- (square), 10- (circle), and 100-year (diamond) return periods. All copulas display similar

Table 3.7: San Diego 100-year marginal (M), conditional (C), and bivariate OWL (m) and precipitation ($mmday^{-1}$) values using the BB1 with annual maximum (AM), annual coinciding (AC), wet season monthly maximum (WMM), and wet season monthly coinciding (WMC) samplings. Conditionals are conditioned on a 25-year event occurring.

	AM		AC		WMM		WMC	
	OWL	Precip	OWL	Precip	OWL	Precip	OWL	Precip
M	2.27	45.07	2.08	45.65	2.26	43.32	2.40	43.34
C1	2.27	48.54	2.10	46.76	2.27	43.98	2.44	44.48
C2	2.27	44.90	2.08	45.60	2.26	43.30	2.40	43.34
C3	2.27	46.35	2.10	46.69	2.27	43.79	2.44	44.42
AND	2.23	34.01	1.85	34.39	2.17	29.29	2.02	29.93
OR	2.27	48.15	2.14	48.83	2.27	45.52	2.47	45.53
K	2.26	42.81	2.02	42.45	2.22	39.68	2.17	40.13
SK	2.27	46.20	2.08	45.65	2.25	40.90	2.32	41.26

values across sampling methods (Fig. 3.11, Table 3.8). For example, the 10-year precipitation with wet season monthly coinciding sampling is 82.49, 81.95, and 81.09 for the Nelsen, Roch-Alegre, and BB1 copulas, respectively. Again, AC sampling severely underestimates precipitation and flooding.

$$\% \; flooding = \frac{precipitation \times area}{volume} \times 100 \tag{3.1}$$

3.4 Discussion

Previous multivariate studies typically use a small, popular group of copulas (e.g., Clayton, Frank, Gumbel, Student t, and Gaussian). Gaussian and Student t copulas were excluded from this study due to their lack of a computationally simple derivative or integral while

the Clayton, Frank, and Gumbel failed to pass the Cramér-von Mises test. Nelsen, BB1, BB5, and Roch-Alegre copulas generally present similar values with the BB5 occasionally presenting more conservative pairs (Fig. 3.6). Well fit copulas concentrate probabilities around more centralized OWL and precipitation values for multivariate events. This is most pronounced at higher (i.e., 100-year) return periods (Fig. 3.6). Given that the resulting copulas exhibit agreement between values (for a given sampling) suggests that choosing a reasonable copula may be sufficient to provide a robust characterization of considered multivariate flooding events.

The choice in sampling imparts a significant influence on event risk interpretation. When maximum versus coinciding sampling is considered, maximum samplings (AM and WMM) tend to provide the largest OWL at low return periods (Fig. 3.7a, c, e, Fig. 3.8, and Table 3.6). At larger return periods, wet season monthly coinciding then provides significantly larger OWLs (Fig. 3.7a, c, e, Fig. 3.9, and Table 3.7). This is observed in the conditionals and bivariates (minus the AND and K hazard scenarios which maximum samplings display the largest OWLs) at all sites. From a logical perspective, coinciding sampling provides a more realistic view of multivariate events (by definition these are pairs that have co-occurred to produce a multivariate flooding event). At long return periods annual coinciding sampling may require a long data record, which is often unavailable. Notably, in this study annual coinciding produced OWL samplings that were substantially lower than any of the other samplings. For example when comparing 100-year OWLs with annual and wet season monthly coinciding samplings, the marginal was 32 cm lower and the AND scenario was 17 cm lower (Table 3.7). Given that sea wall protected urban coastal areas are highly sensitive to even minor elevations differences (e.g., Gallien et al., 2011), this suggests with limited data records annual coinciding sampling should be avoided.

An important note is each probability type appropriately describes a unique event, characterized by OWL and precipitation. Serinaldi (2015) suggests inter-comparing univariate, multivariate, and conditional probabilities and return periods is misleading as each proba-

bility type describes its associated event. Events where only extreme OWL or precipitation is of concern, should simply utilize marginal statistics and follow current FEMA guidelines. Multivariate event analysis may utilize a variety of scenarios. Conditional type distributions become useful when future information on one variable is known (ex., predicted OWL levels). AND scenarios may be applied when both variables exceeding given limits is of concern. The Survival Kendall scenario is an alternative to the AND scenario using a more conservative approach to develop events of concern (Salvadori et al., 2013). An OR scenario should be applied when either multivariate variable exceeding a limit is of concern, whereas the Kendall scenario provides minimum OR events of concern (Salvadori et al., 2011). The benefit of the Kendall and Survival Kendall is all the events along their isolines describe a similar probability space versus the AND and OR isolines describe events with similar probabilities of non-exceedance. It is critical for practitioners and future studies to define concerning flood events within a region since the associated probability will result in varying event risk estimates as seen within this work. The selected probability type will have significant influence on flood risk studies and modeling efforts. A majority of previous studies focus on specific probability types and do not consider multiple flooding pathways. Only a single study explores all the probabilities associated to different extreme events (Serinaldi, 2016).

From a regulatory perspective, FEMA recommends individual (univariate) analysis to develop return periods for multivariate coastal flooding applications (FEMA, 2011, 2016c, 2020), and blending the two hazard mapping results. Fundamentally, this type of approach assumes (event) independence and may underestimate multivariate flood hazards (e.g., Moftakhari et al., 2019; Muñoz et al., 2020). FEMA provides guidelines for coastal-riverine (FEMA, 2020), tide, surge, tide-surge (FEMA, 2016a), surge-riverine (FEMA, 2016c), and tropical storm (or hurricane) type flooding events (FEMA, 2016b). Currently, FEMA does not provide specific guidance for considering high marine water levels and precipitation. However, this work suggests, at high return periods the sampling method is critical to char-

acterizing both univariate and joint probabilities.

Structural scenarios provide a quantitative context to frame flood vulnerability. In the structural failure context, annual coinciding sampling significantly underestimates flooding at all return periods, and annual maximum sampling underestimates severe (i.e., 100-year) events, echoing previous annual maximum and coinciding sampling issues. Similar values between most copulas support the suggestion that choosing a reasonable copula will provide robust results in these types of applications. Precipitation events in the Structural scenario (Table 3.8) range between 33.30 mmday^{-1} and 131.44 mmday^{-1}, resulting between 27.86 % and complete (100 %) backshore flooding. This significant flooding at all return periods suggests severe flood vulnerability, which is validated by frequent closures of PCH. This structural function provides a quick and simple alternative to poorly performing bathtub flood models (e.g., Bernatchez et al., 2011; Gallien et al., 2011, 2014; Gallien, 2016) to quantitatively explore flood severity while accounting for infrastructure and joint probabilities.

The maximum OWL and precipitation observations within the record are 2.33 m and 118.93 mmday^{-1} for Sunset, 2.27 m and 42.11 mmday^{-1} for San Diego, and 2.45 m and 76.83 mmday^{-1} for Santa Monica. Most likely precipitation and OWL pairs in high return periods often exceed the current data record's maximums (e.g. Table 3.7). This study is limited to the available data records and sea level rise clearly imparts a non-stationary trend. Current water level values restricted to today's distribution tails, will become more frequent in the next century (Taherkhani et al., 2020). For example, Wahl et al. (2015) suggests a previously 100-year event in New York is now a 42-year event based on the increasing correlation between extreme precipitation and storm surge events. Similarly, our results suggest increasing precipitation and, particularly, OWL levels.

3.5 Conclusions

Univariate and multivariate event risks from OWL and/or precipitation were explored at three sites in a tidally dominated, semi-arid region. Seventeen copulas were considered. Previous studies typically relied upon a small number of copulas (e.g. Clayton, Frank, Gumbel, Student t, and Gaussian) for multivariate flood assessments. In this case, the Nelsen, BB1, BB5, and Roch-Alegre copulas passed the Cramér-von Misses test and produced similar, quality fits across all sampling methods. Although, in some cases, the BB5 produced conservative results. Copulas exhibit similar most probable pairs (e.g., Fig. 3.5, 3.6) suggesting a number of potential copulas may provide a robust multivariate analysis. The impact of sampling and distribution choice on uni- and multivariate return period values are presented, however uncertainties deserve further characterization. This work focused solely on exploring conditional and joint probabilities of OWL and precipitation in a tidally and wave dominated semi-arid region and would not be applicable to regions experiencing multiple flooding seasons (e.g., Couasnon et al., 2022). Although wave impacts were not included in this assessment, they are fundamental to coastal flooding, particularly in regions subjected to long period swell. Joint probability methods explicitly including wave contributions to multivariate event risk characterizations are needed for future work.

The annual maximum method is widely recognized for hazard assessments (FEMA, 2011, 2016c), and is common practice in flood risk analysis (e.g., Baratti et al., 2012; Bezak et al., 2014; Wahl et al., 2015). Concerningly, this work suggests that annual maximum sampling does not characterize severe flooding potential for extreme events. Water levels are substantially underestimated as annual sampling neglects a large portion of observations (Table 3.7). Generally, maximum samplings produced larger values at minor return periods but significantly underestimated water levels at longer return periods than wet season monthly coinciding sampling. Similarly, annual coinciding type sampling (Tables 3.6, 3.7) grossly underestimate OWLs. Wet season sampling quadruples data pairs (Table 3.1), providing

additional historical joint event information. Further investigation into monthly coinciding and, where appropriate, water year coinciding are needed to develop optimal sampling strategies for given regional conditions.

3.6 Data Availability

NOAA precipitation data is available for download at `https://www.ncei.noaa.gov/metadata/geoportal/rest/metadata/item/gov.noaa.ncdc:C00313/html\#`. Tidal data is available for download on NOAA's Tides & Currents wetbsite (`https://tidesandcurrents.noaa.gov`).

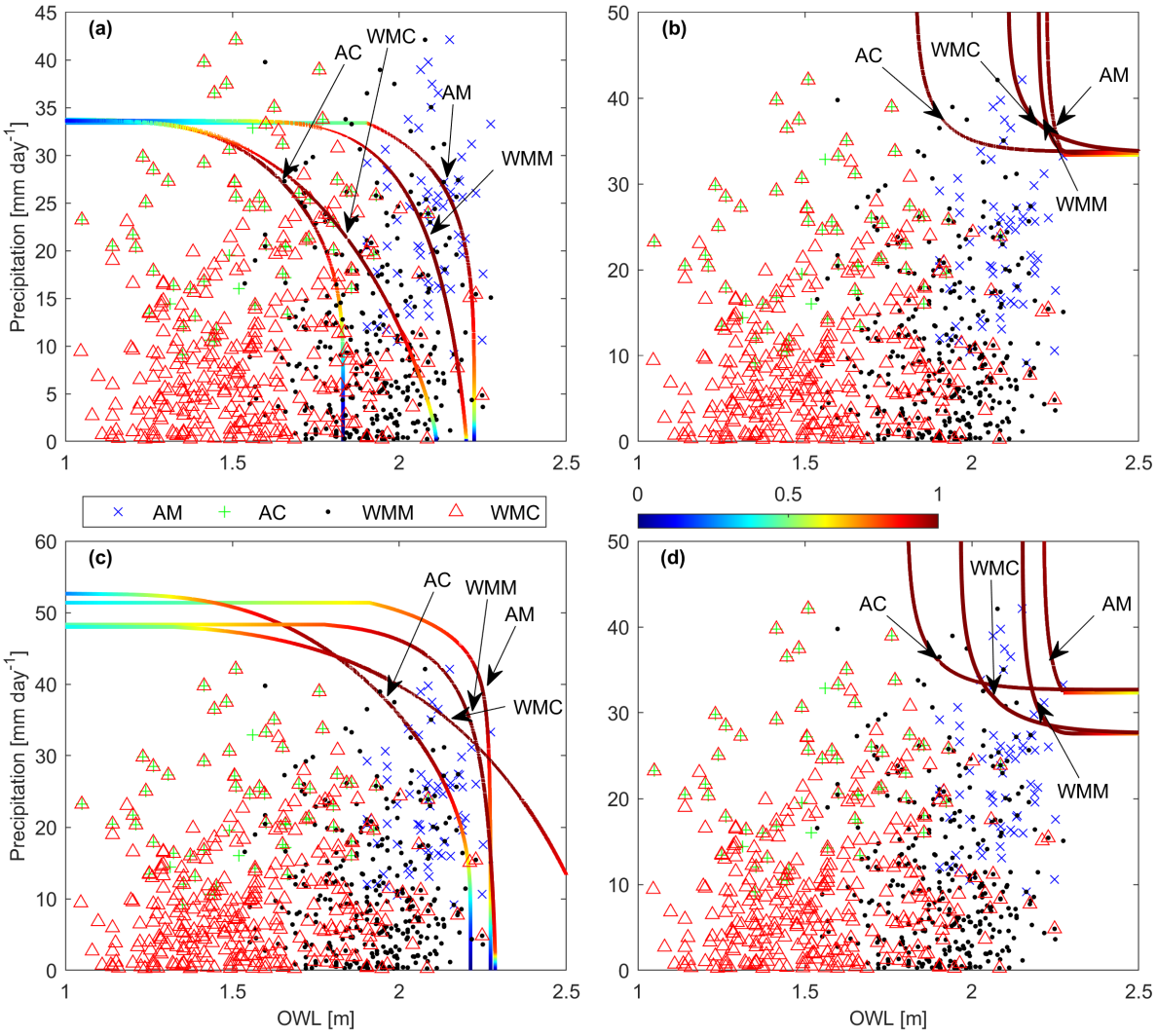

Figure 3.8: San Diego (a) AND, (b) OR, (c) SK, and (d) K hazard scenarios for annual maximum (AM, cross), annual coinciding (AC, plus), wet season monthly maximum (WMM, dot), wet season monthly coinciding (WMC, triangle) data and 10-year isolines using the BB1 copula. Sampling labels point to the mostly likely value on their respective isolines.

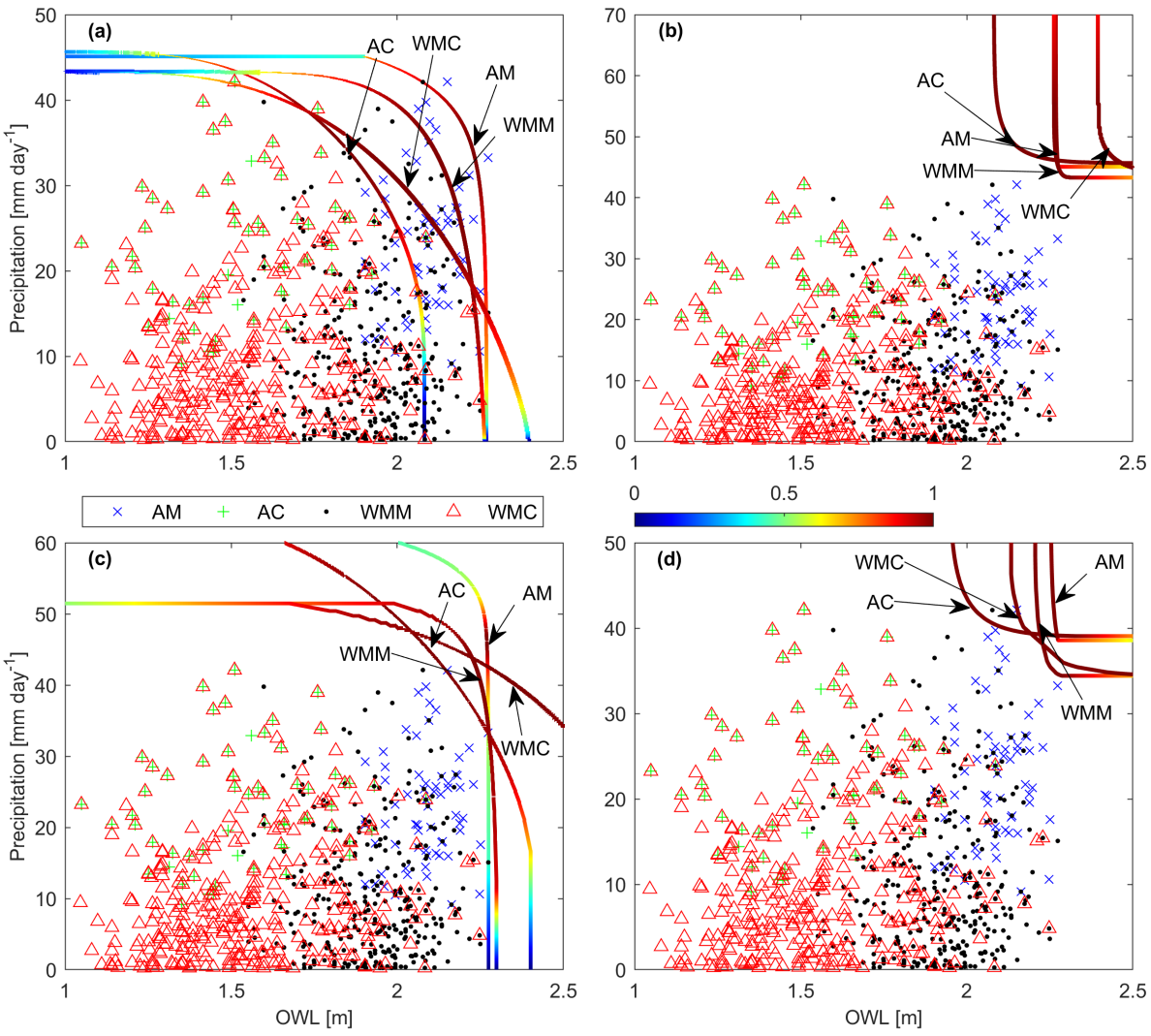

Figure 3.9: San Diego (a) AND, (b) OR, (c) SK, and (d) K hazard scenarios for annual maximum (AM, cross), annual coinciding (AC, plus), wet season monthly maximum (WMM, dot), wet season monthly coinciding (WMC, triangle) data and 100-year isolines using the BB1 copula. Sampling labels point to the mostly likely value on their respective isolines.

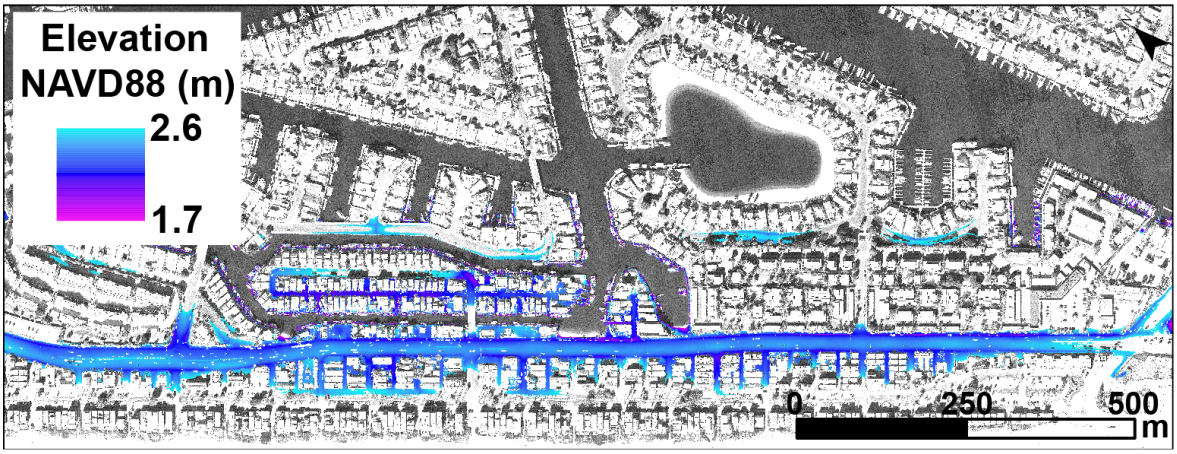

Figure 3.10: Elevations within the Pacific Coast Highway boundary ranging from low (purple) to high (blue). Background imagery from NOAA (Accessed 2020).

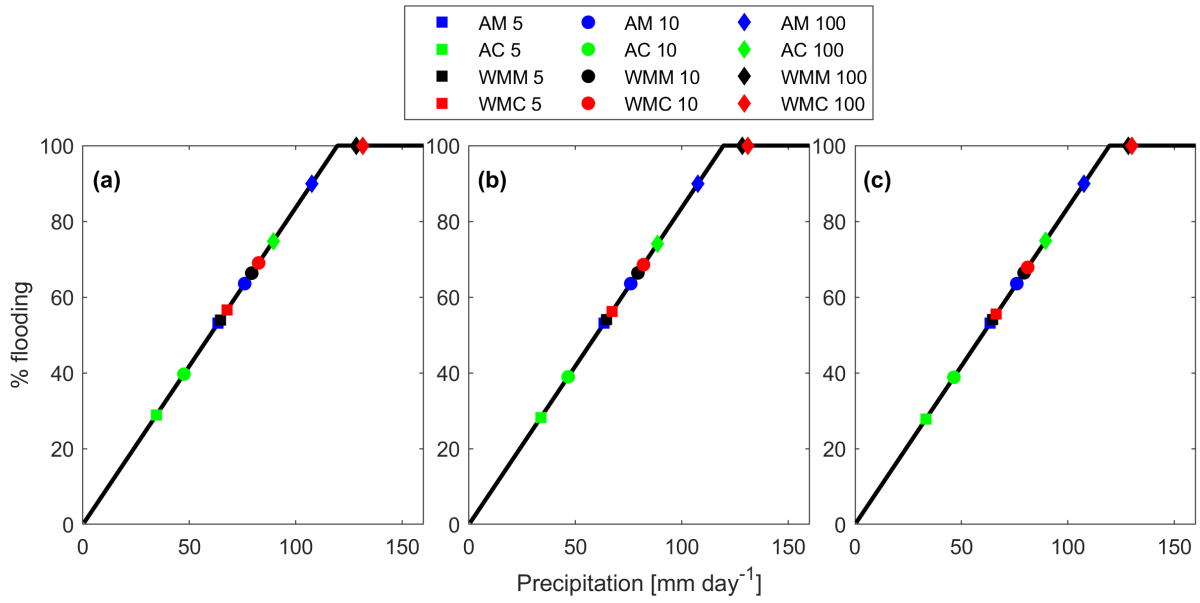

Figure 3.11: Structural scenario 5- (square), 10- (circle), and 100-year (diamond) return periods for annual maximum (AM, blue), annual coinciding (AC, green), wet season monthly maximum (WMM, black), and wet season monthly (WMC, red) data using the (a) Nelsen, (b) Roch-Alegre, and (c) BB1 copulas.

Table 3.8: Precipitation and percent flooding (Ψ) associated to the 5-, 10-, and 100-year return periods (T) using the Nelsen, Roch-Alegre, and BB1 copulas to determine C1 values with annual maximum (AM), annual coinciding (AC), wet season monthly maximum (WMM), and wet season monthly coinciding (WMC) samplings. Precipitation values are in mmday^{-1} and Ψ is a percentage. Values are based off a OWL of ≥ 1.68 m which forces tide valve closure.

T	5-yr.		10-yr.		100-yr.	
	Precip	Ψ	Precip	Ψ	Precip	Ψ
			Nelsen			
AM	63.51	53.14	75.97	63.56	107.44	89.89
AC	34.45	28.82	47.41	39.66	89.39	74.79
WMM	64.51	53.97	79.27	66.32	128.26	100.00
WMC	67.71	56.65	82.49	69.02	131.44	100.00
			Roch-Alegre			
AM	63.51	53.14	75.97	63.56	107.44	89.89
AC	33.70	28.19	46.57	38.97	88.50	74.05
WMM	64.57	54.02	79.34	66.38	128.44	100.00
WMC	67.17	56.20	81.95	68.56	130.92	100.00
			BB1			
AM	63.51	53.14	75.97	63.56	107.44	89.89
AC	33.30	27.86	46.41	38.83	89.44	74.83
WMM	64.60	54.05	79.38	66.42	128.44	100.00
WMC	66.34	55.50	81.09	67.84	130.03	100.00

CHAPTER 4

Quantifying compound flood event uncertainty from wave induced flooding

4.1 Background

Traditionally, compound flooding literature has focused on the combined impacts of river discharge and storm surge events (Table 1 in Lucey and Gallien (2022)). Modeling approaches rarely include wave driven impacts (e.g., Barnard et al., 2019; Johnson, 2019). Similarly, few multivariate copula based studies explicitly consider wave impacts (Table 1.1). Masina et al. (2015) quantified flood risks from wave and water levels and highlighted the critical the importance of considering wave impacts for realistic flood estimates. Wahl et al. (2012) explored compound flood risks caused by storm surge and incident waves and showed flood risks were underestimated when excluding waves. Along the U.S. West Coast wave runup accounts for nearly half of maximum total water levels (Serafin et al., 2017), and Reguero et al. (2019) suggest wave impacts will be amplified in a changing climate. Quantifying multivariate events explicitly accounting for wave impacts is critical to characterizing coastal flooding (e.g., Erikson et al., 2018; Gallien et al., 2018; Barnard et al., 2019).

This study explores wave driven compound coastal flood risk and uncertainties associated with copula choice, sampling methods, utilized rainfall gauge, and record length for various hazard scenarios. Events caused (independently or in combination) by waves, tides, and precipitation are considered since both waves and tides dominate total water level signals along the California Coast (Erikson et al., 2018), and only limited studies account for these

flood pathways (Hawkes, 2008).

4.2 Site description & data

This study focuses on two Southern California beaches, with over 70-years of tide, wave, and precipitation records, to explore uncertainties associated to copula and sampling choice: Sunset Beach in Huntington Beach, California and La Jolla in San Diego, California. San Francisco is used to explore uncertainties associated to data length since its local tide and precipitation records have 100-years of overlap. These locations are densely populated, highly urbanized, and extensively managed to prevent flooding events which would have severe economic, recreational and societal impacts. A single, local precipitation gauge is used to represent the local meteorology for both San Francisco and La Jolla. For Sunset Beach two precipitation stations, Torrance and Long Beach Airports at 9.4 m and at 26.6 m NAVD88, were used to explore uncertainties related to the utilized rainfall gauge. The Torrance and Long Beach precipitation gauges are approximately 11 km and 15.5 km from the LA tide gauge, respectively, and the gauges themselves are approximately 18 km apart. Therefore four sites are explored (Figure 4.1): San Francisco (SF), Torrance (T), Long Beach (LB), and San Diego (SD).

Verified hourly observed water levels (OWLs, m NAVD88) at the San Francisco (Station ID: 9414290), Los Angeles (Station ID: 9410660), and La Jolla (Station ID: 9410230) were downloaded from NOAA's Tides and Currents website (NOAA, Accessed 2022b). Months with no OWL measurements were excluded. Daily precipitation summaries (P, mmday^{-1}) at the Downtown San Francisco (USW00023272), Torrance Airport (USW00003122), Long Beach Airport (USW00023129), and San Diego (USW00093107) stations were downloaded from NOAA's Global Historical Climatology Network daily dataset (NOAA, Accessed 2021a). Daily precipitation observations that were flagged by NOAA (NOAA, Accessed 2021a), were manually verified and removed if necessary before being included in the study. All data are

in UTC time. Table 4.1 presents the overlapping observation periods between OWL and P at each site.

Two sources of wave data are used in this study: the Global Ocean Wave (GOW) reanalysis (Reguero et al., 2012; Shope et al., 2021) and Coastal Data Information Program (CDIP) wave observations (Scripps, Accessed 2021). Both datasets are provided at 100 m alongshore intervals at Scripps Monitoring and Prediction (MOP) lines. MOP Lines 669-678, and 598-618 were used for San Diego and Los Angeles, respectively. CDIP wave buoys along the Southern California Coast have minimal wave records (<30-years). Combining the GOW and CDIP wave records significantly increases data availability resulting in an additional 54- and 51-years at San Diego and Los Angeles, respectively. GOW hindcast data is available in hourly intervals with observations from February 01, 1948 to December 31, 2008, while CDIP wave data is in 30 minutes intervals (i.e., two measurements made per hour). CDIP data is coarsened to one observation per hour to match GOW data; the largest CDIP wave height observation is selected for each hour. The full GOW data record is combined with the CDIP wave buoy data after December 31, 2008 to create each sites' wave record. Total water levels (TWL), the sum of observed water level and wave runup,

$$TWL = OWL + R_{2\%} \tag{4.1}$$

were then calculated using $R_{2\%}$ (Stockdon et al., 2006), which represents the highest two percent of wave runup elevations expected for a given wave height (H_s), wave period (T_p), and beach slope (β). Representative foreshore beach slopes of 0.125 for Los Angeles (Vos et al., 2020) and 0.055 for San Diego (Ludka et al., 2018) were used. $R_{2\%}$ is given by

$$R_{2\%} = 1.1(0.35\beta(H_s L_0)^{0.5} + (\frac{[H_s L_0(0.563\beta^2 + 0.004)]^{0.5}}{2})) \tag{4.2}$$

where the deep water wave length (L_0) is

$$L_0 = (T_p^2 g)/(2\pi). \tag{4.3}$$

Only the largest wave runup value across all the mop lines per hour were used in the final wave dataset for each site. Table 4.2 presents the overlapping observation periods between TWL and P at each site.

Various sampling methods are used to characterize multivariate flood events: annual maximum (AM), annual coinciding (AC), wet season monthly maximum (WMM), and wet season monthly coinciding (WMC). Maximum sampling pairs the largest observations within a given time frame (e.g., year) and may result in pairs that did not historically occur (e.g., a maximum August OWL paired with a maximum precipitation observation from December). However, this paring strategy has been used in multiple studies (e.g., Bezak et al., 2014; Wahl et al., 2015; Lucey and Gallien, 2022), and has been recommended for coastal hazard assessment (FEMA, 2016c). In the case of WMM sampling, months with missing data were reviewed and removed if the tidal peak was absent. Coinciding sampling is commonly used to characterize compound events (Sadegh et al., 2018; Ganguli and Merz, 2019a; Lucey and Gallien, 2022). This sampling strategy selects the largest primary observation (precipitation) within a given time frame (e.g., month, year) and pairs it with the largest secondary observation (OWL or TWL) occurring on that same day. For example, the largest precipitation event recorded within a year will be paired with the largest OWL or TWL measurement that occurred on the day of the precipitation event. Coinciding sampling pairs with three or more OWL measurements missing within the 24-hour accumulated precipitation window were manually reviewed and removed if the tidal peak was not recorded. Southern California's wet season occurs between October to March and provides a majority of the total annual rainfall (Cayan and Roads, 1984; Conil and Hall, 2006; Guirguis and Avissar, 2008). Therefore, wet season monthly samplings only utilize observations from October to March. Figure 4.2 displays the resulting data pairs. Tables 4.1 and 4.2 provide a summary of each sites' associated gauges, observation windows, and number of pairs for OWL-P (Table 4.1)

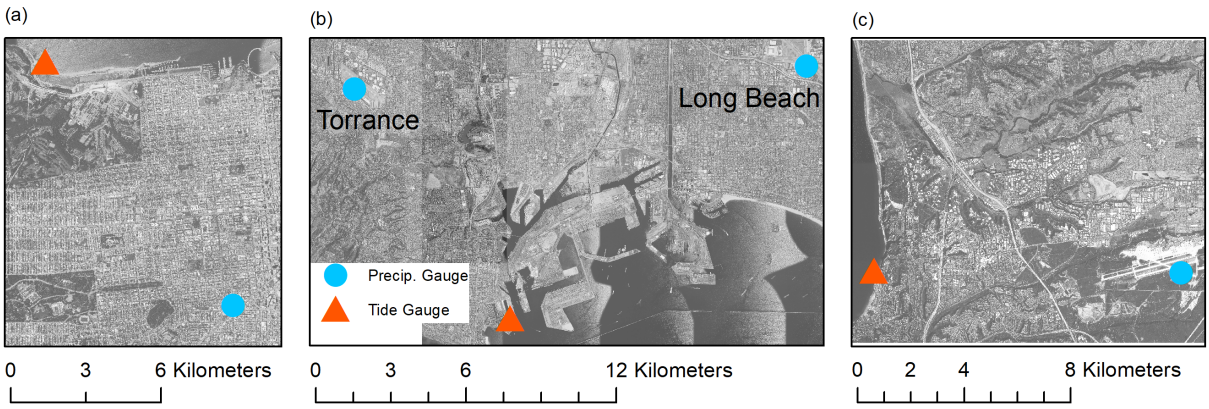

Figure 4.1: Map displaying (a) San Francisco, (b) Long Beach, Torrance, and (c) San Diego sites along with locations of tide gauges (triangle) and precipitation stations (circle). Wave gauges are not displayed because they are deep water wave gauges (far from shore). Aerial imagery from NOAA (Accessed 2022a).

and TWL-P (Table 4.2) events.

4.3 Bootstrapping Method

San Francisco is used to explore uncertainties associated to record length given the extensive observed water level and precipitation records (100-years). Bootstrapping techniques have commonly been used to explore various sources of uncertainty (Genest et al., 2009; Serinaldi, 2013; Tong et al., 2015; Dodangeh et al., 2019) and are utilized to quantify record length uncertainties. The 10- and 100-year observed water levels and precipitation values were estimated with the full 100-year record and various subsets. Ten subsets of 90-, 80-, 70-, 50-, 30-, and 20-years of data were created from the original San Francisco precipitation and tide records for univariate, conditional, and bivariate scenarios using all sampling methods (annual maximum, annual coinciding, wet season monthly maximum, and wet season monthly coinciding). Table 7.2 in the Appendix displays the periods used for each subset. The vari-

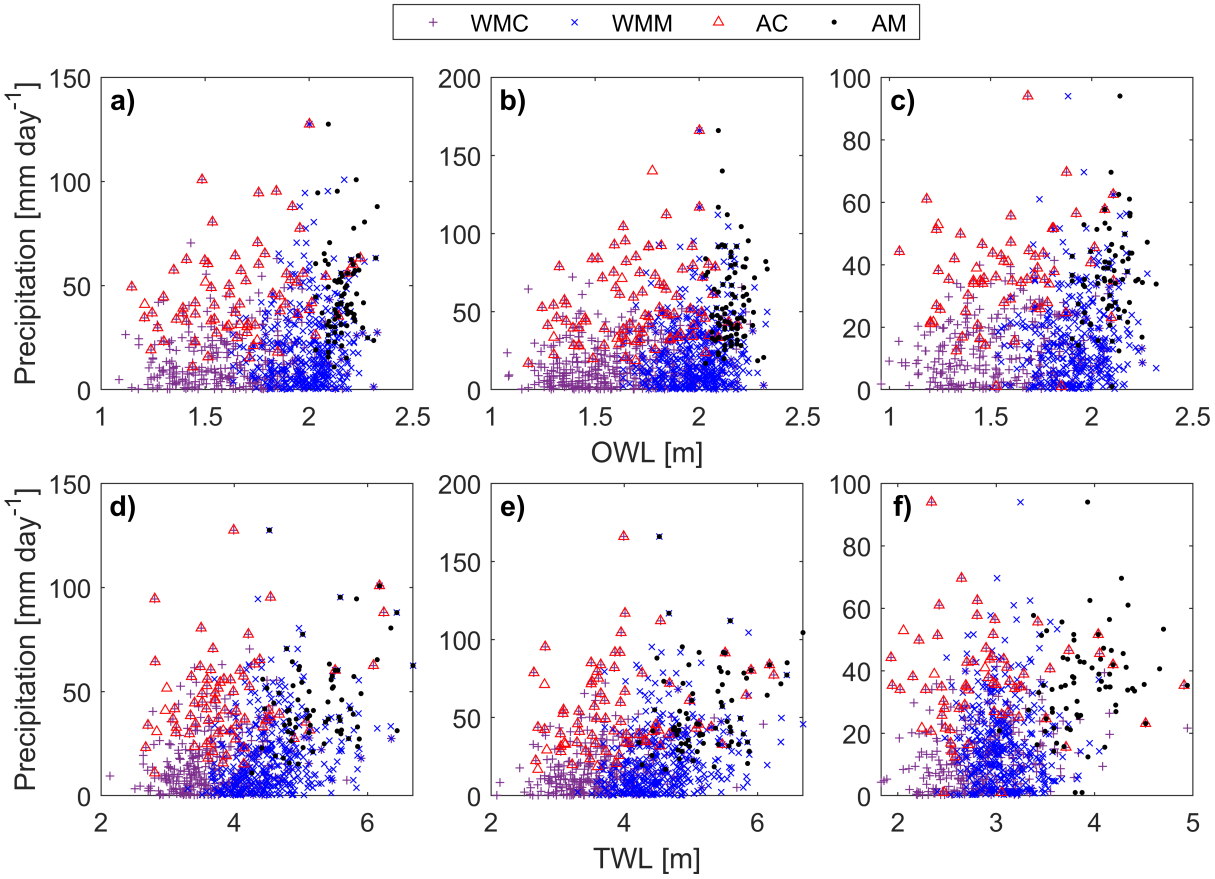

Figure 4.2: Data pairs using annual maximum (AM; dot), annual coinciding (AC; triangle), wet season monthly maximum (WMM; cross), and wet season monthly coinciding (WMC; plus) sampling for (a)(b)(c) OWL-P, (d)(e)(f) TWL-P pairs at (a)(d) Long Beach, (b)(e) Torrance, and (c)(f) San Diego

Table 4.1: Water level and precipitation (P) observations for San Francisco (SF), Torrance (T), Long Beach (LB), and San Diego (SD) using annual maximum (AM), annual coinciding (AC), wet season monthly maximum (WMM), and wet season monthly coinciding (WMC) samplings. The presented SF pairs are when using the full 100-year record.

Site	Tide Gauge	P Gauge	Observation Window	AM Pairs	AC Pairs	WMM Pairs	WMC Pairs
SF	9414290	023272	January 1, 1921 to July 31, 2021	100	100	583	581
T	9410660	003122	January 1, 1932 to July 31, 2021	90	89	469	467
LB	9410660	023129	January 1, 1943 to July 31, 2021	73	73	381	380
SD	9410230	093107	July 1, 1947 to June 30, 2021	71	65	360	356

Table 4.2: Total water level and precipitation information for Torrance (T), Long Beach (LB), and San Diego (SD) using annual maximum (AM), annual coinciding (AC), wet season monthly maximum (WMM), and wet season monthly coinciding (WMC) samplings. The observation windows provided are the combined record of two wave datasets.

Site	Wave Gauge	Observation Window	AM Pairs	AC Pairs	WMM Pairs	WMC Pairs
T	092	February 1, 1948 to July 26, 2021	74	73	378	377
LB	092	February 1, 1948 to July 26, 2021	73	73	381	380
SD	100	February 1, 1948 to June 30, 2021	71	65	366	355

ability and behaviors of estimates associated to sampling size can be visualized with boxplots and further compared to the estimates from the full record. A Nelsen copula is used for all bivariate and conditional estimates, as it frequently passed the Cramér-von Mises test. It should be noted that the best fitting marginal distribution changed depending on the period and sample size and will therefore have some influence on estimates.

4.4 Results

A majority of correlations (67%) were positive and significant at the Torrance, Long Beach, and San Diego sites for OWL-P and TWL-P pairs using all sampling methods. Correlations which were not significant at standard levels ($p > 0.05$) are noted: Long Beach with annual maximum sampling for OWL-P, and annual coinciding sampling for TWL-P. Torrance with annual maximum and coinciding sampling for OWL-P and San Diego with annual maximum and coinciding sampling for OWL-P along with annual coinciding and wet season monthly maximum for TWL-P. The associated marginals generally passed the Chi-squared test at standard levels. Table 7.1 in the Appendix presents the marginal fits and those with below standard significance levels are noted: Long Beach OWL using wet season monthly coinciding sampling for OWL-P pairs, Torrance OWL and P when using wet season monthly maximum and coinciding sampling for OWL-P pairs and annual maximum and coinciding sampling for TWL-P pairs, and San Diego OWL using wet season monthly coinciding for OWL-P pairs.

4.4.1 Copula choice

Uncertainties induced by copula selection were explored at all locations (excluding San Francisco), but the San Diego site annual maximum sampling for TWL-P pairs best illustrates the results in this subsection. In this example, the Clayton, AMH, FGM, Nelsen, Roch-Alegre (Roch.), Fischer-Kock (Fisc.), BB1, and BB5 copulas passed the Cramér-von Mises test. When observing the conditional CDFs (Figure 4.3), there is a general agreement between

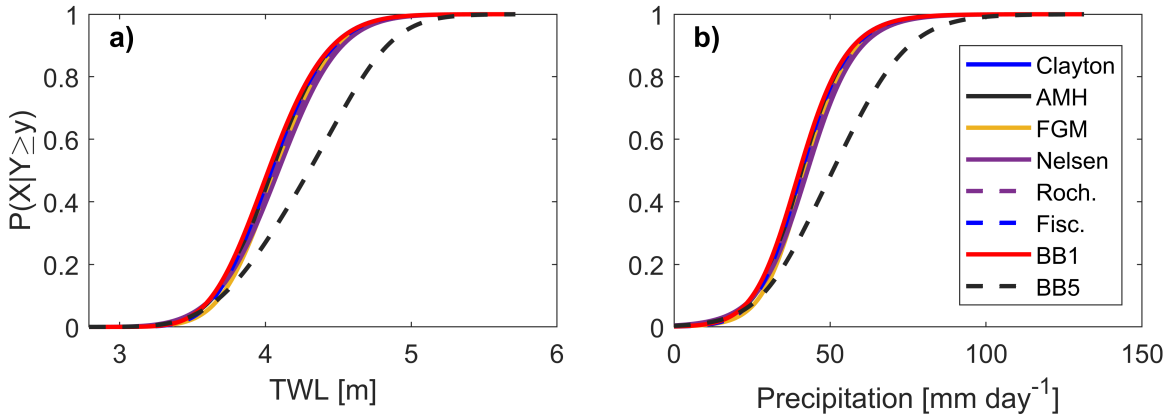

Figure 4.3: Conditional 1 CDFs at San Diego using annual maximum sampling for (a) TWL and (b) P fitted with Clayton, AMH, FGM, Nelsen, Roch-Alegre (Roch.), Fischer-Kock (Fisc.), BB1, and BB5 copulas. The primary variable is conditioned on the secondary variable at a 25-year return period.

the copulas' estimates except BB5 estimates are more conservative. For example, the 10- and 100-year TWL estimates (from the copulas except the BB5) have a range of 8 cm (4.11 m to 4.19 m) and 10 cm (5.05 m to 5.15 m), but BB5 10- and 100-year estimates are larger (5.79 m and 7.41 m).

A similar pattern emerges in the bivariate estimates (Figure 4.4). All copula isolines, except the BB5, present strong agreement. BB5 isolines provide the largest 10- and 100-year (Figures 4.4a, 4.4c) AND estimates, but slightly lower 10-and 100-year (Figures 4.4b, 4.4d) OR estimates. For example, the most likely 10-year AND (Figure 4.4a) TWL and P estimates vary by 2 cm (4.11 m - 4.13 m) and 1 mmday^{-1} (43.77 mmday^{-1} to 44.71 mmday^{-1}) and 100-year AND (Figure 4.4c) TWL and P estiamates vary by 3 cm (4.42 m to 4.45 m) and 1 mmday^{-1} (55.71 mmday^{-1} to 57.05 mmday^{-1}). BB5 TWL and P estimates were larger by 2 cm and 1 mmday^{-1} (4.15 m and 45.19 mmday^{-1}) for the 10-year event and 13 cm and 6 mmday^{-1} (4.58 m and 63.05 mmday^{-1}) for the 100-year event.

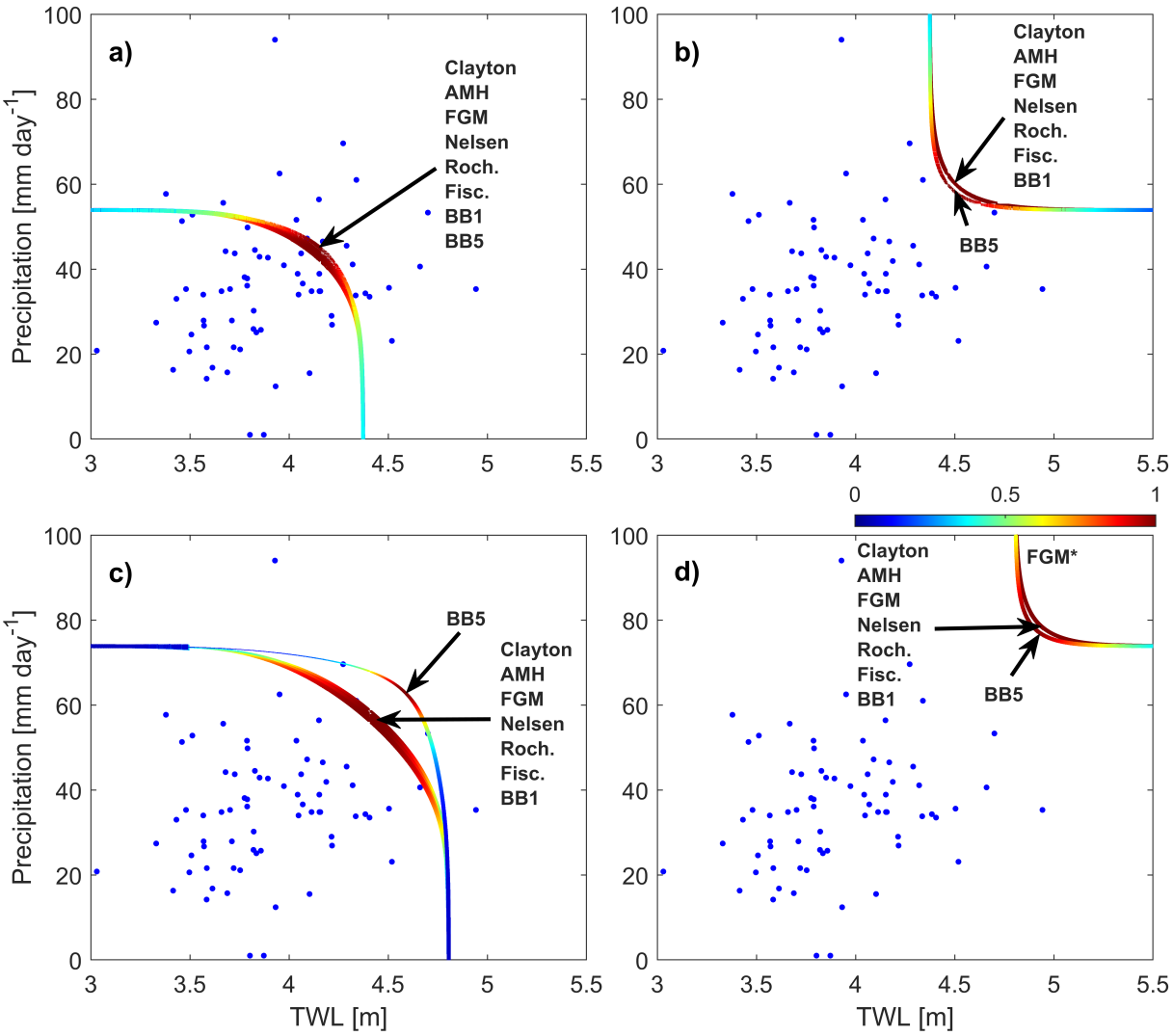

Figure 4.4: (a)(c) AND and (b)(d) OR (a)(b) 10- and (c)(d) 100-year isolines at San Diego using annual maximum sampling for TWL-P pairs fitted with Clayton, AMH, FGM, Nelsen, Roch-Alegre (Roch.), Fischer-Kock (Fisc.), BB1, and BB5 copulas. Arrows point toward the most likely event pair along an isoline generated by the labeled copula. Red and blue locations along an isoline indicate higher and lower probability densities, respectively.

4.4.2 Sampling

The Long Beach site, fitted with a Nelsen copula, was used to best illustrate uncertainties induced by sampling methods. For the univariate case, annual coinciding sampling provides the lowest OWL estimates (Figure 4.5a). The other sampling methods have similar OWL estimates except wet season monthly coinciding sampling provides the largest 100-year OWL estimates (Figure 4.5a). Annual coinciding sampling generally results in the lowest TWL estimates (Figure 4.5c). Maximum samplings (annual and wet season monthly) produce the largest 10-year TWL estimates and wet season monthly maximum provided the largest 100-year TWL estimates (except at San Diego where wet season monthly coinciding sampling provided the largest TWL estimates). OWL and TWL estimates varied depending on sampling method with more variability in TWL estimates than OWL estimates (e.g., 10-year OWL and TWL range between 25 cm of OWL and 1.26 m of TWL; Figure 4.5a, c). Marginal precipitation estimates are generally similar regardless of sampling method, but can diverge at the 100-year return period where annual type samplings exceed those of the wet season monthly samplings (Figure 4.5b, d).

In the conditional case (Figure 4.6), annual coinciding sampling generally result in the lowest OWL (Figure 4.6a) and TWL (Figure 4.6c) values. However, annual coinciding sampling occasionally produced values greater than or similar to other samplings (e.g., 100-year OWL estimates with annual maximum, annual coinciding, and wet season monthly maximum are within a 5 cm range; Figure 4.6a). Wet season monthly coinciding sampling generally provides the largest OWL estimates. Multiple sampling methods provided the largest TWL estimates which varied between locations and the utilized copula. These upper and lower limits result in significant variability for OWL and TWL, and TWL was significantly more variable compared to OWL estimates. For example, there is a 17 cm range between 10-year OWL estimates (Figure 4.6a) and a 1.29 m range between 10-year TWL estimates (Figure 4.6c). Precipitation estimates follow one of two patterns: estimates are grouped as annual samplings and wet season monthly samplings (i.e., similar estimates between annual maxi-

mum and coinciding and between wet season monthly maximum and coinciding samplings; Figure 4.6b), or estimates are similar across sampling choice (e.g., 10-year precipitation estimates have a range of 6 mmday^{-1}; Figure 4.6d).

Across hazard scenarios (Figure 4.7) the annual coinciding sampling method generally results in the smallest OWL and TWL values. There are instances where estimates from an annual coinciding sampling were similar to estimates produced from other samplings (e.g., there is a 5 cm range between 100-year OR OWL values produced by the annual maximum, annual coinciding, and wet season monthly maximum samplings; Figure 4.7f). Estimates from annual maximum and/or wet season monthly maximum sampling resulted in the largest OWL and TWL values except for the 100-year OR scenario where estimates using a wet season monthly coinciding sampling generally generated the largest OWL and TWL values. Similar to the marginal and conditional cases, OWL and TWL estimates vary significantly due to sampling choice. For example, 10-year OWLs had a range of 37 cm (Figure 4.7a) and 10-year TWLs had a range of 1.42 m (Figure 4.7c) in the AND scenario. Precipitation estimates follow the same two behaviors as the conditional cases: estimates are similar between annual samplings and wet season monthly samplings (e.g., Figure 4.7h) or estimates have minimal differences between sampling methods (e.g., 10-year OR precipitation varies by 1 mmday^{-1}; Figure 4.7d). These patterns persist across locations and copulas.

4.4.3 Rainfall gauge choice

Results from using a wet season monthly coinciding sampling and a fitted Nelsen and BB5 copula were used to display uncertainties associated to rainfall gauge choice. Marginal TWL CDFs (Figure 4.8a) show a general agreement, but marginal precipitation estimates differ (Figure 4.8b). Torrance 10- (96 mmday^{-1} versus 77 mmday^{-1}) and 100-year (152 mmday^{-1} versus 115 mmday^{-1}) marginal precipitation estimates were always larger than Long Beach marginal precipitation estimates for all sampling methods including OWL-P results.

Rainfall gauge choice further impacts conditional CDFs (Figure 4.9). Conditional TWL

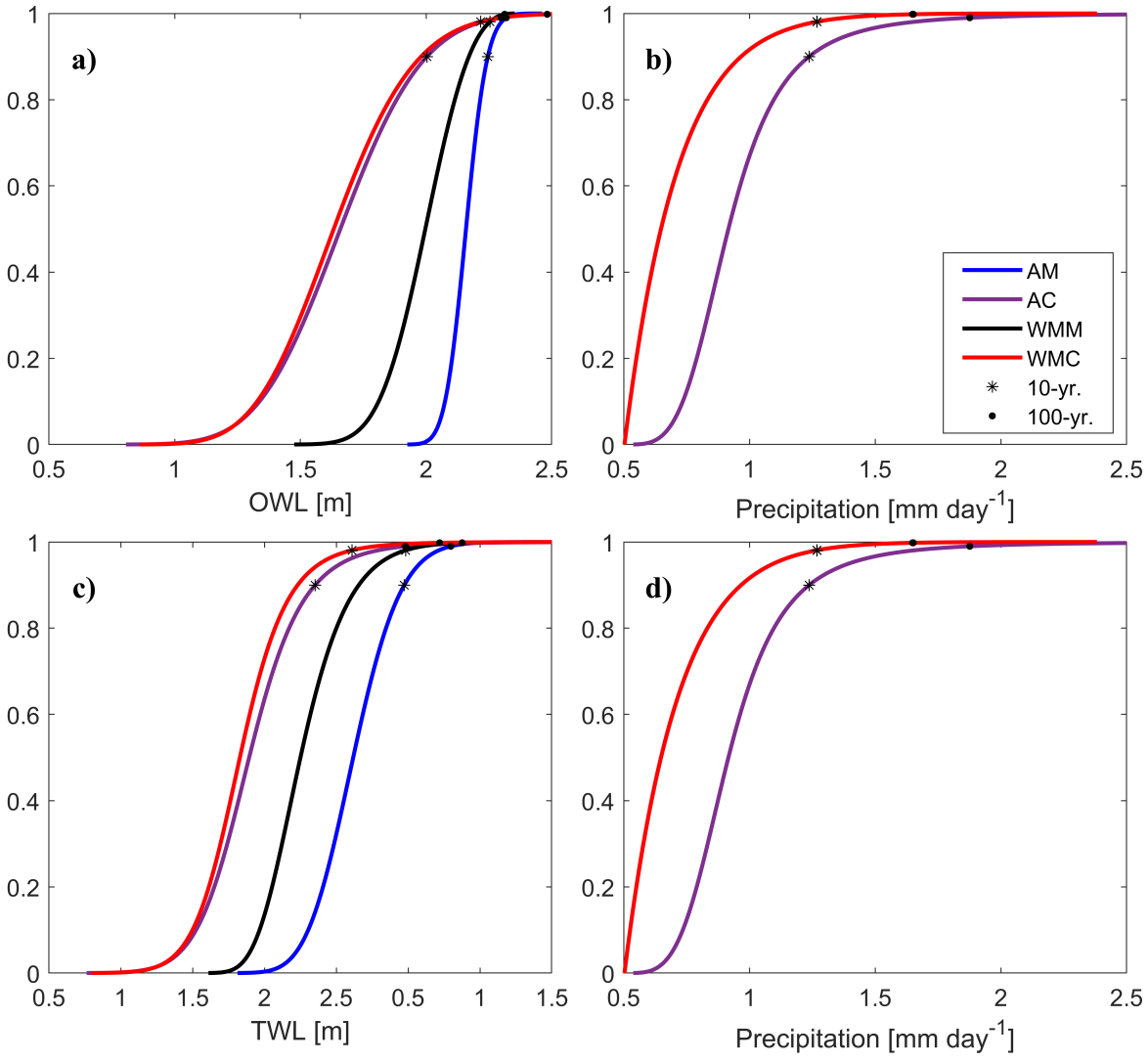

Figure 4.5: Marginal CDFs, with 10- (asterisks) and 100-year (dot) values, at Long Beach using annual maximum (AM), annual coinciding (AC), wet season monthly maximum (WMM), and wet season monthly coinciding (WMC) sampling for (a)OWL-(b)P and (c)TWL-(d)P pairs.

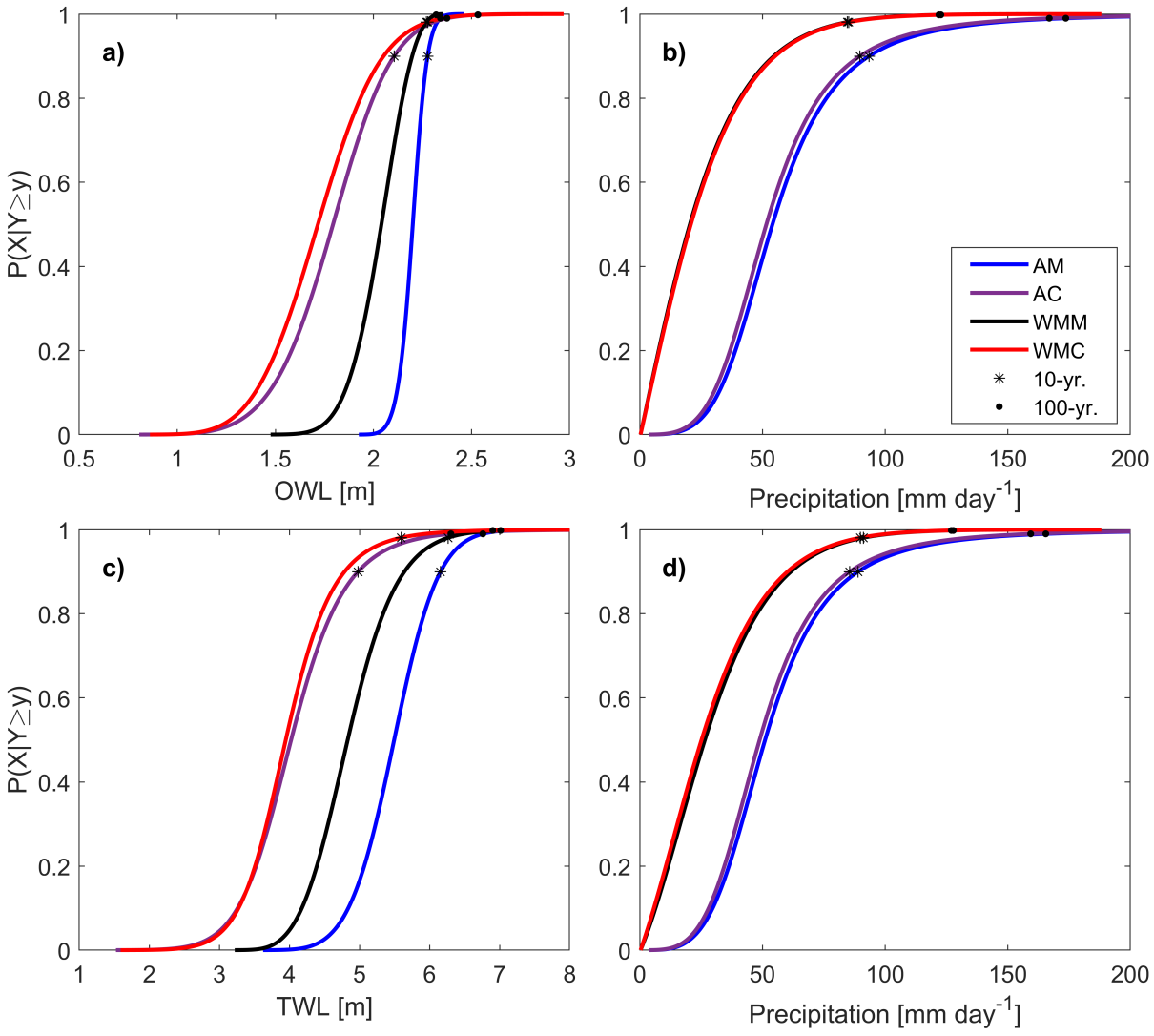

Figure 4.6: Conditional 1 CDFs, with 10- (asterisks) and 100-year (dot) values, at Long Beach using annual maximum (AM), annual coinciding (AC), wet season monthly maximum (WMM), and wet season monthly coinciding (WMC) sampling with a fitted Nelsen copula for (a)OWL-(b)P and (c)TWL-(d)P pairs. The primary variable is conditioned on the secondary variable at a 25-year return period.

estimates vary between Long Beach and Torrance (Figure 4.9a). In this example the 100-year TWL estimate can vary between 6.36 m and 9.73 m (range of 3.37 m) depending on the utilized rainfall gauge. Torrance conditional precipitation estimates generally exceed Long Beach estimates when comparing similar copulas. Figure 4.9b 100-year conditional precipitation estimates vary between 127 $mmday^{-1}$ and 263 $mmday^{-1}$ (range of 136 $mmday^{-1}$) depending on the utilized rainfall gauge and copula. An exception was Long Beach 100-year precipitation estimates were larger or similar to Torrance estimates when using an annual sampling (annual maximum or coinciding).

Bivariate estimates also vary depending on rainfall gauge choice (Figure 4.10). In the AND scenario (Figure 4.10a, c), Torrance and Long Beach TWL estimates were generally similar per copula (e.g., Long Beach and Torrance 100-year TWLs were 5.01 m and 5.10 m using the Nelsen copula). Torrance AND precipitation estimates were always larger than Long Beach. In the OR scenario (Figure 4.10b, d), Torrance precipitation estimates were generally larger than Long Beach. TWL OR estimates typically were larger at Torrance at the 10-year return period (e.g., Torrance and Long Beach TWLs with a BB5 copula were 5.35 m and 5.28 m; Figure4.10b), but Long Beach bivariate estimates were larger at the 100-year return period (e.g., Torrance and Long Beach TWLs with a BB5 copula were 6.16 m and 7.61 m; Figure4.10d). There were cases where Torrance and Long Beach had similar TWL bivariate estimates (e.g., Torrance and Long Beach 100-year TWLs with a Nelsen copula were 5.61 m and 5.56 m; Figure4.10d). Long Beach and Torrance always had similar 10-year bivariate OWLs, but Long Beach had larger 100-year bivariate OWLs. The range between Long Beach and Torrance estimates generally increased at more severe return periods (e.g., there is a 35 cm and 69 cm range for 10- and 100-year AND TWLs; Figure4.10 a, c) for magninal, conditional, and bivariate cases. These behaviors were observed across sampling methods and OWL-P estimates unless noted.

4.4.4 Record length

Figures 4.11 and 4.12 show 10- and 100-year OWL and precipitation estimates from the full record and subsets for the marginal, conditional, and bivariate cases using each sampling method at San Francisco. The variability of the 10- and 100-year OWL and precipitation estimates were the largest within the 20-year subsets (small data record) and the least within the 90-year subsets (ample data record). This variability increases between the 10- to 100-year estimates. For example, the 10- and 100-year OWL has a range of approximately 20 cm and 45 cm, respectively, for the AND scenario using annual maximum sampling with 20-year subsets (Figure 4.11a and 4.12a).

Notably, the variability of the 10- and 100-year OWL and precipitation estimates reduced significantly for marginal, conditional, and bivariate scenarios when utilizing sample sizes greater than or equal to 70-years for all sampling methods (Figures 4.11 and 4.12). Generally when comparing the subset estimates to estimates made from the 100-year record, the medians of the boxplots made from 90-, 80-, and 70-year subsets are similar with the estimates provided by the 100-year record (e.g., Figure 4.11a). However, there is a noticeable difference between the medians from shorter subset lengths and the 100-year record's estimates (e.g., approximately 6 cm difference for the AND scenario using 20-year subsets; Figure 4.11a). Also, the interquartile ranges at shorter subset lengths occasionally do not encompass the estimate calculated using the 100-year record (e.g., 100-year Conditional 1 OWL with 20-year subsets using an annual maximum sampling; Figure 4.12a).

4.5 Discussion

Copula choice, sampling methods, rainfall gauge choice, record length, and the inclusion of waves can impact flood risk estimates. Copulas which pass a Cramér-von Misses test, suggesting a significant fit, display similar estimates with the exception of the BB5 (Figures 4.3, 4.4). This is similar to observations in Lucey and Gallien (2022). From a design or

management perspective, this would require different practices given the different copula estimates at equal return periods and similar sampling methods. For example, if a flood wall must withstand a 10-year OWL exacerbated by at least a 25-year precipitation event (Conditional 1 scenario), the 2.22 m versus 2.60 m estimates provided by the Nelsen and BB5 copulas, when using wet season monthly coinciding sampling, will have different design requirements. This potential under-design (or over-design) of the structure may have significant consequences for urbanized communities. Currently, there is a paucity of studies exploring how various well fitting copulas could impact design scenarios (Lucey and Gallien, 2022).

Sampling choice imparts the largest uncertainties. Annual coinciding sampling generally resulted in the lowest estimates for the marginal (Figure 4.5), conditional (Figure 4.6), and bivariate (Figure 4.7) cases. The annual maximum and wet season monthly (maximum and coinciding) samplings provided the largest estimates depending on the probability scenario (marginal, conditional, AND, OR) and variable in question (OWL, TWL). While it should be expected that different sampling methods will result in different estimates (Engeland et al., 2004; Jarušková and Hanek, 2006; Lucey and Gallien, 2022), quantifying the range of estimates based on various sampling methods is novel. Generally, annual coinciding sampling, on the lower end, and one of the other samplings, on the higher end, envelope the possible range of estimates. This could be beneficial for management and design applications as a method to quantify the uncertainty associated with sampling methods. There is also a limited pool of studies exploring the impacts sampling methods could have on design scenarios (Engeland et al., 2004; Tu et al., 2018; Lucey and Gallien, 2022).

Rainfall gauge choice has the potential to influence flood risk estimates. There is a significant amount of uncertainty associated to univariate (Figure 4.8), conditional (Figure 4.9), and bivariate (Figure 4.10) estimates depending on the utilized rainfall gauge, echoing previous findings on uncertainty associated to model inputs (Coveney and Fotheringham, 2011; Bates et al., 2014; Sampson et al., 2014). Urban microclimates (Pacific Energy Center,

Accessed 2022; World Meteorological Organization, 2008; Barry and Blanken, 2016) are likely driving these differences. Urbanization has been shown to alter precipitation patterns around cities (Han et al., 2014; Pour et al., 2020) which, in turn, influences urban flood developments (Huong and Pathirana, 2013; Pathirana et al., 2014; Pour et al., 2020). Accurate flood risk assessments and studies at coastal urban communities must account for the possible influence of microclimates when selecting a rainfall station. Future work should further explore microclimate and chosen rainfall gauge induced uncertainties and their propagation into flood estimates.

Waves inclusion alters uncertainty. TWL and OWL are fundamentally different variables, accordingly TWL-P and OWL-P results vary. Copula choice behaviors for TWL-P and OWL-P estimates were similar (Figure 4.4), but sampling behaviors differed (Figure 4.7). The largest estimates of TWL-P most frequently resulted from utilizing a maximum type sampling (annual or wet season monthly maximum) versus the wet season monthly coinciding as noted for OWL-P estimates. TWL consistently had much larger variability in its estimates versus OWL estimates. For example when using annual maximum sampling at Long Beach, the 10-year (univariate) OWL and TWL are estimated to be 2.25 m and 5.95 m (Figure 4.5a, c). This is a drastic difference in the estimated 10-year event and should emphasize the importance in accounting for all potential flooding pathways (Gallien et al., 2018), especially waves for Southern California studies (e.g., Erikson et al., 2018).

Data length was shown to largely influence estimates. Similar to previous studies (Su and Tung, 2013; Sadegh et al., 2017; Dodangeh et al., 2019), the variability of the 10- and 100-year OWL and P estimates were the largest within the 20-year subsets and the smallest within the 90-year subsets (i.e., there was more uncertainty in estimates when using a limited data record). This is visualized in Figure 4.11a where there is a 3 cm and 24 cm range of 10-year AND OWLs when using subsets with 90- and 20-year lengths. Figure 4.13 further highlights this uncertainty, the isolines created by the 100-year record (red line) and subsets (black lines) strongly agree when using the 90-year subsets (Figure

4.13b) but vary dramatically when using the 20-year subsets (Figure 4.13a). Uncertainties further increase when comparing the ranges of the 10- and 100-year estimates (e.g., there is a 24 cm and 30 cm range of 10- and 100-year OWLs when using subsets with 20-year lengths for the AND scenario with annual maximum sampling; Figure 4.11a and 4.12a), also noted by Dodangeh et al. (2019) (i.e., recognizes more uncertainty associated with higher return period estimates). Most importantly, the variability of the 10- and 100-year OWL and precipitation estimates significantly reduce for the marginal, conditional, and bivariate cases when utilizing sample sizes greater than or equal to 70-years for all sampling methods (Figures 4.11, 4.12). This reduction in uncertainty when utilizing larger records suggests an inadequate sample size can generate biased estimates largely due to the poor characterization of the dependence structure between variables. Abnormalities (e.g., Figure 4.12e Conditional 1) can be attributed to marginals which did not pass the Chi Square test at standard levels and/or insignificant correlations.

It should be noted climatic conditions, non-stationarity, and/or alternative sampling methods may affect results. Wave direction (Masina et al., 2015) and El Niño-Southern Oscillation patterns (ENSO; Allan and Komar, 2006) were explored, but datasets filtered by wave direction (e.g., events with waves originating from the North Pacific) or ENSO season (El Niño years) typically resulted in an insufficient number of pairs (e.g., San Diego OWL-P pairs with annual maximum sampling decreased from 71-pairs to 34-pairs when only considering El Niño years). Peaks over threshold sampling (Jarušková and Hanek, 2006) was also utilized, but the resulting datasets had either insignificant or negligible correlations (correlations < 0.04). While peaks over threshold sampling, wave direction, and ENSO resulted in negligible correlations or limited data availability, these should not be discounted as other studies have found success by considering these variables (Allan and Komar, 2006; De Michele et al., 2007; Masina et al., 2015; Liu et al., 2018) and sampling method (Jarušková and Hanek, 2006; Tu et al., 2018; Ghanbari et al., 2021). Future work should expand to consider all available flooding pathways, variables, and sampling methods

which could contribute to flooding events, exacerbate current trends, and better characterize variable relations.

4.6 Conclusions

Uncertainties owing to sampling methods, copula choice, selected rainfall gauge, and record length were explored by considering events caused by OWL-P and TWL-P events in densely populated, urban coastal communities. Univariate, conditional, and bivariate situations were considered. Copulas passing a Cramér-von Misses test produced similar flood event estimates except estimates from the BB5 copula were often more conservative. Various sampling methods were employed: annual maximum, annual coinciding, wet season monthly maximum, and wet season monthly coinciding. Estimates largely varied depending on sampling method. However, uncertainties induced by sampling could be constrained by using the lowest and highest estimates produced by a variety of sampling methods. Microclimates were suspected to drive the differences between Long Beach and Torrance event estimates and the disagreement between estimates at these local sites present the chosen rainfall gauge as a critical source of uncertainty. There is a substantial difference between observed and total water level estimates and their variability (> 1 m). In some cases, waves account of over half of the TWL estimates. This emphasizes the importance of explicitly including wave impacts is open coast flooding applications.

Available record length significantly impacted marginal and multivariate estimates. Variability was the largest and smallest at 20- and 90-years worth of data, echoing previous studies (Su and Tung, 2013; Sadegh et al., 2017; Dodangeh et al., 2019). Estimates at larger return periods also had increased ranges of variability, also noted by Dodangeh et al. (2019). However, estimates were typically constrained with records of at least 70-years and this could serve as a reasonable record length to minimize flood risk estimate uncertainties. Future work should explore the uncertainties from other sampling methods (e.g., peaks over

threshold), variables (e.g., ENSO season), and events (e.g., OWL-$R_{2\%}$) and their influence on flood risk estimates. Additionally, the contribution of non-stationary processes (e.g., sea level rise) should be determined and accounted for within estimates.

4.7 Data Availability

NOAA precipitation data is available for download at `https://www.ncei.noaa.gov/metadata/geoportal/rest/metadata/item/gov.noaa.ncdc:C00313/html\#`. Tidal data is available for download on NOAA's Tides & Currents website (`https://tidesandcurrents.noaa.gov`). GOW hindcast data is available at `https://www.sciencebase.gov/catalog/item/5ee17ff582ce3bd58d7be907`. CDIP wave observations are available at `https://cdip.ucsd.edu/m/`.

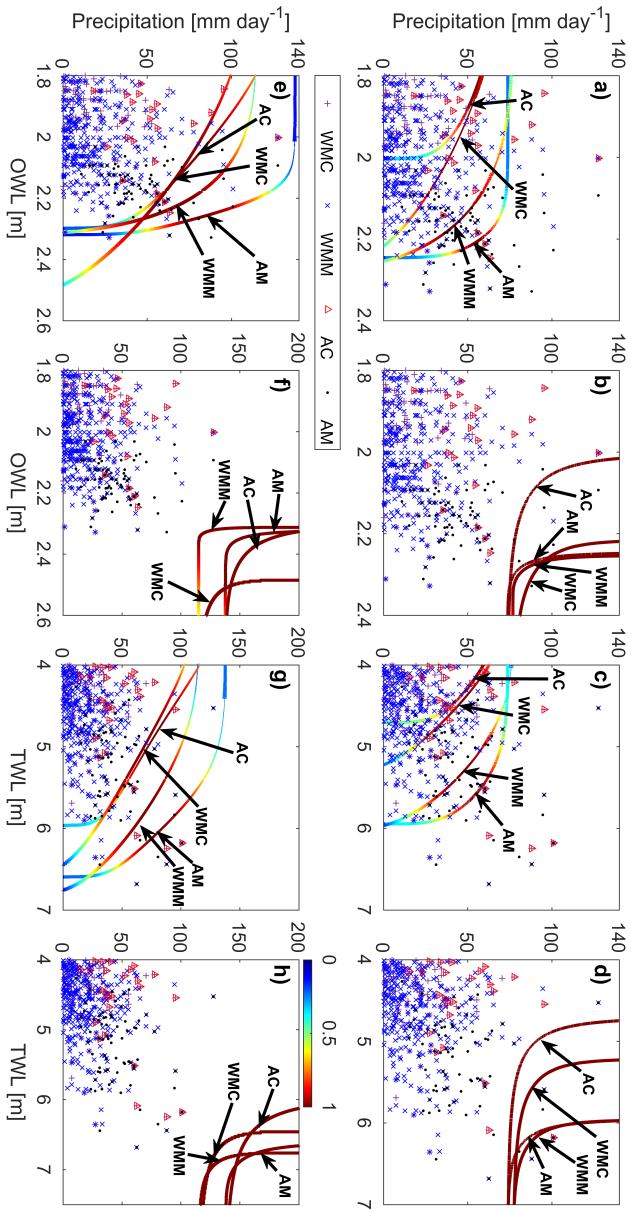

Figure 4.7: (a)(c)(e)(g)AND and (b)(d)(f)(h)OR (a)(b)(c)(d)10- and (e)(f)(g)(h)100-year isolines at Long Beach using annual maximum (AM; dot), annual coinciding (AC; triangle), wet season monthly maximum (WMM; cross), and wet season monthly coinciding (WMC; plus) sampling with a fitted Nelsen copula for (a)(b)(e)(f)OWL-P and (c)(d)(g)(h)TWL-P pairs. Arrows point toward the most likely event pair along an isoline generated by the labeled copula. Red and blue locations along an isoline indicate higher and lower probability densities, respectively.

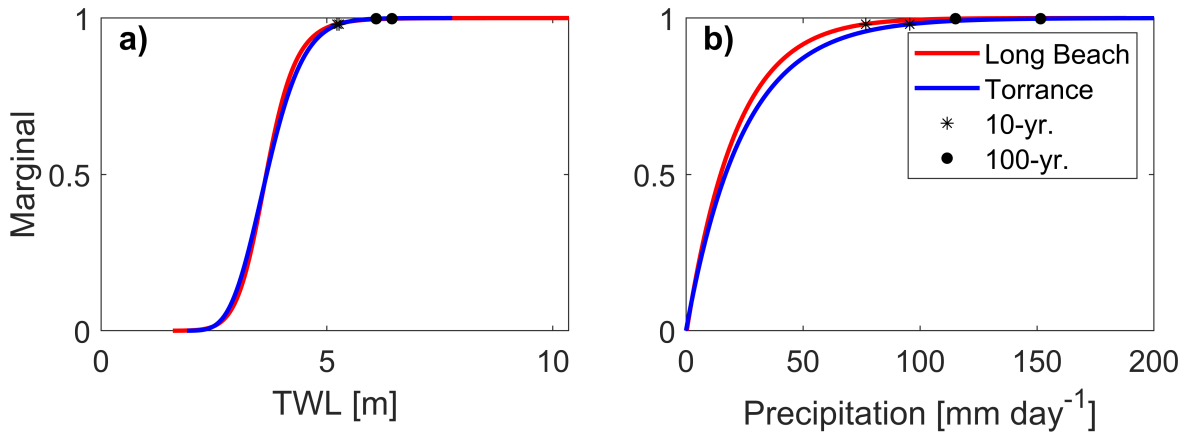

Figure 4.8: Marginal CDFs, with 10- (asterisk) and 100-year (dot) values, at Long Beach and Torrance using a wet season monthly coinciding (WMC) sampling for (a) TWL-(b) P pairs.

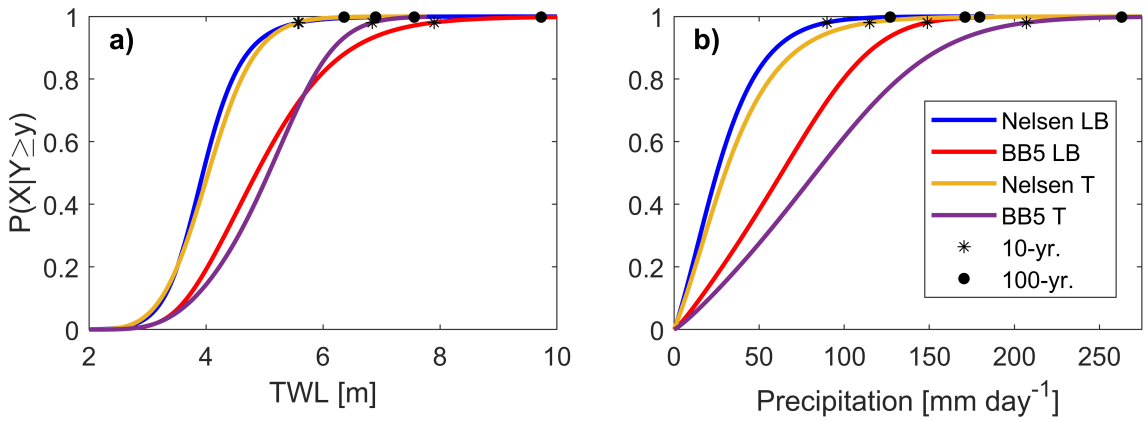

Figure 4.9: Conditional 1 CDFs, with 10- (asterisk) and 100-year (dot) values, at Long Beach (LB) and Torrance (T) using a wet season monthly coinciding (WMC) sampling with a fitted Nelsen and BB5 copula for (a) TWL-(b) P pairs. The primary variable is conditioned on the secondary variable at a 25-year return period.

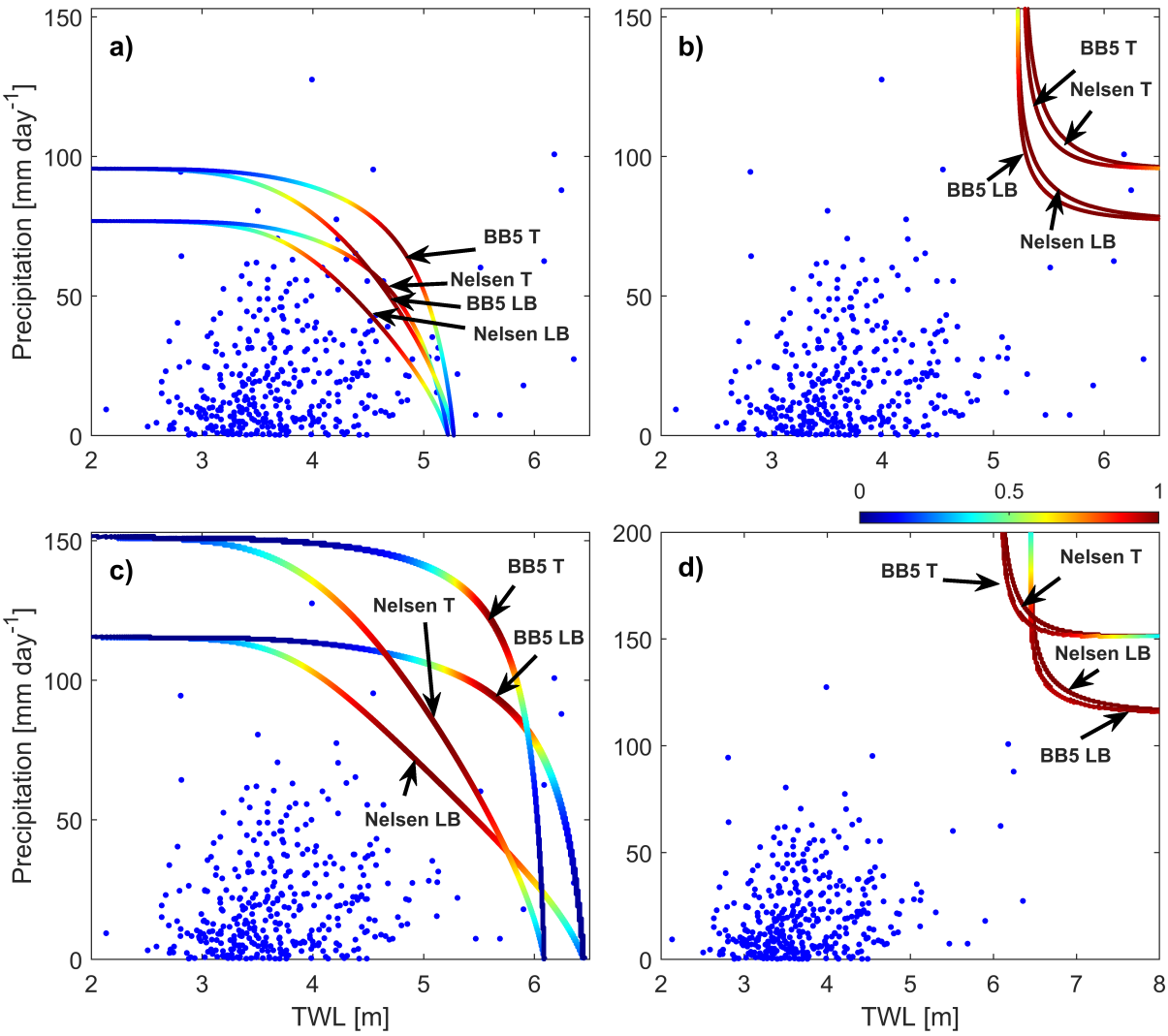

Figure 4.10: (a)(c) AND and (b)(d) OR (a)(b) 10- and (c)(d) 100-year isolines at Long Beach (LB) and Torrance (T) using a wet season monthly coinciding (WMC) sampling with a fitted Nelsen and BB5 copula for TWL-P pairs. Arrows point toward the most likely event pair along an isoline generated by the labeled copula. Red and blue locations along an isoline indicate higher and lower probability densities, respectively.

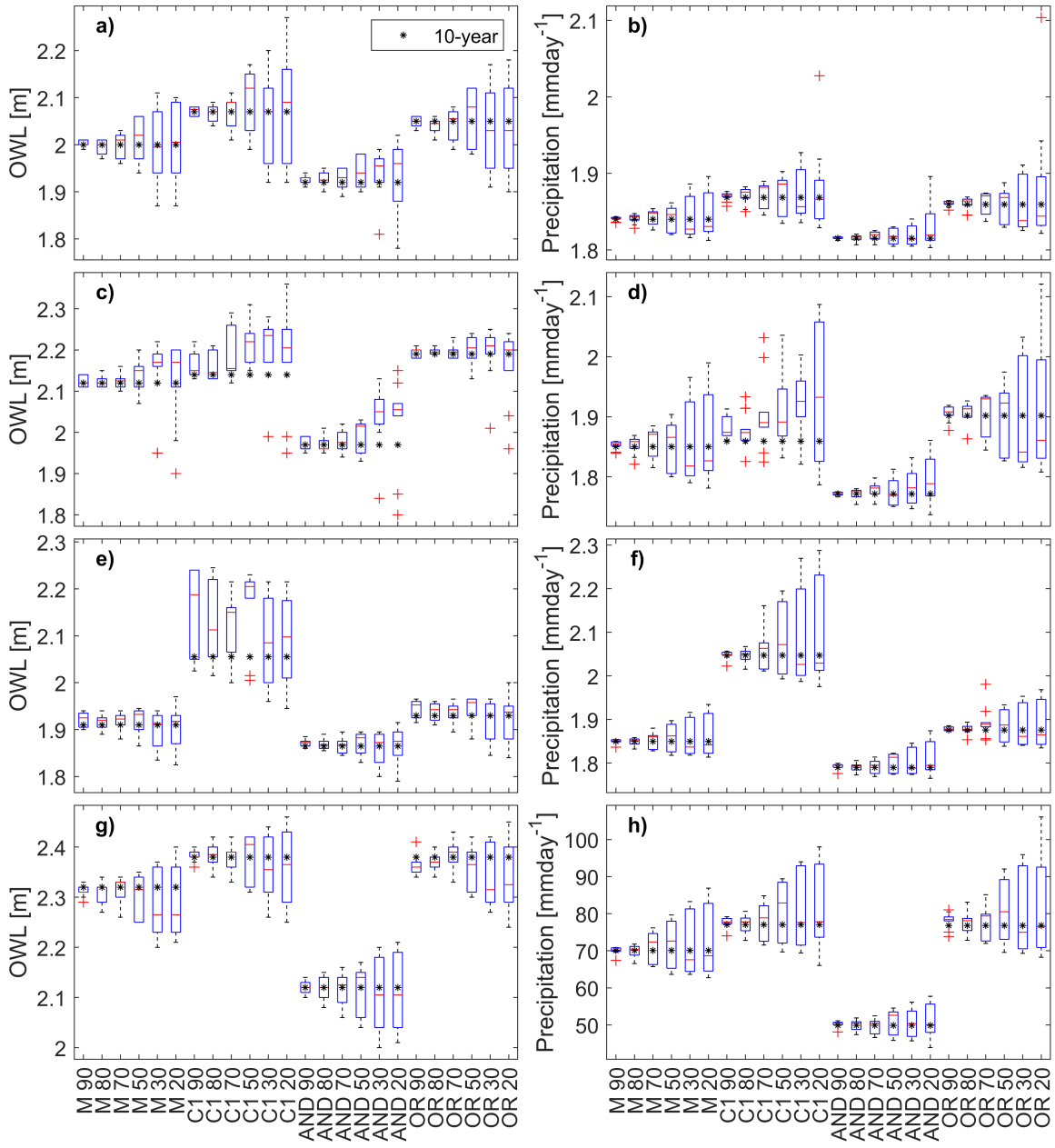

Figure 4.11: 10-year marginal (M), Conditional 1 (C1), AND, and OR (a)(c)(e)(g) observed water levels (OWL) and (b)(d)(f)(h) precipitation estimates using 90-, 80-, 70-, 50-, 30-, and 20-year subsets with (a)(b) annual maximum, (c)(d) annual coinciding, (e)(f) wet season monthly maximum, and (g)(h) wet season monthly coinciding sampling. Asterisks indicate the 10-year estimate based from the 100-year record and crosses indicate outliers which are more than 1.5 times the interquartile range.

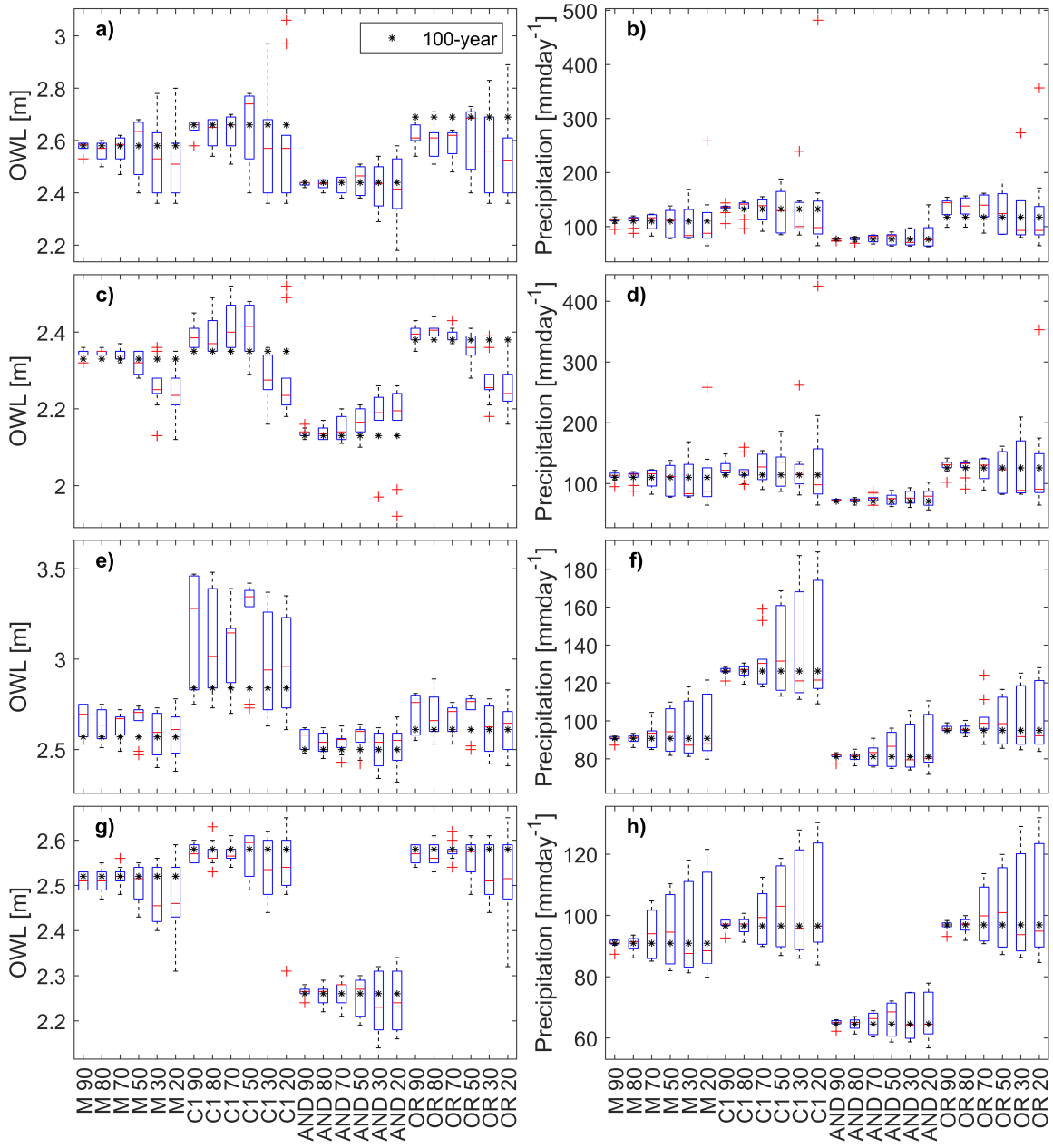

Figure 4.12: 100-year marginal (M), Conditional 1 (C1), AND, and OR (a)(c)(e)(g) observed water levels (OWL) and precipitation (b)(d)(f)(h) estimates using 90-, 80-, 70-, 50-, 30-, and 20-year subsets with annual maximum (a)(b), annual coinciding (c)(d), wet season monthly maximum (e)(f), and wet season monthly coinciding sampling (g)(h). Asterisks indicate the 100-year estimate based from the 100-year record and crosses indicate outliers which are more than 1.5 times the interquartile range.

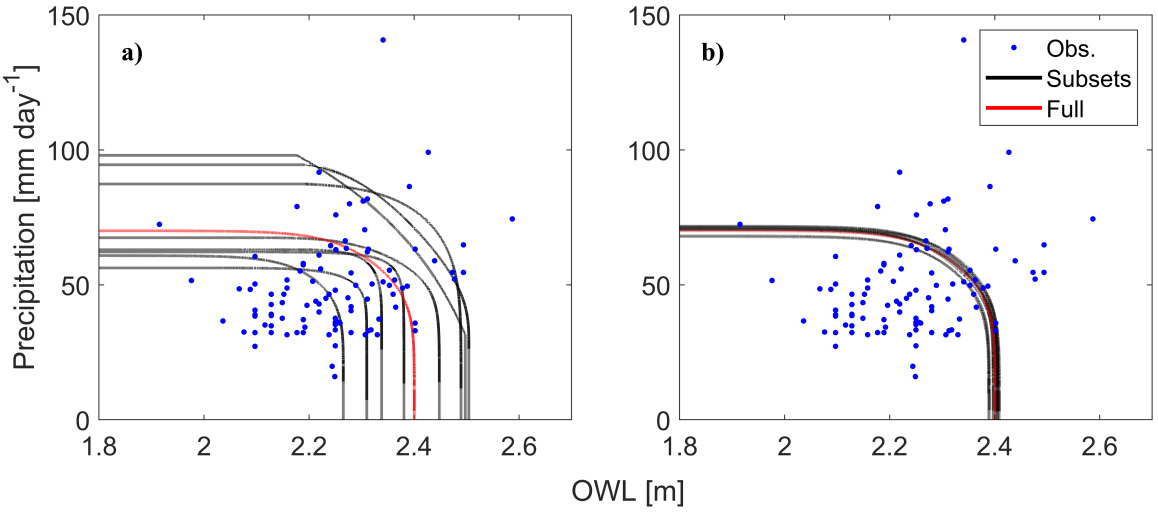

Figure 4.13: 10-year isolines for observed water levels (OWL) and precipitation pairs from (a) 20- and (b) 90-year subsets with annual maximum sampling for the AND scenario (isolines representative of Figure 4.11a) at San Francisco. Black and red lines correspond to isolines created by subsets and the full 100-year record, respectively, while the markers represent observation (Obs.) pairs from the 100-year record.

CHAPTER 5

Hybrid statistical-numerical modeling for compound flood risk assessment and uncertainty quantification

5.1 Background

Recently, a hybrid approach combining copulas and numerical models has developed. Often studies apply copulas after modeling efforts to consider dependencies between variables (Bevacqua et al., 2019, 2020; Couasnon et al., 2020; Ganguli et al., 2020; Santos et al., 2021; Tanim and Goharian, 2021; Xu et al., 2022). For example, Xu et al. (2022) models tropical cyclone events and subsequently uses copulas to determine peak water level-precipitation pairs for design purposes in an area without water level records. Only limited studies utilize copulas to provide inputs to numerical models and determine the flood risk likely experienced by an area (Sebastian et al., 2017; Couasnon et al., 2018; Didier et al., 2019; Moftakhari et al., 2019). Moftakhari et al. (2019) presents a methodology to improve on FEMA's guidelines for riverine-coastal compound flooding (FEMA, 2015) by creating copulas for ocean water levels and streamflow and then modelling those events to establish the possible floodplain. Although the hybrid statistical-numerical modeling is rapidly developing, it is unknown how statistical uncertainties will impact flood maps.

Previous studies have explored multiple sources of uncertainty and their influences on events estimates and numerical models outcomes (Table 1.3). Significant event pair variability has been observed depending on the utilized sampling methods (Mazas and Hamm, 2017; Lucey and Gallien, 2023). Observation record length present a critical source of un-

certainty (Genest et al., 2009; Su and Tung, 2013; Tong et al., 2015; Sadegh et al., 2017; Dodangeh et al., 2019; Lucey and Gallien, 2023). Teng et al. (2017) characterized uncertainties pertaining numerical modeling (e.g., model structure, inputs, parameters, validation data quality, landscape cover, and nonstationarity) and suggested methodologies to account for uncertainty. However, it is unknown how statistical event characterization (e.g., record length, sampling strategy, observational data) influence flood maps. This study explores how statistical modeling (i.e., copula choice, sampling methods, event choice, and record length) impacts flood estimates. Univariate and multivariate statistics are determined and used as numerical model inputs. Uncertainty is quantified utilizing modeled flood event characteristics (e.g., areal extent, depth, flood volume)

5.2 Data & Study Sites

Two extensively managed, densely populated, urbanized Southern California beaches were used to explore uncertainties, Sunset Beach and Newport Beach. These sites have over 70-years of precipitation and tide observations to develop copulas while minimizing uncertainty from data availability (Lucey and Gallien, 2023) and benefit from previous flood validation data (Gallien et al., 2011, 2014; Tang and Gallien, 2023). Figure 5.1 displays the location of the utilized precipitation and tide gauges along the sites.

5.2.1 Tide & Precipitation

Verified hourly and 6-minute observed water levels (OWLs, m NAVD88) at the Los Angeles (Station ID: 9410660) were downloaded from NOAA's Tides and Currents website (NOAA, Accessed 2023b). Months with no OWL measurements were excluded. Daily precipitation summaries (P, mmday^{-1}) at the Long Beach Airport (USW00023129) and Newport Beach Harbor (USC00046175) stations were downloaded from NOAA's Global Historical Climatology Network dataset (NOAA, Accessed 2023a). Sunset Beach utilizes the Long Beach

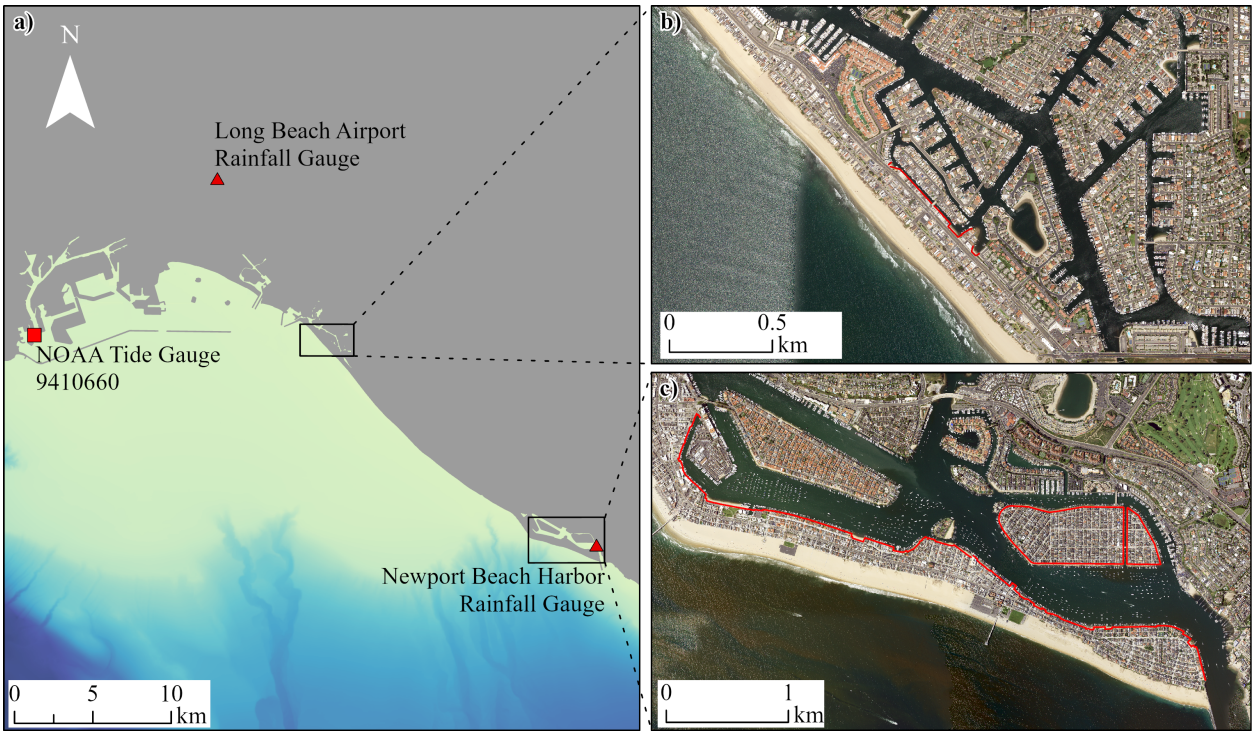

Figure 5.1: (a) Location of data gauges and the study sites. Subsets display (b) Sunset Beach and (c) Newport Beach domains with seawalls delineated as red lines.

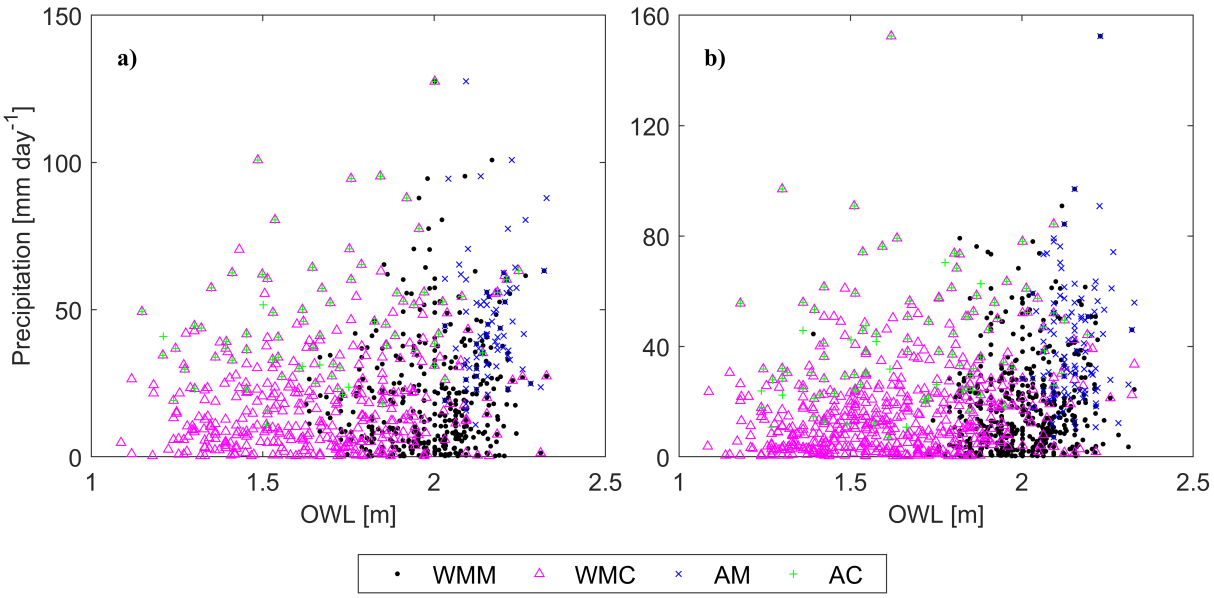

Figure 5.2: Pairs of observed water level (OWL; m) and precipitation (mmday^{-}1) using annual maximum (AM; cross), annual coinciding (AC; plus), wet season monthly maximum (WMM; dot), and wet season monthly coinciding (WMC; triangle) samplings at (a) Sunset Beach and (b) Newport Beach

Airport precipitation observations, while Newport Beach utilizes the Newport Beach Harbor precipitation data. Daily precipitation observations flagged by NOAA (NOAA, Accessed 2023a) were removed if necessary. All data are in UTC time. Table 5.1 presents the overlapping observation periods between OWL and P at each site. All locations utilize the same observed water level observations.

5.3 Numerical Modeling

Shock capturing full nonlinear shallow water (NLSW) models have proven to provide accurate flood estimates in complex urban environments without specific parameter tuning (e.g., Gallien et al., 2011; Akoh et al., 2017; Xie et al., 2019; Moftakhari et al., 2019; Rong et al., 2020; Stephens et al., 2022). Similarly, a number of 2D NLSW models have been

Table 5.1: Observed Water level (OWL) and precipitation (P) observations for Sunset (S) and Newport Beach (NB) using annual maximum (AM), annual coinciding (AC), wet season monthly maximum (WMM), and wet season monthly coinciding (WMC) samplings.

Site	OWL Gauge	P Gauge	Observation Window	AM Pairs	AC Pairs	WMM Pairs	WMC Pairs
S	9410660	USW00023129	January 1, 1943 to March 31, 2023	75	75	387	388
NB	9410660	USC00046175	November 28, 1923 to March 31, 2023	101	100	531	531

successfully used in coastal (Table 1.2), and compound flooding applications (e.g., Herdman et al., 2018; Shen et al., 2019; Muñoz et al., 2020; Nederhoff et al., 2021). Delft3D flow (`http://oss.deltares.nl/web/delft3dfm`) solves full 2D NLSW equations using a shock-capturing scheme (Kramer and Stelling, 2008; Toro and Garcia-Navarro, 2007; Toro, 2013), and has been successfully used to model complex coastal environments (e.g., Martyr-Koller et al., 2017; Kumbier et al., 2018; Ganguli et al., 2020; Muñoz et al., 2020; Paprotny et al., 2020; Nederhoff et al., 2021; Xu et al., 2022; Tang and Gallien, 2023). Delft3D-FM is open source, widely used, boundary fitting, and employs a shock capturing numerical scheme appropriate to urban environments. Accordingly, Delft3D-FM is selected for all hydrodynamic modeling in this work.

Infrastructure presents a particular challenge in urban coastal flood modeling and is critical to resolve within numerical modeling applications (Fewtrell et al., 2011; Gallien et al., 2011, 2014; Wang et al., 2018). Gallien et al. (2011); Gallien (2016); Tang and Gallien (2023) collected infrastructure and validation data in various California (e.g., Surfside-Sunset, Newport Beach, Imperial Beach). Sea wall elevations were measured using a Stonex S900A and incorporated into the Delft3D model using elevated nodes along mesh edges. In this work, urban drainage infrastructure is not incorporated into the model domains since information

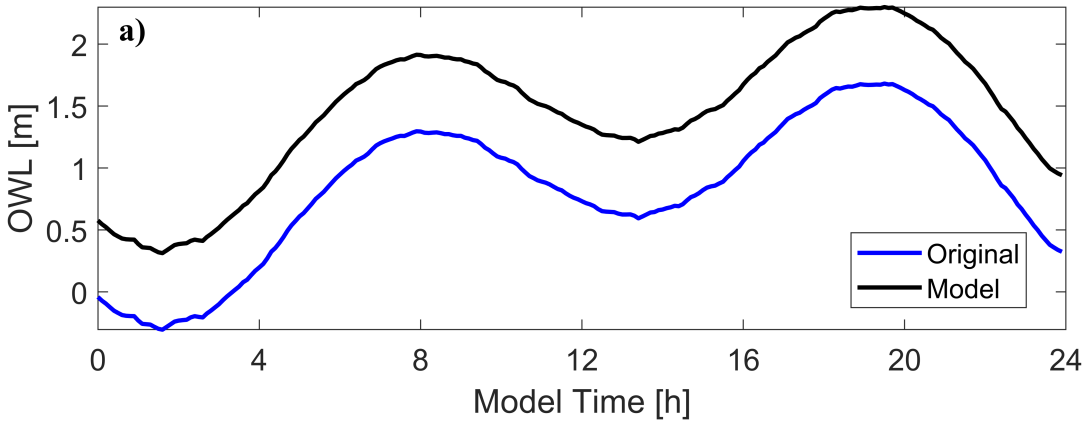

Figure 5.3: Example of model (a) observed water level (m) inputs for 24-hours simulation window. Black lines indicated the model input after modification (if needed) of the original data signal (blue line).

on drainage infrastructure is not publicly available. Topobathy for the Newport Beach model utilizes LiDAR topography datasets provided by the City of Newport Beach and U.S. Army Corps of Engineer's bathymetric surveys as utilized in Gallien et al. (2011). Sunset Beach topobathy data is composed of multiple DEM sources and surveys provided by Table 2 in Tang and Gallien (2023).

Simulations were run for 24-hours of model time where precipitation events were spatially and temporally uniform. A great diurnal range tide cycle (referred to as the "base tide") from the Los Angeles tide gauge from approximately mean lower low water to mean higher high water levels (-0.04m and 1.63m NAVD88 respectively, NOAA2023a) provides the ocean water level forcing. Ocean water levels were created by raising the base tide to the estimated event while maintaining the tidal range and peaks of the signal. For example (Figure 5.3), 67 cm is added to the 24-hour base tide signal for a 10-year event with a peak of 2.3 m (i.e., 1.63 m plus 0.67 m is 2.3 m) over the simulation window. Flood metrics presented in the results include flooded area (m^2) and volume (m^3) and the maximum flood depth difference between events at each grid cell (m).

5.4 Results

Table 7.3 in the Appendix presents the marginal fits and those with below standard significance levels are noted: observed water level marginals with annual coinciding and wet season monthly maximum and coinciding samplings at Newport Beach, precipitation marginals with wet season monthly maximum and coinciding samplings at Newport Beach, and observed water level marginals with wet season monthly coinciding sampling at Sunset Beach. Figure 7.3 presents marginal CDF plots. Correlations were positive and significant at all locations except when using an annual maximum sampling.

5.4.1 Copula choice

Copula choice impacts on modeled flood estimates were quantified with Clayton, Nelsen, Roch-Alegre (Roch.), Fischer-Kock (Fisc.), BB1, and BB5 copulas. These copulas passed a Cramér-von Misses test at Sunset or Newport Beach. Compound event estimates between copulas were generally similar, but BB5 estimates occasionally produced greater event estimates. Observed water level estimates varied by 3 cm and 12 cm, and precipitation estimates varied by 2.35 mmday^{-1} and 19.78 mmday^{-1} for 10- and 100-year events at Sunset Beach when using an annual coinciding sampling (Figure 5.4; Table 7.5). Additionally, BB5 observed water level and precipitation event estimates were the largest compared to the other copula estimates in this example (Figure 5.4; Table 7.5).

The most likely compound events using an annual coinciding sampling at Sunset Beach (Figure 5.4; Table 7.5) were then modeled to quantify copula choice influence on model estimates (Figure 5.5). Univariate 10-year precipitation was 72.89 mmday^{-1} and OWL was 2.01 m. Compound AC OWL ranged from 1.82 m to 1.85 m. Precipitation values were between 76.66 mmday^{-1} to 99.44 mmday^{-1} (Figure 5.4, Table 7.5). The 10-year OWL is beneath the sea wall level (approximately 2.4 m), no flooding was observed. The flooded area for multivariate events was minimally variable, 87,870 m^3 to 88,280 m^3 depending on

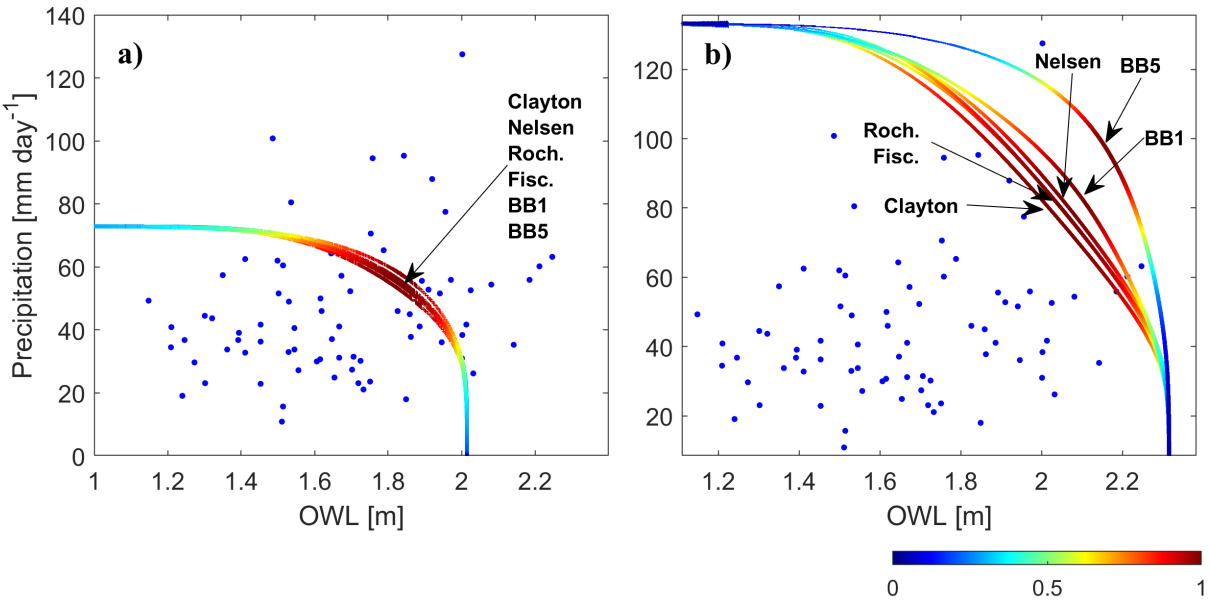

Figure 5.4: Isolines for (a) 10- and (b) 100-year compound events at Sunset Beach using an annual coinciding sampling and Clayton, Nelsen, Roch-Alegre (Roch.), Fischer-Kock (Fisc.), BB1, and BB5 copulas. Dots display pairs of observed water level (OWL; m) and precipitation (P; mmday^{-1}) events. Arrows point to the most likely event along an isoline and indicate the copula used to generate that isoline. Probability density is gradated along the isolines from low (blue) to high (red) density.

copula (Table 5.2).

Similarly, trivial flood volumes variations (less than 1%) were observed between copulas, 96 m^3, and 577 m^3 for the 10- and 100-year flood events, respectively. Again, the BB5 provided the largest flood (or most conservative) events compared to the other copulas (Table 5.2). Copulas aside from the BB5 copula only varied by 45 m^3 and 209 m^3 for the 10- and 100-year flood event (Table 5.2). Only minor differences at a maximum of 3 cm and 6 cm in the maximum flood depths for the 10- and 100-year event were observed (Figure 5.5). In this particular case, precipitation clearly dominates the flooding signal and results are insensitive to copula choice.

Table 5.2: Modeled maximum flooded area (10^3 m^2) and volume (Vol.; 10^2 m^3) for 10- and 100-year compound and univariate, observed water level (OWL) and precipitation (P), events using an annual coinciding sampling at Sunset Beach. Compound events were created using a Clayton, Nelsen, Roch-Alegre (Roch.), Fischer-Kock (Fisc.), BB1, and BB5 copula passing a Cramér-von Misses test for one or more cases.

	Clayton	Nelsen	Roch.	Fisc.	BB1	BB5	OWL	P
				10-year				
Area	87.87	88.05	88.01	87.99	87.92	88.28	0	90.96
Vol.	88.05	88.51	88.38	88.36	88.22	89.02	0	95.46
				100-year				
Area	91.46	91.79	91.69	91.69	92.20	93.63	14.74	96.06
Vol.	96.97	97.97	97.57	97.56	99.06	102.75	15.16	109.57

5.4.2 Sampling

Figure 5.6 shows the 10- and 100-year isolines for multivariate events comprised of high marine water levels and precipitation using a Nelsen copula. The most likely compound

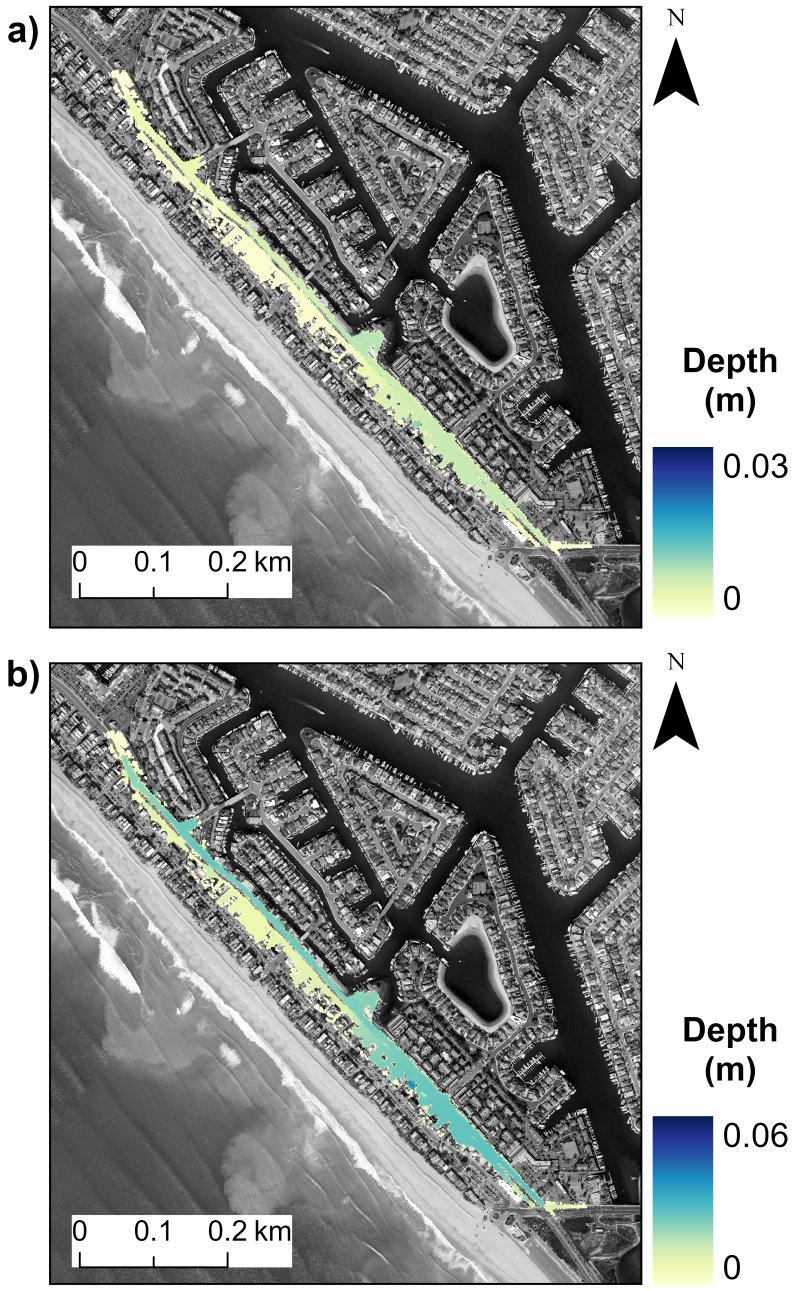

Figure 5.5: Differences in (a) 10- and (b) 100-year maximum flood depths per grid cell at Sunset Beach. Events were created using an annual coinciding sampling and Clayton, Nelsen, Roch-Alegre (Roch.), Fischer-Kock (Fisc.), BB1, and BB5 copulas' most likely events in Figure 5.4 and Table 7.5. The difference in the maximum flood depths are gradated from minor (yellow) to significant (blue) depth changes.

events and all sampling methods at Sunset Beach (Figure 5.6; Table 7.4) were modeled to quantify sampling method influences of on model outcomes (Figure 5.7; Table 5.3). Here, flood metrics varied depending only slightly on the utilized sampling method. Compound flood volumes varied by 692 m^3 and 652 m^3 for the 10- and 100-year event depending on the utilized sampling (Table 5.3). 10- and 100-year events created with an annual type sampling resulted in the largest flood metrics, and events created from an annual maximum sampling resulted in the largest flooding compared to events produced from the other sampling methods (Table 5.3). Sampling methods also influenced the maximum flood depths to a maximum of 8 cm, primarily concentrated at low-elevation regions and coastal-inland entrances (Figure 5.7).

Table 5.3: Modeled maximum flooded area (10^3 m^2) and volume (Vol.; 10^2 m^3) for 10- and 100-year marginal, observed water levels (OWL) and precipitation (P), and compound events (AND) using annual maximum (AM), annual coinciding (AC), wet season monthly maximum (WMM), and wet season monthly coinciding (WMC) samplings at Sunset Beach. Compound events were created using the Nelsen copula passing a Cramér-von Misses test

	AND		OWL		P	
	Area	Vol.	Area	Vol.	Area	Vol.
10-year						
AM	89.05	90.99	0.54	0.20	90.96	95.46
AC	88.05	88.51	0	0	90.96	95.46
WMM	86.51	85.13	0.54	0.20	91.34	96.56
WMC	86.19	84.07	0	0	91.34	96.57
100-year						
AM	92.86	100.71	14.74	15.16	96.06	109.57
AC	91.79	97.97	14.74	15.16	96.06	109.57
WMM	90.73	95.34	12.33	11.69	94.59	105.50
WMC	90.31	94.18	99.81	191.07	94.59	105.50

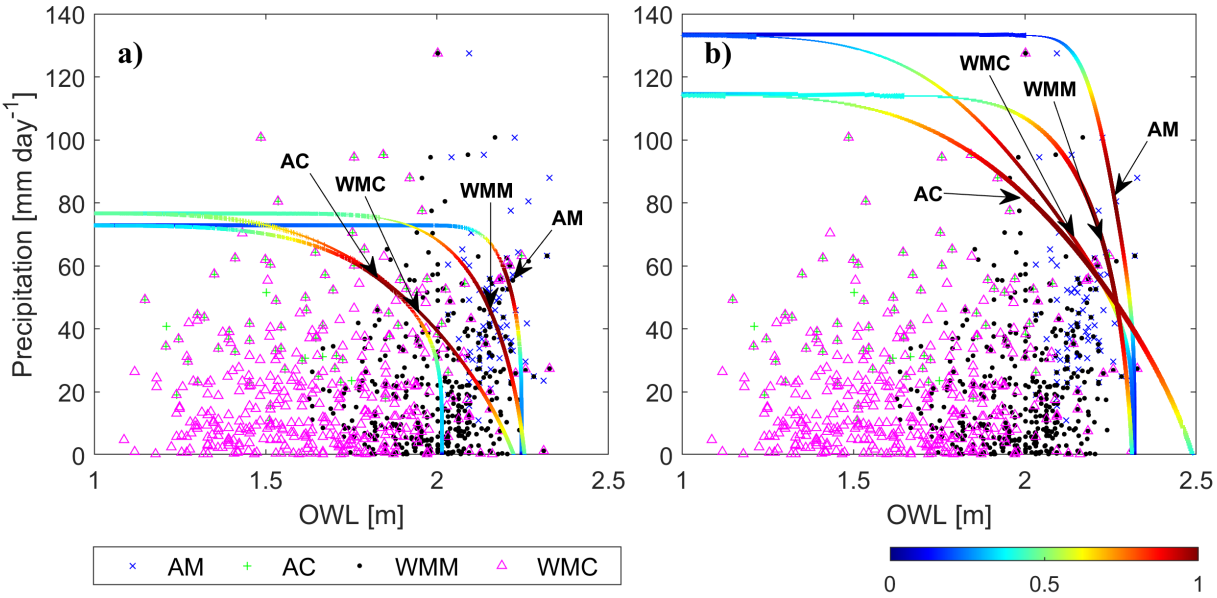

Figure 5.6: Isolines for (a) 10- and (b) 100-year compound events at Sunset Beach using a Nelsen copula and various samplings. Markers display pairs of observed water level (OWL; m) and precipitation (P; mmday^{-}1) using annual maximum (AM; cross), annual coinciding (AC; plus), wet season monthly maximum (WMM; dot), and wet season monthly coinciding (WMC; triangle) samplings. Arrows point to the most likely event along an isoline and indicate the sampling method used to generate that isoline. Probability density is gradated along the isolines from low (blue) to high (red) density.

5.4.3 Multivariate events sharing a common return period

Isolines created using an annual coinciding sampling and a Gaussian copula passing a Cramér-von Misses test at Sunset Beach were used to observe the variability of flood extent estimates along an isoline (Figure 5.8; Table 5.4). Five events along the 10- and 100-year isolines were modeled: three around the center of the isoline, where the most probable events lie, and two utilizing the estimated univariate observed water level or precipitation event. This results in a 10-year observed water level and precipitation range of 0.96 m and 61 mmday^{-1} and a 100-year observed water level and precipitation range of 1.05 m and 113 mmday^{-1} (Table 5.4). Modeling the events in Figure 5.8 produced flood volumes varying by 7,039 m^3 and 5,152 m^3 for the 10- and 100-year events (Tables 5.5). The maximum flood depth varied up to 0.4 m and 0.2 m for the 10- and 100-year events (Figure 5.9), with the largest variability occurring at the center (Figure 5.9a) and western (Figure 5.9b) portions of the domain.

Table 5.4: 10- and 100-year compound observed water level (OWL; m) and precipitation (P; mmday^{-1}) events at Sunset Beach created with an annual coinciding sampling and Gaussian copula passing a Cramér-von Misses test.

	OWL [m]		P [mmday^{-1}]	
	10	100	10	100
Case 1	2.01	2.32	11.78	20.70
Case 2	1.84	2.09	55.00	83.93
Case 3	1.69	2.03	64.77	93.67
Case 4	1.94	2.15	43.56	74.60
Case 5	1.05	1.26	72.89	133.30

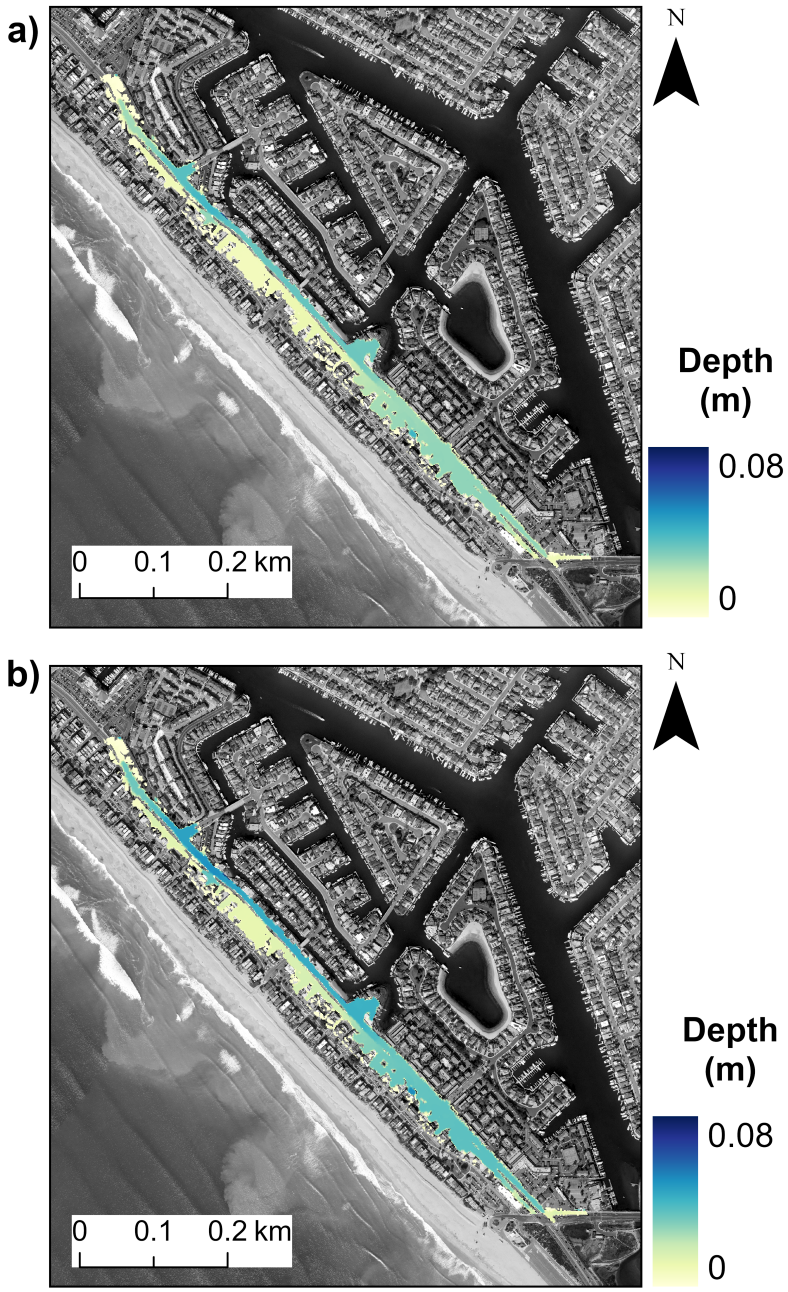

Figure 5.7: Differences in (a) 10- and (b) 100-year maximum flood depths per grid cell at Sunset Beach. Events were created using a Nelsen copula and an annual maximum and coinciding, and wet season monthly maximum and coinciding samplings' most likely events in Figure 5.6 and Table 7.4. The difference in the maximum flood depths are gradated from minor (yellow) to significant (blue) depth changes.

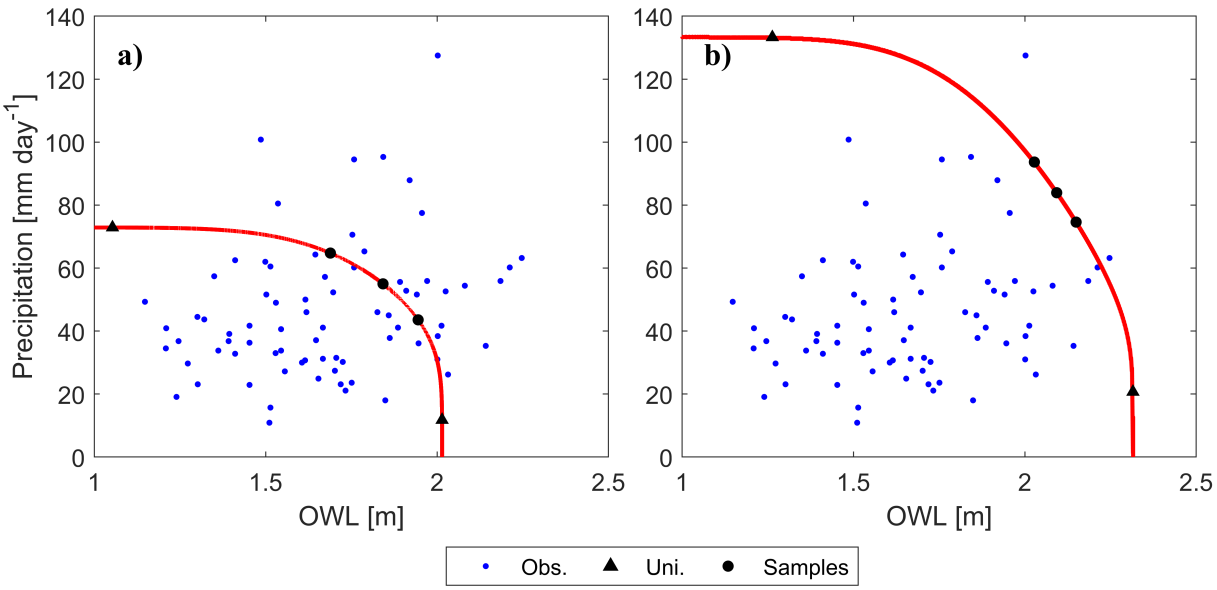

Figure 5.8: (a) 10- and (b) 100-year isolines made with using a Gaussian copula and an annual coinciding sampling at Sunset Beach. Triangles are where the marginal observed water level (OWL) or precipitation (P) intersect the isoline while circles are samples at the 35th, 50th, and 65th percentile along the isoline.

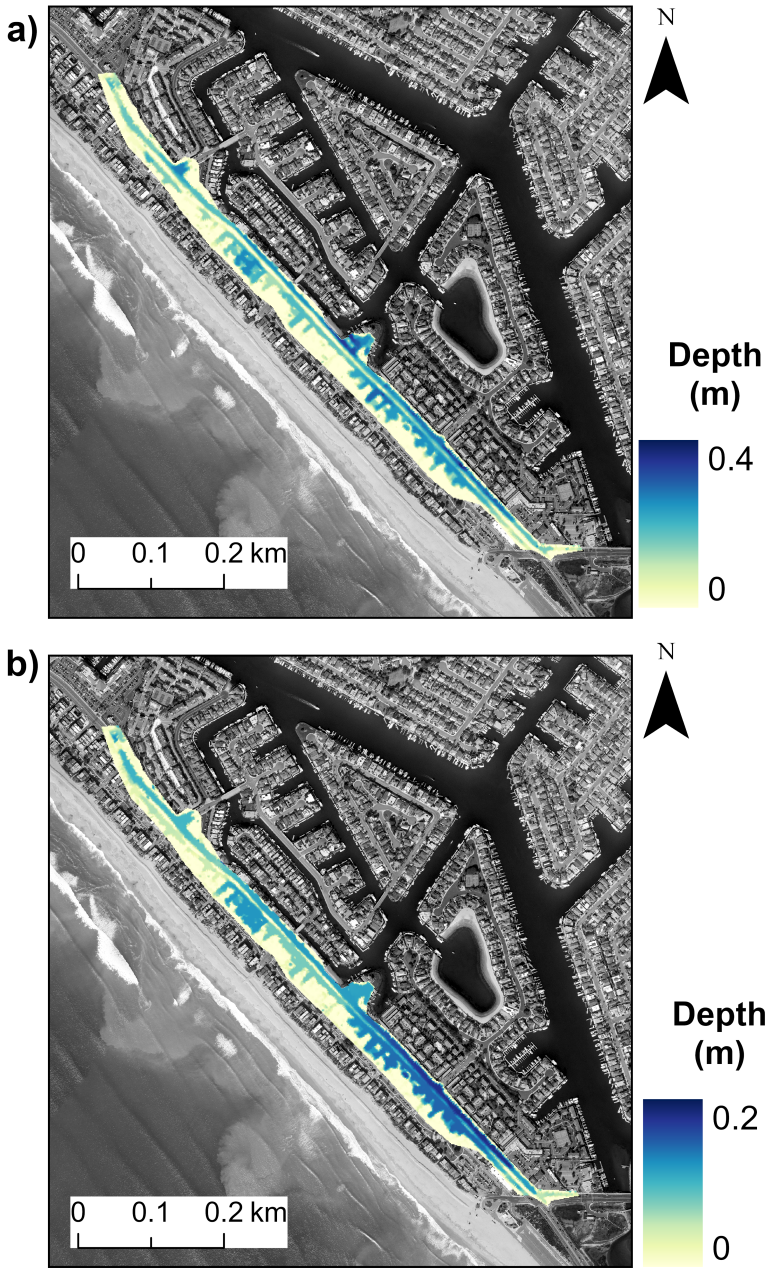

Figure 5.9: Differences in (a) 10- and (b) 100-year maximum flood depths (m) per grid cell at Sunset Beach using the marked events on the isolines shown in Figure 5.8 and listed in Table 5.4. Events were created using an annual coinciding sampling and Gaussian copula passing a Cramér-von Misses test. The difference in the maximum flood depths are gradated from minor (yellow) to significant (blue) depth changes.

Table 5.5: Modeled maximum flooded area (10^3 m^2) and volume (Vol.; 10^2 m^3) for 10- and 100-year compound observed water level (OWL) and precipitation (P) events at Sunset Beach. Compound events were created using an annual coinciding sampling and Gaussian copula passing a Cramér-von Misses test.

	Case 1	Case 2	Case 3	Case 4	Case 5
10-year					
Area	52.20	88.04	89.39	86.12	90.21
Vol.	22.83	88.47	91.64	83.91	93.22
100-year					
Area	73.13	92.16	93.03	91.28	95.58
Vol.	56.40	98.86	101.15	96.55	107.92

5.4.4 Record length

The uncertainties associated with record length were assessed at Newport Beach using the annual maximum and coinciding, and wet season monthly maximum and coinciding samplings with a Nelsen copula which generally passed a Cramér-von Misses test. Significant variability amount exists in observed water level and precipitation estimates when using short data records (<70-years) and further increases between the 10- and 100-year event estimates (Figure 5.10). For example, 10- and 100-year marginal observed water level estimates vary by 17 cm and 44 cm when utilizing record lengths of 20-years and a wet season monthly coinciding sampling (Figure 5.10g). Estimates made when using at least 70-year records tend to be well constrained (Figure 5.10). AND observed water level estimates generally vary less than 3 cm for the 10- and 100-year events when utilizing 90-year record lengths (Figure 5.10a, c, e, g).

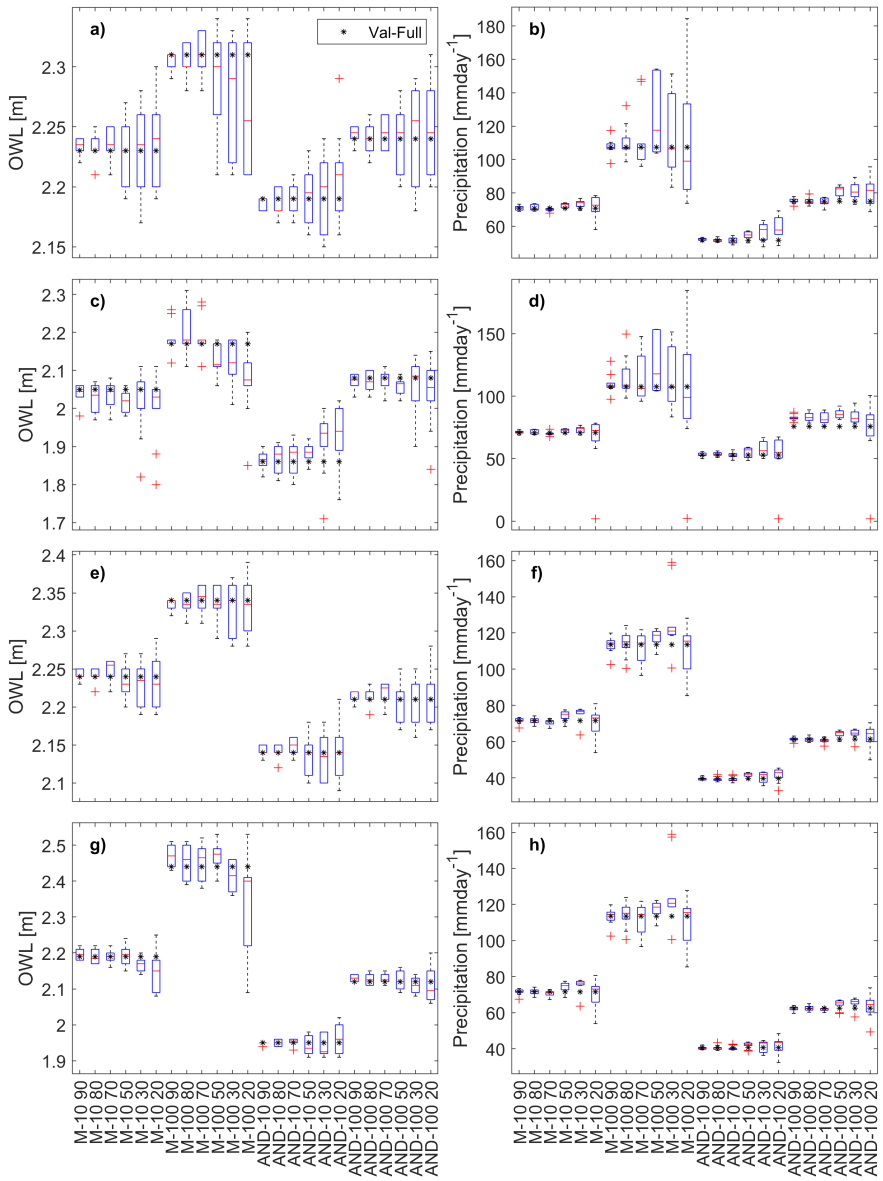

Figure 5.10: 10-year marginal (M-10), 100-year marginal (M-100), 10-year AND (AND-10), and 100-year AND (AND-100) (a)(c)(e)(g) observed water levels (OWL) and (b)(d)(f)(h) precipitation estimates using 90-, 80-, 70-, 50-, 30-, and 20-year subsets with (a)(b) annual maximum, (c)(d) annual coinciding, (e)(f) wet season monthly maximum, and (g)(h) wet season monthly coinciding sampling. Asterisks indicate the 10- or 100-year estimate based from the full record (Val-full) and crosses indicate outliers which are more than 1.5 times the interquartile range. All cases used a Nelsen copula.

Compound events were modeled at Newport Beach (Figure 5.11) using an annual maximum sampling. 10-year maximum compound flood depths varied up to 30 cm and 8 cm when utilizing the estimates with 20- (Figure 5.11a) and 90-year records (Figure 5.11b). The domain's northwest corner and east island significantly differ in flood depths when using 20-year subsets (Figure 5.11a). In contrast, the domain has minimal to moderate differences when using 90-year subsets (Figure 5.11b). 10-year compound events from 20- and 90- subsets (Figure 5.11) produced flooded areas varying by 93,600 m^2 and 14,413 m^2, respectively (Figure 5.12). Generally, modeled flood area and volume variability progressively decreased as the utilized data record length increased (Figure 5.12).

5.5 Discussion

Uncertainties from sampling methods, copula choice, record length, and chosen isoline events affect flood prediction. Sampling methods impart significant uncertainties onto event estimates (Lucey and Gallien, 2023), however this does not always translate into fundamentally different outcomes. Annual coinciding estimates produced the lowest observed water level estimates versus other sampling method estimates (Table 7.4) as previously observed (Lucey and Gallien, 2022, 2023), but did not translate into the lowest flood metrics. Annual samplings generally had larger flood metrics (and greater precipitation estimates) compared to wet season monthly samplings for 10- and 100-year marginal and compound events (Table 5.3). Precipitation is a dominant driver in flood developments in urban areas (Gaitan et al., 2016; Huang et al., 2018; Vorobevskii et al., 2020) and cases that had larger precipitation estimates, regardless of the estimated observed water level, produced larger flood metrics. For example, the 10-year compound event flood volume was 8,850 m^3 and 8,513 m^3 when using an annual coinciding (observed water level and precipitation of 1.84 m and 55 $mmday^{-1}$) versus wet season monthly maximum (observed water level and precipitation of 2.16 m and 44 $mmday^{-1}$) sampling. Here, sampling methods only trivially affected modeled flood es-

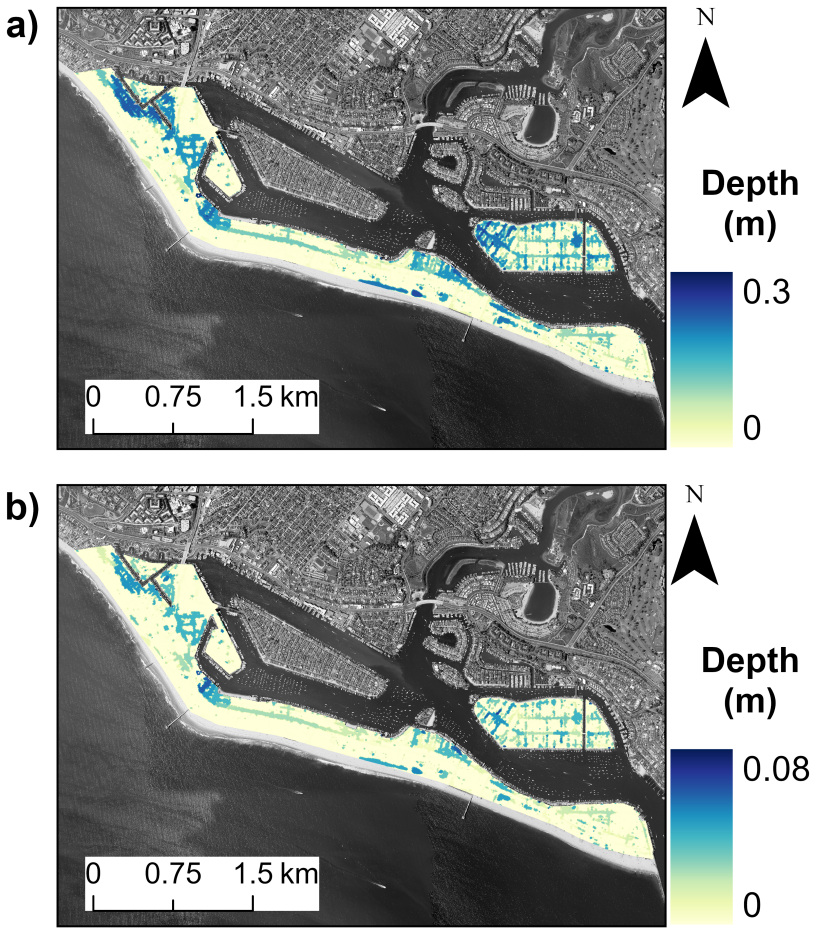

Figure 5.11: Differences in flood depths (m) for 10-year AND events using (a) 20- and (b) 90-year subsets at Newport Beach. Events were created using a Nelsen copula and an annual maximum sampling. The difference in the maximum flood depths are gradated from minor (yellow) to significant (blue) depth changes.

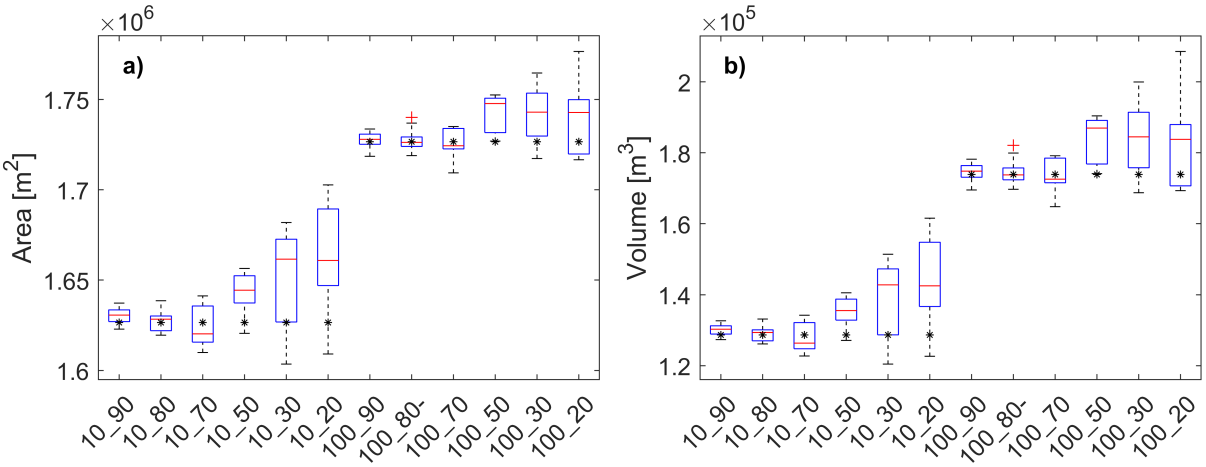

Figure 5.12: Modeled compound flooded (a) area (m^2) and (b) volume (m^3) at Newport Beach when using various subset sizes with an annual maximum sampling and a Nelsen copula. X-axis labels indicate the return period (10- or 100-year) and subset size (90-, 80-, 70-, 50-, 30-, and 20-year) used for the estimates. Asterisks indicate the 10- or 100-year flood area or volume based from the full record (Val-full) and crosses indicate outliers which are more than 1.5 times the interquartile range.

timates. It should be noted drainage infrastructure is not represented within the current models and is known to influence urban flooding (Gallien et al., 2011, 2014; Shen et al., 2019; Rong et al., 2020). Additionally, Tang and Gallien (2023) showed that the Surfside-Sunset maximum flood volume is constrained by the flood wall and that approximately 25 mm of precipitation fills the basin and begins discharging over the seawall into the bay. This suggests that sampling time windows and drainage infrastructure play a key role in accurate compound flood event modeling.

Copulas passing a Cramér-von Misses test generally produced similar event (previously observed by Lucey and Gallien (2022, 2023)) and flood estimates excluding the BB5 copula which occasionally resulted in larger values (Figure 5.4). The conservative nature of the BB5 copula was previously observed Lucey and Gallien (2023). The range of compound flood volume (2,169 m^3 to 738 m^3) and area (96 m^2 to 45m^2) is substantially reduced when excluding the BB5 flood metrics (Table 5.2). Only minor variability was observed in maximum flood depths for the 10-year event (Figure 5.4a) and slightly increased for the 100-year event (Figure 5.4b). These results may suggest copula selection as a minor source of uncertainty, assuming copulas pass a Cramér-von Misses (or alternative goodness of fit) test. Future work should further explore which copulas provide more conservative estimates (e.g., BB5 copula), which have a consistent agreement, and if the dependencies between event variables (e.g., waves and tide, precipitation and temperature, streamflow and tide) indicate particular copula choices.

If a copula function is used without its probability density function (De Michele et al., 2007; Wahl et al., 2012; Sadegh et al., 2017), it is necessary to understand what events to choose along an isoline and their implications on flood developments. Compound events of concern should be constrained between marginal intersections on the isoline (triangles in Figure 5.8). In this example, the largest flooding events occurred together with the highest precipitation event (where the precipitation marginal intersected the isoline) and not around the center of the isoline where the most likely event commonly occurs. There was also

less variability in the 100-year versus 10-year flood volumes (7,039 2,169 m^3 versus 5,152 m^3) and areas (38,013 m^2 versus 22,450 m^2) even though the magnitude for the 100-year flood events were higher (Table 5.5). This suggests flooding is reaching a saturation point or a volumetric capacity during the 100-year events. Drainage infrastructure is critical in flooding development (Gallien et al., 2011, 2014; Shen et al., 2019; Rong et al., 2020; Tang and Gallien, 2023). Future work must integrate drainage infrastructure into models when accounting for pluvial-induced flooding which is modulated by marine water levels.

Multiple studies have explored the influence of record length on event magnitudes (Genest et al., 2009; Su and Tung, 2013; Tong et al., 2015; Sadegh et al., 2017; Dodangeh et al., 2019; Lucey and Gallien, 2023), but examination of event magnitude flooding outcomes is novel. Similar to Lucey and Gallien (2023), event estimates from shorter record lengths increase variability. In this study, utilizing longer records ($\geq$70 years) constrained estimates (Figure 5.10). The maximum difference in flood depth between subsets changes from 30 cm to 8 cm when using 20- (Figure 5.11a) and 90-year (Figure 5.11b) subsets indicating significant variability per grid cell. Figure 5.11a (10-year event with 20-year subsets) has a range of 93,600 m^2 of flooding, and multiple zones indicating significant changes to the maximum flood depths. Figure 5.11b (10-year event with 90-year subsets) has a range of 14,413 m^2 of flooding, and most of the domain indicates minor changes to flood depth.

Additional sources of uncertainty exist beyond the scope of this particular study. For example, numerical model inputs (e.g., topography, bathymetry, flood protection infrastructure operation) are known to contribute to flood map uncertainty (Coveney and Fotheringham, 2011; Bates et al., 2014; Sampson et al., 2014; Saint-Geours et al., 2015). Future work quantifying flood map uncertainties and investigating uncertainty bounds within hybrid statistical-numerical modeling studies should be undertaken. Waves can contribute to significant flooding (Erikson et al., 2018; Gallien et al., 2018; Lucey and Gallien, 2023) and should be accounted for in areas where they affect flooding. Integrating overland flows and wave overtopping (Smith et al., 2012; Wadey et al., 2012; Gallien, 2016; Gallien et al., 2018)

into coupled hydrodynamic models is necessary to consider the role wave related flooding in compound events. Stationarity had been a typical assumption when conducting frequency analysis studies. Accounting for non-stationarity is critical for future work as it amplifies flood risk estimate uncertainties (Naseri and Hummel, 2022).

5.6 Conclusions

This work utilized a statistical-modeling hybrid framework to determine univariate and bivariate (compound) observed water level and precipitation flooding events in highly urbanized coastal regions while quantifying uncertainties in model flood estimates originating from coupla choice, sampling methods, record length, and event choice. Copulas passing a Cramér-von Misses test resulted in similar event estimates, translating into model flood estimates with negligible differences. The BB5 copuls consistently provided the most conservative (i.e., largest) events compared with other copulas. Event estimates were created with an annual maximum, annual coinciding, wet season monthly maximum, and wet season monthly coinciding. Annual type events produced larger precipitation estimates resulting in larger flood estimates even when other sampling methods had larger observed water level estimates. Utilizing data records of at least 70-years resulted in minimal event estimate variability and significant reductions in modeled flood extent and depth.

Flood estimates vary widely depending on the event choice along an isoline. Modeled results were noticeably greater when precipitation estimates were larger, suggesting the dominant role of precipitation in urban flooding (Gaitan et al., 2016; Huang et al., 2018; Vorobevskii et al., 2020). However, drainage infrastructure alters flood estimates (Gallien et al., 2011, 2014; Shen et al., 2019; Rong et al., 2020), and future work must account for urban drainage infrastructure to improve the accuracy of flood model estimates and quantification of errors attributed to uncertainty sources. Additionally, wave events occur within limited time windows and their flooding outcomes are predicated on marine water levels.

Research is needed to determine appropriate time sampling windows for transient events. Future work should consider the possibility of compounding or amplifying uncertainties due to non-stationary data (Naseri and Hummel, 2022), model inputs (Coveney and Fotheringham, 2011; Bates et al., 2014; Sampson et al., 2014; Saint-Geours et al., 2015), or coinciding critical uncertainty sources (e.g., minimal data records for a non-stationary variable) within a study.

5.7 Data Availability

NOAA precipitation data is available for download at `https://www.ncei.noaa.gov/maps/alltimes/`. NOAA DEM data (topography, bathymetry, areal imagery) is available for download at NOAA's Digital Coast: Data Access Viewer (`https://coast.noaa.gov/dataviewer/#/lidar/search/where:ID=8658`). Tidal data is available for download on NOAA's Tides & Currents website (`https://tidesandcurrents.noaa.gov`).

CHAPTER 6

Conclusions and Future Work

Coastal flooding caused by precipitation, observed water levels, and waves were assessed at highly urbanized coastal communities while accounting for uncertainties and quantifying the implications of methodologies. A hybrid statistical-numerical modeling framework was developed to quantify statistical characterization impacts on flooding outcomes. Uncertainties stemming from copula choice, sampling methods, record length, selected rainfall gauge, and event choice were considered. Previous studies typically relied upon a small number of copulas (e.g. Clayton, Frank, Gumbel, Student t, and Gaussian) for multivariate flood risk assessments, but copulas such as the Nelsen, BB1, BB5, and Roch-Alegre passed Cramér-von Misses tests indicating alternative copulas may be more appropriate for coastal flood hazards. Utilizing copulas passing a Cramér-von Misses test to determine event or flood estimates present similar results suggesting a number of potential copulas may provide for a robust multivariate analysis. Certain copulas, such as the BB5 copula, produce more conservative event and flood estimates and future work should identify which copulas best characterize coastal flooding in wave and tidally dominated applications.

Sampling methods imparted a critical source of uncertainty. Various sampling methods were employed: annual maximum, annual coinciding, wet season monthly maximum, and wet season monthly coinciding. An annual maximum sampling is commonly used in practice (FEMA, 2011, 2016c) and studies (e.g., Baratti et al., 2012; Bezak et al., 2014; Wahl et al., 2015), but may not characterize severe flooding potential. Annual coinciding sampling repeatedly resulted in lower observed water level estimates compared to estimates made with

other sampling methods. Utilizing sampling methods with higher sampling frequencies (i.e., wet season type samplings) benefit from additional data pairs potentially improving the characterization of event dependencies. However, modeling events generated form various sampling methods showed that events with larger precipitation estimates resulted in larger flooding metrics. The largest flood events were produced with annual type samplings.

Available record length imparted the most uncertainty into both flood event pairs and the resulting flood maps. Event estimates had significant variability when utilizing minimal data records (< 70 years), but were well constrained when using at least 70-years of records. Using longer data records further translated to significant reductions in model flood variability across the domain and at each grid cell. Novel to this work, microclimates were suspected to drive the differences between local event estimates and the disagreement between local estimates present data source, in this case chosen rainfall gauge, as a critical source of uncertainty. Additionally, event and model flood estimates greatly varied depending on the utilized event pair along an isoline.

While critical sources of uncertainty were quantified, other factors need to be accounted for in future studies. Flooding results were greater when precipitation estimates were larger, suggesting a dominant role of precipitation in urban flooding (Gaitan et al., 2016; Huang et al., 2018; Vorobevskii et al., 2020). Exclusion of drainage infrastructure is a limitation of this work and deserves consideration since it is known to control flood development (Gallien et al., 2011, 2014; Shen et al., 2019; Rong et al., 2020). Sea level rise will increase and intensify both tidal and wave driven flooding (e.g., Tang and Gallien, 2023). Waves significantly impact event estimates (Serafin et al., 2017; Reguero et al., 2019). Explicitly accounting for wave impacts is critical to characterizing coastal flooding (e.g., Erikson et al., 2018; Gallien et al., 2018; Barnard et al., 2019). Long term, vulnerable coastal sites may shift from pluvial to marine dominated flooding and highlight the critical need to consider non-stationarity. Other sources of uncertainty (e.g., ENSO influence, topobathy inputs, event window timing) should also be accounted for in future work. Hybrid statistical-numerical frameworks must

continue to be applied to environments with different dominate flood drivers and studies should explore their benefits over traditional statistical or numerical modeling methods.

CHAPTER 7

Appendix

7.1 Additional Information for Chapter 3

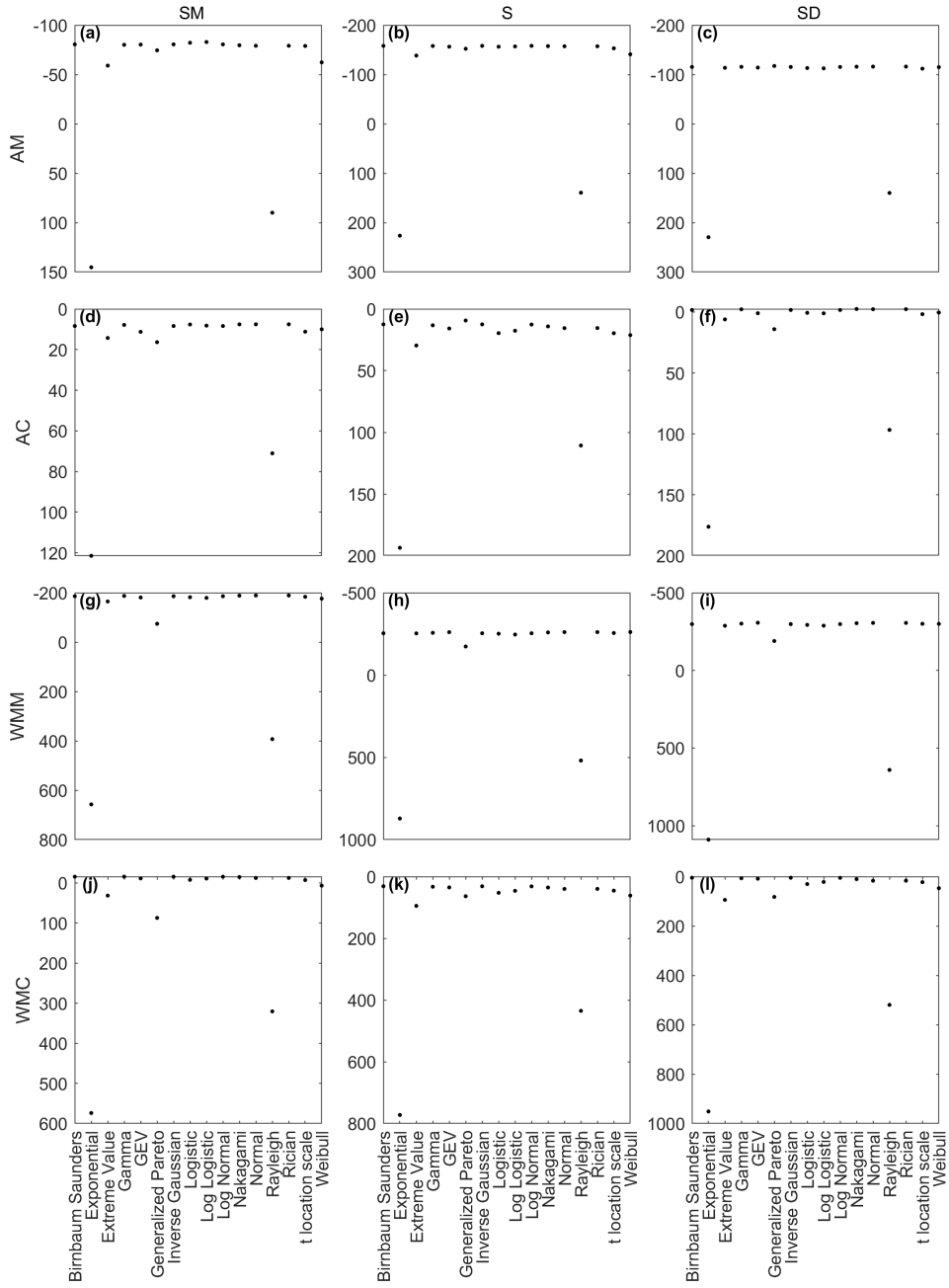

Figure 7.1: Marginal OWL BIC values per fitted copula for Santa Monica (left column), Sunset (middle column), and San Diego (right column) using (a)(b)(c) annual maximum, (d)(e)(f) annual coinciding, (g)(h)(i) wet season monthly maximum, and (j)(k)(l) wet season monthly coinciding. The Y-axis is orientated to display best BIC (top) to worse BIC (bottom).

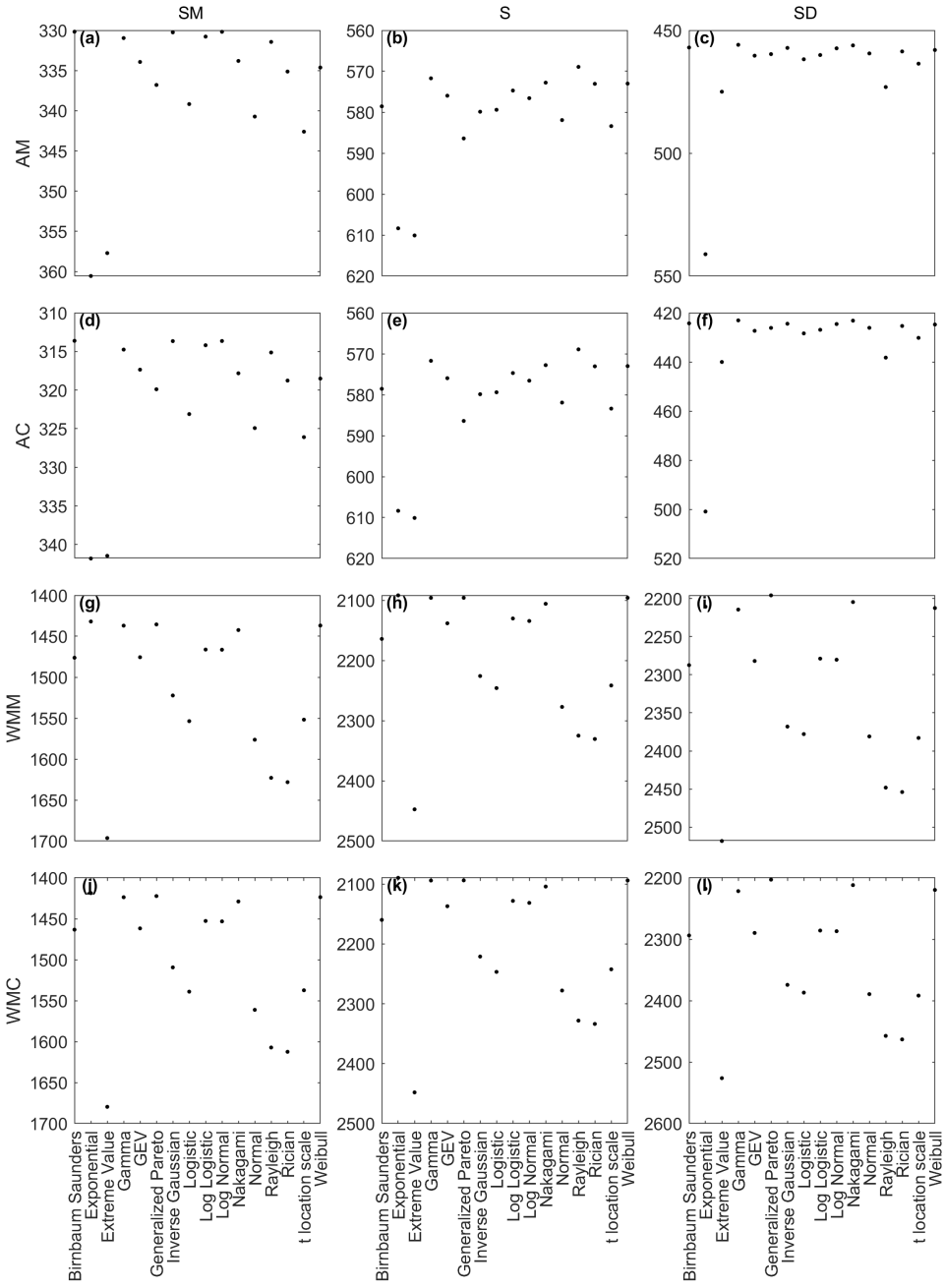

Figure 7.2: Marginal precipitation BIC values per fitted copula for Santa Monica (left column), Sunset (middle column), and San Diego (right column) using (a)(b)(c) annual maximum, (d)(e)(f) annual coinciding, (g)(h)(i) wet season monthly maximum, and (j)(k)(l) wet season monthly coinciding. The Y-axis is orientated to display best BIC (top) to worse BIC (bottom).

7.2 Additional Information for Chapter 4

Table 7.1: Fitted observed (OWL) and total water level (TWL), and precipitation (P) univariate distributions using annual maximum (AM) and coinciding (AC), and wet season monthly maximum (WMM) and coinciding (WMC) samplings. San Francisco marginals were fitted when using the 100-year record. Distributions with an star (*) indicate fits with below standard levels of significance ($\alpha < 0.05$).

OWL-P					
Sampling	Variable	San Francisco	Torrance	Long Beach	San Diego
AM	OWL	L	BS	BS	Normal
	P	L	BS	L	Logistic
AC	OWL	Nakagami	Weibull	Nakagami	Gamma
	P	L	BS	L	Logistic
WMM	OWL	Gamma	Normal*	GEV	Normal
	P	Nakagami*	GP*	GP	GP
WMC	OWL	Gamma	BS*	Gamma*	GP*
	P	Nakagami*	GP*	GP	GP
TWL-P					
AM	TWL	-	IG*	IG	IG
	P	-	BS	L	Logistic
AC	TWL	-	GP*	L	L
	P	-	BS	L	Logistic
WMM	TWL	-	GEV	GEV	GEV
	P	-	Exponential	GP	GP
WMC	TWL	-	LN	L	L
	P	-	Exponential	GP	GP

BS - Birnbaum-Saunders; GP - Generalized Pareto; L - Log logistic

LN - Log Normal; GEV - Generalized Extreme Value; IG - Inverse Gaussian

Table 7.2: The periods used for the 90-, 80-, 70-, 50-, 30-, and 20-years of subsets created from the original San Francisco record. There are ten different periods per subset length.

Subset size (years)	Periods
90	1931-2021, 1921-1930 and 1941-2021, 1921-1940 and 1951-2021, 1921-1950 and 1961-2021, 1921-1960 and 1972-2021, 1921-1970 and 1982-2021, 1921-1981 and 1992-2021, 1921-1991 and 2002-2021, 1921-2001 and 2012-2021, 1921-2011
80	1941-2021, 1921-1930 and 1951-2021, 1921-1940 and 1961-2021, 1921-1950 and 1972-2021, 1921-1960 and 1982-2021, 1921-1965 and 1987-2021, 1921-1970 and 1992-2021, 1921-1981 and 2002-2021, 1921-1991 and 2012-2021, 1921-2001
70	1951-2021, 1921-1930 and 1961-2021, 1921-1935 and 1966-2021, 1921-1940 and 1972-2021, 1921-1945 and 1977-2021, 1921-1950 and 1982-2021, 1921-1960 and 1992-2021, 1921-1970 and 2002-2021, 1921-1981 and 2012-2021, 1921-1991
50	1921-1970, 1926-1976, 1931-1981, 1941-1991, 1946-1996, 1951-2001, 1956-2006, 1961-2011, 1966-2016, 1972-2021
30	1921-1950, 1931-1960, 1936-1965, 1941-1970, 1951-1981, 1961-1991, 1972-2001, 1982-2011, 1987-2016, 1992-2021
20	1921-1940, 1931-1950, 1941-1960, 1951-1970, 1961-1981, 1972-1991, 1982-2001, 1987-2006, 1992-2011, 2002-2021

7.3 Additional Information for Chapter 5

Table 7.3: Best fitting observed water level (OWL) and precipitation (P) univariate distributions for each location using annual maximum (AM), annual coinciding (AC), wet season monthly coinciding (WMM), and wet season monthly coinciding (WMC) samplings. Distributions with a star (*) indicate the distribution did not have standard levels of significance ($p \leq 0.05$).

Sampling	Variable	Long Beach-Sunset	Newport
AM	OWL	BS	BS
	P	L	G
AC	OWL	NA	GP*
	P	L	G
WMM	OWL	GEV	N*
	P	GP	GP*
WMC	OWL	G*	G*
	P	GP	GP*

BS - Birnbaum-Saunders; GP - Generalized Pareto; G - Gamma
N - Normal; L - Log logistic; NA - Nakagami

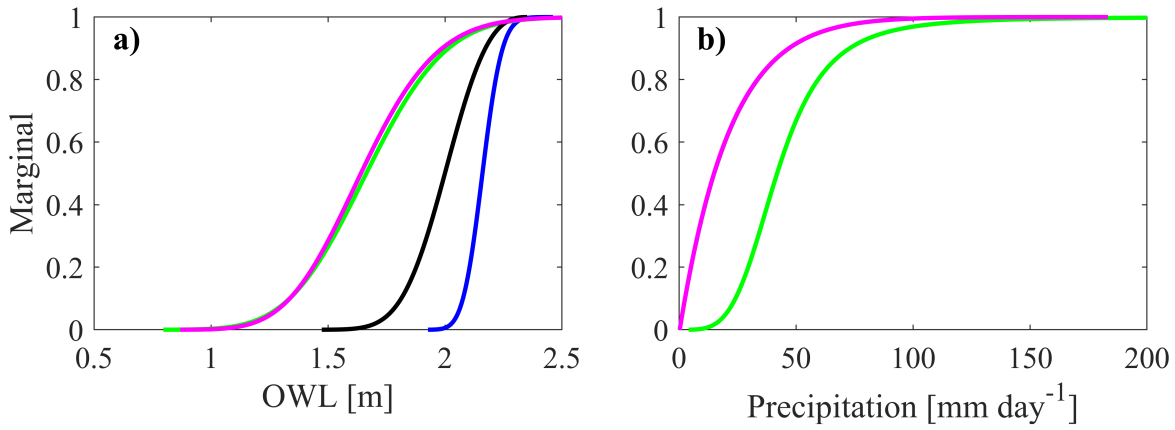

Figure 7.3: Univariate cumulative distribution function plots for observed water level (OWL) and precipitation (P) at Long Beach using an annual maximum (AM; blue), annual coinciding (AC; green), wet season monthly coinciding (WMM; black), and wet season monthly coinciding (WMC; magenta) sampling.

Table 7.4: 10- and 100-year events for marginal, observed water levels (OWL) and precipitation (P), and compound events (AND) using annual maximum (AM), annual coinciding (AC), wet season monthly maximum (WMM), and wet season monthly coinciding (WMC) samplings at Sunset Beach. Compound events were created using the Nelsen copula passing a Cramér-von Misses test.

	OWL [m]		P [mmday^{-1}]	
Sampling	10	100	10	100
AND				
AM	2.21	2.26	55.87	81.27
AC	1.84	2.07	54.96	80.12
WMM	2.16	2.23	44.10	66.46
WMC	1.96	2.14	43.98	66.30
Marginal				
AM	2.25	2.32	72.89	133.30
AC	2.01	2.32	72.89	133.30
WMM	2.25	2.31	76.66	113.87
WMC	2.22	2.49	76.70	114.05

Table 7.5: 10- and 100-year events for marginal (Uni.), observed water levels (OWL) and precipitation (P), and compound events using an annual coinciding sampling at Sunset Beach. Compound events were created using a Clayton, Nelsen, Roch-Alegre (Roch.), Fischer-Kock (Fisc.), BB1, and BB5 copula passing a Cramér-von Misses test for one or more cases.

	OWL		P	
	[m]		[mmday^{-1}]	
Sampling	10	100	10	100
Clayton	1.82	2.04	53.93	76.66
Nelsen	1.84	2.07	54.96	80.12
Roch.	1.83	2.06	54.69	78.75
Fisc.	1.84	2.06	54.57	78.68
BB1	1.83	2.09	54.31	83.95
BB5	1.85	2.16	56.29	96.44
Uni.	2.01	2.32	72.89	133.30

Bibliography

Aghakouchak, A.: Entropy copula in hydrology and climatology, Journal of Hydrometeorology, 15, 2176–2189, 2014.

Akoh, R., Ishikawa, T., Kojima, T., Tomaru, M., and Maeno, S.: High-resolution modeling of tsunami run-up flooding: a case study of flooding in Kamaishi city, Japan, induced by the 2011 Tohoku tsunami, Natural Hazards and Earth System Sciences, 17, 1871–1883, 2017.

Allan, J. C. and Komar, P. D.: Climate controls on US West Coast erosion processes, Journal of coastal research, 22, 511–529, 2006.

Anandalekshmi, A., Panicker, S. T., Adarsh, S., Siddik, A. M., Aloysius, S., and Mehjabin, M.: Modeling the concurrent impact of extreme rainfall and reservoir storage on Kerala floods 2018: a Copula approach, Modeling Earth Systems and Environment, 5, 1283–1296, 2019.

Arega, F. and Sanders, B. F.: Dispersion model for tidal wetlands, Journal of Hydraulic Engineering, 130, 739–754, 2004.

Ayantobo, O. O., Wei, J., and Wang, G.: Modeling Joint Relationship and Design Scenarios Between Precipitation, Surface Temperature, and Atmospheric Precipitable Water Over Mainland China, Earth and Space Science, 8, e2020EA001 513, 2021.

Baratti, E., Montanari, A., Castellarin, A., Salinas, J., Viglione, A., and Bezzi, A.: Estimating the flood frequency distribution at seasonal and annual time scales., Hydrology & Earth System Sciences, 16, 2012.

Barnard, P. L., Erikson, L. H., Foxgrover, A. C., Hart, J. A. F., Limber, P., O'Neill, A. C., van Ormondt, M., Vitousek, S., Wood, N., Hayden, M. K., et al.: Dynamic flood modeling essential to assess the coastal impacts of climate change, Scientific reports, 9, 1–13, 2019.

Barry, R. G. and Blanken, P. D.: Microclimate and local climate, Cambridge University Press, 2016.

Bates, P. D., Dawson, R. J., Hall, J. W., Horritt, M. S., Nicholls, R. J., Wicks, J., and Hassan, M. A. A. M.: Simplified two-dimensional numerical modelling of coastal flooding and example applications, Coastal Engineering, 52, 793–810, 2005.

Bates, P. D., Pappenberger, F., and Romanowicz, R. J.: Uncertainty in flood inundation modelling, in: Applied uncertainty analysis for flood risk management, pp. 232–269, 2014.

Beck, H. E., Zimmermann, N. E., McVicar, T. R., Vergopolan, N., Berg, A., and Wood, E. F.: Present and future Köppen-Geiger climate classification maps at 1-km resolution, Scientific data, 5, 1–12, 2018.

Bell, J. E., Herring, S. C., Jantarasami, L., Adrianopoli, C., Benedict, K., Conlon, K., Escobar, V., Hess, J., Luvall, J., Garcia-Pando, C., et al.: Ch. 4: Impacts of extreme events on human health, Tech. rep., US Global Change Research Program, Washington, DC, 2016.

Bernatchez, P., Fraser, C., Lefaivre, D., and Dugas, S.: Integrating anthropogenic factors, geomorphological indicators and local knowledge in the analysis of coastal flooding and erosion hazards, Ocean & Coastal Management, 54, 621–632, 2011.

Bevacqua, E., Maraun, D., Vousdoukas, M. I., Voukouvalas, E., Vrac, M., Mentaschi, L., and Widmann, M.: Higher probability of compound flooding from precipitation and storm surge in Europe under anthropogenic climate change, Science advances, 5, eaaw5531, 2019.

Bevacqua, E., Vousdoukas, M. I., Zappa, G., Hodges, K., Shepherd, T. G., Maraun, D., Mentaschi, L., and Feyen, L.: More meteorological events that drive compound coastal flooding are projected under climate change, Communications earth & environment, 1, 1–11, 2020.

Bezak, N., Brilly, M., and Šraj, M.: Comparison between the peaks-over-threshold method and the annual maximum method for flood frequency analysis, Hydrological Sciences Journal, 59, 959–977, 2014.

Bray, S. N. and McCuen, R. H.: Importance of the assumption of independence or dependence among multiple flood sources, Journal of Hydrologic Engineering, 19, 1194–1202, 2014.

Brown, J. D., Spencer, T., and Moeller, I.: Modeling storm surge flooding of an urban area with particular reference to modeling uncertainties: A case study of Canvey Island, United Kingdom, Water Resources Research, 43, 2007.

Cañizares, R. and Irish, J. L.: Simulation of storm-induced barrier island morphodynamics and flooding, Coastal Engineering, 55, 1089–1101, 2008.

Cayan, D. R. and Roads, J. O.: Local relationships between United States West Coast precipitation and monthly mean circulation parameters, Monthly Weather Review, 112, 1276–1282, 1984.

Cea, L., French, J., and Vázquez-Cendón, M.: Numerical modelling of tidal flows in complex estuaries including turbulence: An unstructured finite volume solver and experimental validation, International Journal for Numerical Methods in Engineering, 67, 1909–1932, 2006.

Chen, W.-B. and Liu, W.-C.: Modeling flood inundation induced by river flow and storm surges over a river basin, Water, 6, 3182–3199, 2014.

Chen, Y., Li, J., Pan, S., Gan, M., Pan, Y., Xie, D., and Clee, S.: Joint probability analysis of extreme wave heights and surges along China's coasts, Ocean Engineering, 177, 97–107, 2019.

Church, J., Clark, P., Cazenave, A., Gregory, J., Jevrejeva, S., Levermann, A., Merrifield, M., Milne, G., Nerem, R., Nunn, P., Payne, A., Pfeffer, W., Stammer, D., and Unnikrishnan, A.: Sea Level Change, in: Climate Change 2013: The Physical Science Basis. Contribution of Working Group I to the Fifth Assessment Report of the Intergovernmental Panel on Climate Change, edited by Stocker, T., Qin, D., Plattner, G.-K., Tignor, M., Allen, S., Boschung, J., Nauels, A., Xia, Y., Bex, V., and Midgley, P., pp. 1137–1216, Cambridge University Press, Cambridge, United Kingdom and New York, NY, USA, 2013.

Conil, S. and Hall, A.: Local regimes of atmospheric variability: A case study of Southern California, Journal of Climate, 19, 4308–4325, 2006.

Corbella, S. and Stretch, D.: Multivariate return periods of sea storms for coastal erosion risk assessment, Natural Hazards and Earth System Sciences, 12, 2699–2708, 2012.

Couasnon, A., Sebastian, A., and Morales-Nápoles, O.: A copula-based Bayesian network for modeling compound flood hazard from riverine and coastal interactions at the catchment scale: An application to the Houston Ship Channel, Texas, Water, 10, 1190, 2018.

Couasnon, A., Eilander, D., Muis, S., Veldkamp, T. I., Haigh, I. D., Wahl, T., Winsemius, H. C., and Ward, P. J.: Measuring compound flood potential from river discharge and storm surge extremes at the global scale, Natural Hazards and Earth System Sciences, 20, 489–504, 2020.

Couasnon, A., Scussolini, P., Tran, T., Eilander, D., Muis, S., Wang, H., Keesom, J., Dullaart, J., Xuan, Y., Nguyen, H., et al.: A flood risk framework capturing the seasonality of and dependence between rainfall and sea levels–an application to Ho Chi Minh City, Vietnam, Water Resources Research, p. e2021WR030002, 2022.

Coveney, S. and Fotheringham, A. S.: The impact of DEM data source on prediction of flooding and erosion risk due to sea-level rise, International Journal of Geographical Information Science, 25, 1191–1211, 2011.

Dawson, R. J., Dickson, M. E., Nicholls, R. J., Hall, J. W., Walkden, M. J., Stansby, P. K., Mokrech, M., Richards, J., Zhou, J., Milligan, J., et al.: Integrated analysis of risks of coastal flooding and cliff erosion under scenarios of long term change, Climatic Change, 95, 249–288, 2009.

De Michele, C. and Salvadori, G.: A generalized Pareto intensity-duration model of storm rainfall exploiting 2-copulas, Journal of Geophysical Research: Atmospheres, 108, 2003.

De Michele, C., Salvadori, G., Canossi, M., Petaccia, A., and Rosso, R.: Bivariate statistical approach to check adequacy of dam spillway, Journal of Hydrologic Engineering, 10, 50–57, 2005.

De Michele, C., Salvadori, G., Passoni, G., and Vezzoli, R.: A multivariate model of sea storms using copulas, Coastal Engineering, 54, 734–751, 2007.

DeGroot, M. H. and Schervish, M. J.: Probability and Statistics, Pearson Education, 4 edn., 2014.

Didier, D., Baudry, J., Bernatchez, P., Dumont, D., Sadegh, M., Bismuth, E., Bandet, M., Dugas, S., and Sévigny, C.: Multihazard simulation for coastal flood mapping: Bathtub versus numerical modelling in an open estuary, Eastern Canada, Journal of Flood Risk Management, 12, e12 505, 2019.

Dodangeh, E., Shahedi, K., Solaimani, K., Shiau, J.-T., and Abraham, J.: Data-based bivariate uncertainty assessment of extreme rainfall-runoff using copulas: comparison between annual maximum series (AMS) and peaks over threshold (POT), Environmental monitoring and assessment, 191, 1–18, 2019.

Engeland, K., Hisdal, H., and Frigessi, A.: Practical extreme value modelling of hydrological floods and droughts: a case study, Extremes, 7, 5–30, 2004.

Erikson, L. H., Espejo, A., Barnard, P. L., Serafin, K. A., Hegermiller, C. A., O'Neill, A., Ruggiero, P., Limber, P. W., and Mendez, F. J.: Identification of storm events and contiguous coastal sections for deterministic modeling of extreme coastal flood events in response to climate change, Coastal Engineering, 140, 316–330, 2018.

Esberto, M. D. P.: Probability Distribution Fitting of Rainfall Patterns in Philippine Regions for Effective Risk Management, Environment and Ecology Research, 6, 178–86, 2018.

Favre, A.-C., El Adlouni, S., Perreault, L., Thiémonge, N., and Bobée, B.: Multivariate hydrological frequency analysis using copulas, Water resources research, 40, 2004.

FEMA: Coastal construction manual: Principles and practices of planning, siting, designing, constructing, and maintaining residential buildings in coastal areas, 2011.

FEMA: Guidance for Flood Risk Analysis and Mapping; Combined Coastal and Riverine Floodplain, 2015.

FEMA: Guidance for Flood Risk Analysis and Mapping: Coastal Water Levels, https://www.fema.gov/sites/default/files/2020-02/Coastal_Wate_Levels_Guidance_May_2016.pdf, 2016a.

FEMA: Guidance for Flood Risk Analysis and Mapping: Statistical Simulation Methods, https://www.fema.gov/sites/default/files/documents/fema_coastal-statistical-simulation-methods_nov-2016.pdf, 2016b.

FEMA: Guidance for Flood Risk Analysis and Mapping: Coastal Flood Frequency and Extreme Value Analysis, https://www.fema.gov/sites/default/files/2020-02/Coastal_Flood_Frequency_and_Extreme_Value_Analysis_Guidance_Nov_2016.pdf, 2016c.

FEMA: Guidance for Flood Risk Analysis and Mapping: Combined Coastal and River-

ine Floodplain, https://www.fema.gov/sites/default/files/documents/coastal_riverine_guidance_dec_2020.pdf, 2020.

Fewtrell, T. J., Duncan, A., Sampson, C. C., Neal, J. C., and Bates, P. D.: Benchmarking urban flood models of varying complexity and scale using high resolution terrestrial LiDAR data, Physics and Chemistry of the Earth, Parts A/B/C, 36, 281–291, 2011.

Flick, R. E.: A comparison of California tides, storm surges, and mean sea level during the El Niño winters of 1982-83 and 1997-98, Shore & Beach, 66, 7–11, 1998.

Flick, R. E.: California tides, sea level, and waves—Winter 2015-2016, Shore & Beach, 84, 25–30, 2016.

Gaitan, S., Van de Giesen, N., and Ten Veldhuis, J.: Can urban pluvial flooding be predicted by open spatial data and weather data?, Environmental Modelling & Software, 85, 156–171, 2016.

Gallegos, H. A., Schubert, J. E., and Sanders, B. F.: Two-dimensional, high-resolution modeling of urban dam-break flooding: A case study of Baldwin Hills, California, Advances in water resources, 32, 1323–1335, 2009.

Gallien, T.: Validated coastal flood modeling at Imperial Beach, California: Comparing total water level, empirical and numerical overtopping methodologies, Coastal Engineering, 111, 95–104, 2016.

Gallien, T., Schubert, J., and Sanders, B.: Predicting tidal flooding of urbanized embayments: A modeling framework and data requirements, Coastal Engineering, 58, 567–577, 2011.

Gallien, T., Sanders, B., and Flick, R.: Urban coastal flood prediction: Integrating wave overtopping, flood defenses and drainage, Coastal Engineering, 91, 18–28, 2014.

Gallien, T., O'Reilly, W., Flick, R., and Guza, R.: Geometric properties of anthropogenic flood control berms on southern California beaches, Ocean & Coastal Management, 105, 35–47, 2015.

Gallien, T., Kalligeris, N., Delisle, M., Tang, B., Lucey, J., and Winters, M.: Coastal flood modeling challenges in defended urban backshores, Geosciences, 8, 450, 2018.

Ganguli, P. and Merz, B.: Trends in compound flooding in northwestern Europe during 1901–2014, Geophysical Research Letters, 46, 10 810–10 820, 2019a.

Ganguli, P. and Merz, B.: Extreme coastal water levels exacerbate fluvial flood hazards in Northwestern Europe, Scientific reports, 9, 1–14, 2019b.

Ganguli, P. and Reddy, M. J.: Probabilistic assessment of flood risks using trivariate copulas, Theoretical and applied climatology, 111, 341–360, 2013.

Ganguli, P., Paprotny, D., Hasan, M., Güntner, A., and Merz, B.: Projected changes in compound flood hazard from riverine and coastal floods in northwestern Europe, Earth's Future, 8, e2020EF001 752, 2020.

Genest, C., Rémillard, B., and Beaudoin, D.: Goodness-of-fit tests for copulas: A review and a power study, Insurance: Mathematics and economics, 44, 199–213, 2009.

Ghanbari, M., Arabi, M., Kao, S.-C., Obeysekera, J., and Sweet, W.: Climate Change and Changes in Compound Coastal-Riverine Flooding Hazard Along the US Coasts, Earth's Future, p. e2021EF002055, 2021.

Gräler, B., van den Berg, M., Vandenberghe, S., Petroselli, A., Grimaldi, S., De Baets, B., and Verhoest, N.: Multivariate return periods in hydrology: a critical and practical review focusing on synthetic design hydrograph estimation, Hydrology and Earth System Sciences, 17, 1281–1296, 2013.

Gregory, J. M., Griffies, S. M., Hughes, C. W., Lowe, J. A., Church, J. A., Fukimori, I., Gomez, N., Kopp, R. E., Landerer, F., Le Cozannet, G., et al.: Concepts and terminology for sea level: Mean, variability and change, both local and global, Surveys in Geophysics, 40, 1251–1289, 2019.

Guirguis, K. J. and Avissar, R.: A precipitation climatology and dataset intercomparison for the western United States, Journal of Hydrometeorology, 9, 825–841, 2008.

Han, J.-Y., Baik, J.-J., and Lee, H.: Urban impacts on precipitation, Asia-Pacific Journal of Atmospheric Sciences, 50, 17–30, 2014.

Hanson, L. S. and Vogel, R.: The probability distribution of daily rainfall in the United States, in: World Environmental and Water Resources Congress 2008: Ahupua'A, pp. 1–10, 2008.

Hanson, S., Nicholls, R., Ranger, N., Hallegatte, S., Corfee-Morlot, J., Herweijer, C., and Chateau, J.: A global ranking of port cities with high exposure to climate extremes, Climatic change, 104, 89–111, 2011.

Hao, Z. and Singh, V. P.: Compound Events under Global Warming: A Dependence Perspective, Journal of Hydrologic Engineering, 25, 03120 001, 2020.

Hawkes, P. J.: Joint probability analysis for estimation of extremes, Journal of Hydraulic Research, 46, 246–256, 2008.

Hawkes, P. J., Gouldby, B. P., Tawn, J. A., and Owen, M. W.: The joint probability of waves and water levels in coastal engineering design, Journal of hydraulic research, 40, 241–251, 2002.

Heberger, M., Cooley, H., Herrera, P., Gleick, P. H., and Moore, E.: Potential impacts of increased coastal flooding in California due to sea-level rise, Climatic Change, 109, 229–249, 2011.

Herdman, L., Erikson, L., and Barnard, P.: Storm surge propagation and flooding in small tidal rivers during events of mixed coastal and fluvial influence, Journal of Marine Science and Engineering, 6, 158, 2018.

Horstman, E., Dohmen-Janssen, M., and Hulscher, S.: Modeling tidal dynamics in a mangrove creek catchment in Delft3D, in: Coastal dynamics, vol. 2013, pp. 833–844, 2013.

Horton, B. P., Rahmstorf, S., Engelhart, S. E., and Kemp, A. C.: Expert assessment of sea-level rise by AD 2100 and AD 2300, Quaternary Science Reviews, 84, 1–6, 2014.

Huang, H., Chen, X., Zhu, Z., Xie, Y., Liu, L., Wang, X., Wang, X., and Liu, K.: The changing pattern of urban flooding in Guangzhou, China, Science of the Total Environment, 622, 394–401, 2018.

Huong, H. T. L. and Pathirana, A.: Urbanization and climate change impacts on future urban flooding in Can Tho city, Vietnam, Hydrology and Earth System Sciences, 17, 379–394, 2013.

Husak, G. J., Michaelsen, J., and Funk, C.: Use of the gamma distribution to represent monthly rainfall in Africa for drought monitoring applications, International Journal of Climatology: A Journal of the Royal Meteorological Society, 27, 935–944, 2007.

Irish, J. L. and Cañizares, R.: Storm-wave flow through tidal inlets and its influence on bay flooding, Journal of waterway, port, coastal, and ocean engineering, 135, 52–60, 2009.

Jane, R., Cadavid, L., Obeysekera, J., and Wahl, T.: Multivariate statistical modelling of the drivers of compound flood events in South Florida, Natural Hazards and Earth System Sciences Discussions, pp. 1–30, 2020.

Jarušková, D. and Hanek, M.: Peaks over threshold method in comparison with block-maxima method for estimating high return levels of several Northern Moravia precipitation and discharges series, Journal of Hydrology and Hydromechanics, 54, 309–319, 2006.

Jeong, D. I., Sushama, L., Khaliq, M. N., and Roy, R.: A copula-based multivariate analysis of Canadian RCM projected changes to flood characteristics for northeastern Canada, Climate dynamics, 42, 2045–2066, 2014.

Johnson, D. R.: Improved methods for estimating flood depth exceedances within storm surge protection systems, Risk Analysis, 39, 890–905, 2019.

Karmakar, S. and Simonovic, S.: Bivariate flood frequency analysis. Part 2: a copula-based approach with mixed marginal distributions, Journal of Flood Risk Management, 2, 32–44, 2009.

Kim, Y.-T., Park, J.-H., Choi, B.-H., Kim, D. H., and Kwon, H.-H.: A Bivariate Frequency Analysis of Extreme Wave Heights and Periods Using a Copula Function in South Korea, Journal of Coastal Research, pp. 566–570, 2018.

Knowles, N.: Potential inundation due to rising sea levels in the San Francisco Bay region, San Francisco Estuary and Watershed Science, 8, 2010.

Kramer, S. C. and Stelling, G. S.: A conservative unstructured scheme for rapidly varied flows, International journal for numerical methods in fluids, 58, 183–212, 2008.

Kumbier, K., Carvalho, R. C., Vafeidis, A. T., and Woodroffe, C. D.: Investigating compound flooding in an estuary using hydrodynamic modelling: a case study from the Shoalhaven River, Australia, Natural Hazards and Earth System Sciences, 18, 463–477, 2018.

Leonard, M., Westra, S., Phatak, A., Lambert, M., van den Hurk, B., McInnes, K., Risbey, J., Schuster, S., Jakob, D., and Stafford-Smith, M.: A compound event framework for understanding extreme impacts, Wiley Interdisciplinary Reviews: Climate Change, 5, 113–128, 2014.

Li, T., Guo, S., Chen, L., and Guo, J.: Bivariate flood frequency analysis with historical information based on copula, Journal of Hydrologic Engineering, 18, 1018–1030, 2013.

Lian, J., Xu, K., and Ma, C.: Joint impact of rainfall and tidal level on flood risk in a coastal city with a complex river network: a case study of Fuzhou City, China, Hydrology and Earth System Sciences, 17, 679, 2013.

Liu, Z., Cheng, L., Hao, Z., Li, J., Thorstensen, A., and Gao, H.: A framework for exploring joint effects of conditional factors on compound floods, Water Resources Research, 54, 2681–2696, 2018.

Lucey, J. T. D. and Gallien, T. W.: Characterizing multivariate coastal flooding events in a semi-arid region: the implications of copula choice, sampling, and infrastructure, Natural Hazards and Earth System Sciences, 22, 2145–2167, https://doi.org/10.5194/nhess-22-2145-2022, 2022.

Lucey, J. T. D. and Gallien, T. W.: Quantifying compound flood event uncertainties in a wave and tidally dominated coastal region: The impacts of copula selection, sampling, record length, and precipitation gauge selection (in review), Flood Risk Management, 2023.

Ludka, B. C., Guza, R. T., and O'Reilly, W.: Nourishment evolution and impacts at four southern California beaches: A sand volume analysis, Coastal Engineering, 136, 96–105, 2018.

Marcos, M., Rohmer, J., Vousdoukas, M. I., Mentaschi, L., Le Cozannet, G., and Amores, A.: Increased extreme coastal water levels due to the combined action of storm surges and wind waves, Geophysical Research Letters, 46, 4356–4364, 2019.

Martinelli, L., Zanuttigh, B., and Corbau, C.: Assessment of coastal flooding hazard along the Emilia Romagna littoral, IT, Coastal Engineering, 57, 1042–1058, 2010.

Martyr-Koller, R., Kernkamp, H., Van Dam, A., Van Der Wegen, M., Lucas, L., Knowles, N., Jaffe, B., and Fregoso, T.: Application of an unstructured 3D finite volume numerical

model to flows and salinity dynamics in the San Francisco Bay-Delta, Estuarine, Coastal and Shelf Science, 192, 86–107, 2017.

Masina, M., Lamberti, A., and Archetti, R.: Coastal flooding: A copula based approach for estimating the joint probability of water levels and waves, Coastal Engineering, 97, 37–52, 2015.

Mazas, F. and Hamm, L.: An event-based approach for extreme joint probabilities of waves and sea levels, Coastal Engineering, 122, 44–59, 2017.

Merkens, J.-L., Reimann, L., Hinkel, J., and Vafeidis, A. T.: Gridded population projections for the coastal zone under the Shared Socioeconomic Pathways, Global and Planetary Change, 145, 57–66, 2016.

Mignot, E., Paquier, A., and Haider, S.: Modeling floods in a dense urban area using 2D shallow water equations, Journal of Hydrology, 327, 186–199, 2006.

Mitková, V. B. and Halmová, D.: Joint modeling of flood peak discharges, volume and duration: a case study of the Danube River in Bratislava, Journal of Hydrology and Hydromechanics, 62, 186–196, 2014.

Moftakhari, H., Schubert, J. E., AghaKouchak, A., Matthew, R. A., and Sanders, B. F.: Linking statistical and hydrodynamic modeling for compound flood hazard assessment in tidal channels and estuaries, Advances in Water Resources, 128, 28–38, 2019.

Moftakhari, H. R., AghaKouchak, A., Sanders, B. F., and Matthew, R. A.: Cumulative hazard: The case of nuisance flooding, Earth's Future, 5, 214–223, 2017.

Muñoz, D., Moftakhari, H., and Moradkhani, H.: Compound Effects of Flood Drivers and Wetland Elevation Correction on Coastal Flood Hazard Assessment, Water Resources Research, 56, e2020WR027 544, 2020.

Naseri, K. and Hummel, M. A.: A Bayesian copula-based nonstationary framework for compound flood risk assessment along US coastlines, Journal of Hydrology, 610, 128 005, 2022.

Neal, J., Villanueva, I., Wright, N., Willis, T., Fewtrell, T., and Bates, P.: How much physical complexity is needed to model flood inundation?, Hydrological Processes, 26, 2264–2282, 2012.

Nederhoff, K., Saleh, R., Tehranirad, B., Herdman, L., Erikson, L., Barnard, P. L., and Van der Wegen, M.: Drivers of extreme water levels in a large, urban, high-energy coastal estuary–A case study of the San Francisco Bay, Coastal Engineering, 170, 103 984, 2021.

Nicholls, R. J.: Planning for the impacts of sea level rise, Oceanography, 24, 144–157, 2011.

Nicholls, R. J., Wong, P. P., Burkett, V., Codignotto, J., Hay, J., McLean, R., Ragoonaden, S., Woodroffe, C. D., Abuodha, P., Arblaster, J., et al.: Coastal systems and low-lying areas, 2007.

NOAA: Extreme Water Levels, Online, https://tidesandcurrents.noaa.gov/est/est_station.shtml?stnid=9410660, Accessed 2019a.

NOAA: US Hourly Precipitation Data, Online, https://www.ncei.noaa.gov/metadata/geoportal/rest/metadata/item/gov.noaa.ncdc:C00313/html#, Accessed 2019b.

NOAA: Tides & Currents, Online, https://tidesandcurrents.noaa.gov, Accessed 2019c.

NOAA: 2018 NAIP 4-Band 8 Bit Imagery : California, Online, https://coast.noaa.gov/dataviewer/#/imagery/search/-13145277.048600255,3989719.0716587296,-13141378.760157712,3992489.913934067/details/9159, Accessed 2020.

NOAA: Global Historical Climatology Network daily (GHCNd), Online, https://www.ncei.noaa.gov/products/land-based-station/global-historical-climatology-network-daily, Accessed 2021a.

NOAA: NOAA: Office For COastal Management, Online, https://coast.noaa.gov/states/california.html, Accessed 2021b.

NOAA: 2018 NAIP 4-Band 8 Bit Imagery : California, Online, https://coast.noaa.gov/dataviewer/#/imagery/search/-13145277.048600255,3989719.0716587296,-13141378.760157712,3992489.913934067/details/9159, Accessed 2022a.

NOAA: Tides & Currents, Online, https://tidesandcurrents.noaa.gov, Accessed 2022b.

NOAA: Global Historical Climatology Network daily (GHCNd), Online, https://www.ncei.noaa.gov/products/land-based-station/global-historical-climatology-network-daily, Accessed 2023a.

NOAA: Tides & Currents, Online, https://tidesandcurrents.noaa.gov, Accessed 2023b.

Pacific Energy Center: Guide to California's climate zones and bioclimatic design, https://www.pge.com/includes/docs/pdfs/about/edusafety/training/pec/toolbox/arch/climate/california_climate_zones_01-16.pdf, Accessed 2022.

Pakoksung, K. and Takagi, M.: Mixed Zero-Inflation Method and Probability Distribution in Fitting Daily Rainfall Data, Engineering Journal, 21, 63–80, 2017.

Paprotny, D., Vousdoukas, M. I., Morales-Nápoles, O., Jonkman, S. N., and Feyen, L.: Compound flood potential in Europe, Hydrology and Earth System Sciences Discussions, pp. 1–34, 2018.

Paprotny, D., Vousdoukas, M. I., Morales-Nápoles, O., Jonkman, S. N., and Feyen, L.: Pan-European hydrodynamic models and their ability to identify compound floods, Natural Hazards, 101, 933–957, 2020.

Pathirana, A., Denekew, H. B., Veerbeek, W., Zevenbergen, C., and Banda, A. T.: Impact of urban growth-driven landuse change on microclimate and extreme precipitation—A sensitivity study, Atmospheric Research, 138, 59–72, 2014.

Poulin, A., Huard, D., Favre, A.-C., and Pugin, S.: Importance of tail dependence in bivariate frequency analysis, Journal of Hydrologic Engineering, 12, 394–403, 2007.

Pour, S. H., Abd Wahab, A. K., Shahid, S., Asaduzzaman, M., and Dewan, A.: Low impact development techniques to mitigate the impacts of climate-change-induced urban floods: Current trends, issues and challenges, Sustainable Cities and Society, 62, 102 373, 2020.

Purvis, M. J., Bates, P. D., and Hayes, C. M.: A probabilistic methodology to estimate future coastal flood risk due to sea level rise, Coastal engineering, 55, 1062–1073, 2008.

Radfar, S., Shafieefar, M., Akbari, H., Galiatsatou, P. A., and Mazyak, A. R.: Design of a rubble mound breakwater under the combined effect of wave heights and water levels, under present and future climate conditions, Applied Ocean Research, 112, 102 711, 2021.

Reddy, M. J. and Ganguli, P.: Bivariate flood frequency analysis of upper Godavari River flows using Archimedean copulas, Water Resources Management, 26, 3995–4018, 2012.

Reguero, B., Menéndez, M., Méndez, F., Mínguez, R., and Losada, I.: A Global Ocean Wave (GOW) calibrated reanalysis from 1948 onwards, Coastal Engineering, 65, 38–55, 2012.

Reguero, B. G., Losada, I. J., and Méndez, F. J.: A recent increase in global wave power as a consequence of oceanic warming, Nature communications, 10, 1–14, 2019.

Requena, A., Mediero, L., and Garrote, L.: A bivariate return period based on copulas for hydrologic dam design: accounting for reservoir routing in risk estimation, Hydrology and Earth System Sciences, 17, 3023, 2013.

Rong, Y., Zhang, T., Zheng, Y., Hu, C., Peng, L., and Feng, P.: Three-dimensional urban flood inundation simulation based on digital aerial photogrammetry, Journal of Hydrology, 584, 124 308, 2020.

Sadegh, M., Ragno, E., and AghaKouchak, A.: Multivariate Copula Analysis Toolbox (MvCAT): describing dependence and underlying uncertainty using a Bayesian framework, Water Resources Research, 53, 5166–5183, 2017.

Sadegh, M., Moftakhari, H., Gupta, H. V., Ragno, E., Mazdiyasni, O., Sanders, B., Matthew, R., and AghaKouchak, A.: Multihazard scenarios for analysis of compound extreme events, Geophysical Research Letters, 45, 5470–5480, 2018.

Saint-Geours, N., Grelot, F., Bailly, J.-S., and Lavergne, C.: Ranking sources of uncertainty in flood damage modelling: a case study on the cost-benefit analysis of a flood mitigation project in the O rb D elta, F rance, Journal of Flood Risk Management, 8, 161–176, 2015.

Salvadori, G.: Bivariate return periods via 2-copulas, Statistical Methodology, 1, 129–144, 2004.

Salvadori, G. and De Michele, C.: Frequency analysis via copulas: Theoretical aspects and applications to hydrological events, Water resources research, 40, 2004.

Salvadori, G. and De Michele, C.: On the use of copulas in hydrology: theory and practice, Journal of Hydrologic Engineering, 12, 369–380, 2007.

Salvadori, G. and De Michele, C.: Multivariate multiparameter extreme value models and return periods: A copula approach, Water resources research, 46, 2010.

Salvadori, G., Durante, F., and De Michele, C.: On the return period and design in a multivariate framework, Hydrology and Earth System Sciences, 15, 3293–3305, 2011.

Salvadori, G., Durante, F., and De Michele, C.: Multivariate return period calculation via survival functions, Water Resources Research, 49, 2308–2311, 2013.

Salvadori, G., Tomasicchio, G., and D'Alessandro, F.: Practical guidelines for multivariate analysis and design in coastal and off-shore engineering, Coastal Engineering, 88, 1–14, 2014.

Salvadori, G., Durante, F., Tomasicchio, G., and D'alessandro, F.: Practical guidelines for the multivariate assessment of the structural risk in coastal and off-shore engineering, Coastal Engineering, 95, 77–83, 2015.

Salvadori, G., Durante, F., De Michele, C., Bernardi, M., and Petrella, L.: A multivariate copula-based framework for dealing with hazard scenarios and failure probabilities, Water Resources Research, 52, 3701–3721, 2016.

Sampson, C. C., Fewtrell, T. J., O'Loughlin, F., Pappenberger, F., Bates, P. B., Freer, J. E., and Cloke, H. L.: The impact of uncertain precipitation data on insurance loss estimates using a flood catastrophe model, Hydrology and Earth System Sciences, 18, 2305–2324, 2014.

Sanders, B. F.: Hydrodynamic modeling of urban flood flows and disaster risk reduction, in: Oxford research encyclopedia of natural hazard science, 2017.

Sanders, B. F., Schubert, J. E., and Gallegos, H. A.: Integral formulation of shallow-water equations with anisotropic porosity for urban flood modeling, Journal of hydrology, 362, 19–38, 2008.

Santos, V. M., Casas-Prat, M., Poschlod, B., Ragno, E., Van Den Hurk, B., Hao, Z., Kalmár, T., Zhu, L., and Najafi, H.: Statistical modelling and climate variability of compound surge and precipitation events in a managed water system: a case study in the Netherlands, Hydrology and Earth System Sciences, 25, 3595–3615, 2021.

Savant, G., McAlpin, T. O., and Trahan, C. J.: Streamline Upwind Petrov-Galerkin–Based shallow water model for large-scale geophysical flows in cartesian and spherical coordinates, Journal of Waterway, Port, Coastal, and Ocean Engineering, 145, 04019 017, 2019a.

Savant, G., Trahan, C. J., Pettey, L., McAlpin, T. O., Bell, G. L., and McKnight, C. J.: Urban and overland flow modeling with dynamic adaptive mesh and implicit diffusive wave equation solver, Journal of Hydrology, 573, 13–30, 2019b.

Schubert, J. E. and Sanders, B. F.: Building treatments for urban flood inundation models and implications for predictive skill and modeling efficiency, Advances in Water Resources, 41, 49–64, 2012.

Schubert, J. E., Sanders, B. F., Smith, M. J., and Wright, N. G.: Unstructured mesh generation and landcover-based resistance for hydrodynamic modeling of urban flooding, Advances in Water Resources, 31, 1603–1621, 2008.

Scripps: Coastal Data Information Program (CDIP) Wave Bouy Data, Online, `https://cdip.ucsd.edu/m/deployment/station_view/`, Accessed 2021.

Sebastian, A.: Compound flooding, in: Coastal Flood Risk Reduction, pp. 77–88, Elsevier, 2022.

Sebastian, A., Dupuits, E., and Morales-Nápoles, O.: Applying a Bayesian network based on Gaussian copulas to model the hydraulic boundary conditions for hurricane flood risk analysis in a coastal watershed, Coastal Engineering, 125, 42–50, 2017.

Seneviratne, S., Nicholls, N., Easterling, D., Goodess, C., Kanae, S., Kossin, J., Luo, Y., Marengo, J., McInnes, K., Rahimi, M., Reichstein, M., Sorteberg, A., Vera, C., and Zhang, X.: Changes in climate extremes and their impacts on the natural physical environment, in: Managing the Risks of Extreme Events and Disasters to Advance Climate Change Adaptation: A Special Report of Working Groups I and II of the Intergovernmental Panel on Climate Change, edited by Field, C., Barros, V., Stocker, T., Qin, D., Dokken, D., Ebi, K., Mastrandrea, M., Mach, K., Plattner, G.-K., Allen, S., Tignor, M., , and Midgley, P., pp. 109–230, Cambridge University Press, Cambridge, UK, and New York, NY, USA, 2012.

Serafin, K. A., Ruggiero, P., and Stockdon, H. F.: The relative contribution of waves, tides, and nontidal residuals to extreme total water levels on US West Coast sandy beaches, Geophysical Research Letters, 44, 1839–1847, 2017.

Serinaldi, F.: An uncertain journey around the tails of multivariate hydrological distributions, Water Resources Research, 49, 6527–6547, 2013.

Serinaldi, F.: Dismissing return periods!, Stochastic Environmental Research and Risk Assessment, 29, 1179–1189, 2015.

Serinaldi, F.: Can we tell more than we can know? The limits of bivariate drought analyses in the United States, Stochastic Environmental Research and Risk Assessment, 30, 1691–1704, 2016.

Shen, Y., Morsy, M. M., Huxley, C., Tahvildari, N., and Goodall, J. L.: Flood risk assessment and increased resilience for coastal urban watersheds under the combined impact of storm tide and heavy rainfall, Journal of Hydrology, 579, 124–159, 2019.

Shiau, J.: Return period of bivariate distributed extreme hydrological events, Stochastic environmental research and risk assessment, 17, 42–57, 2003.

Shope, J., Erikson, L., Barnard, P., Storlazzi, C., Hardy, M., , and Doran, K.: Modeled extreme total water levels along the U.S. west coast, 2021.

Sklar, M.: Fonctions de repartition an dimensions et leurs marges, Publ. inst. statist. univ. Paris, 8, 229–231, 1959.

Smith, R. A., Bates, P. D., and Hayes, C.: Evaluation of a coastal flood inundation model using hard and soft data, Environmental Modelling & Software, 30, 35–46, 2012.

Stephens, T. A., Savant, G., Sanborn, S. C., Wallen, C. M., and Roy, S.: Monolithic multiphysics simulation of compound flooding, Journal of Hydraulic Engineering, 148, 05022 003, 2022.

Stockdon, H. F., Holman, R. A., Howd, P. A., and Sallenger Jr, A. H.: Empirical parameterization of setup, swash, and runup, Coastal engineering, 53, 573–588, 2006.

Su, H.-T. and Tung, Y.-K.: Incorporating uncertainty of distribution parameters due to sampling errors in flood-damage-reduction project evaluation, Water Resources Research, 49, 1680–1692, 2013.

Swift Jr, L. W. and Schreuder, H. T.: Fitting daily precipitation amounts using the SB distribution, Monthly Weather Review, 109, 2535–2540, 1981.

Symonds, A. M., Vijverberg, T., Post, S., van der Spek, B.-J., Henrotte, J., and Sokolewicz, M.: Comparison between Mike 21 FM, Delft3D and Delft3D FM flow models of western port bay, Australia, COASTAL ENGINEERING, p. 2, 2016.

Taherkhani, M., Vitousek, S., Barnard, P. L., Frazer, N., Anderson, T. R., and Fletcher, C. H.: Sea-level rise exponentially increases coastal flood frequency, Scientific reports, 10, 1–17, 2020.

Tang, B. and Gallien, T. W.: Predicting compound coastal flooding in urban catchments: Hydraulic infrastructure implications, in review, Journal of Marine Science and Enginering, 2023.

Tanim, A. H. and Goharian, E.: Developing a hybrid modeling and multivariate analysis framework for storm surge and runoff interactions in urban coastal flooding, Journal of Hydrology, 595, 125 670, 2021.

Tebaldi, C., Strauss, B. H., and Zervas, C. E.: Modelling sea level rise impacts on storm surges along US coasts, Environmental Research Letters, 7, 014 032, 2012.

Teng, J., Jakeman, A. J., Vaze, J., Croke, B. F., Dutta, D., and Kim, S.: Flood inundation modelling: A review of methods, recent advances and uncertainty analysis, Environmental modelling & software, 90, 201–216, 2017.

Thompson, C. M. and Frazier, T. G.: Deterministic and probabilistic flood modeling for

contemporary and future coastal and inland precipitation inundation, Applied Geography, 50, 1–14, 2014.

Tong, X., Wang, D., Singh, V., Wu, J., Chen, X., and Chen, Y.: Impact of data length on the uncertainty of hydrological copula modeling, Journal of Hydrologic Engineering, 20, 05014 019, 2015.

Toro, E. F.: Riemann solvers and numerical methods for fluid dynamics: a practical introduction, Springer Science & Business Media, 2013.

Toro, E. F. and Garcia-Navarro, P.: Godunov-type methods for free-surface shallow flows: A review, Journal of Hydraulic Research, 45, 736–751, 2007.

Tu, X., Du, Y., Singh, V. P., and Chen, X.: Joint distribution of design precipitation and tide and impact of sampling in a coastal area, International Journal of Climatology, 38, e290–e302, 2018.

USACE: Coastal risk reduction and resilience, 2013.

Van Thanh, N., Le, D. T., Thinh, N. A., Lan, T. D., and Hens, L.: Shifting challenges for coastal green cities, Vietnam Journal of Earth Sciences, 39, 109–129, 2017.

Villaneueva, I. and Wright, N.: Linking Riemann and storage cell methods for flood predictions, Proc. Inst. Civ. Eng. Waste Resour. Manag, 159, 27–33, 2006.

Volpi, E. and Fiori, A.: Hydraulic structures subject to bivariate hydrological loads: Return period, design, and risk assessment, Water Resources Research, 50, 885–897, 2014.

Vorobevskii, I., Al Janabi, F., Schneebeck, F., Bellera, J., and Krebs, P.: Urban floods: linking the overloading of a storm water sewer system to precipitation parameters, Hydrology, 7, 35, 2020.

Vos, K., Harley, M. D., Splinter, K. D., Walker, A., and Turner, I. L.: Beach slopes from satellite-derived shorelines, Geophysical Research Letters, 47, e2020GL088 365, 2020.

Wadey, M. P., Nicholls, R. J., and Hutton, C.: Coastal flooding in the Solent: An integrated analysis of defences and inundation, Water, 4, 430–459, 2012.

Wahl, T., Mudersbach, C., and Jensen, J.: Assessing the hydrodynamic boundary conditions for risk analyses in coastal areas: a multivariate statistical aaproach based on Copula functions, Natural Hazards and Earth System Science, 12, 495–510, 2012.

Wahl, T., Jain, S., Bender, J., Meyers, S. D., and Luther, M. E.: Increasing risk of compound flooding from storm surge and rainfall for major US cities, Nature Climate Change, 5, 1093, 2015.

Wang, Y., Chen, A. S., Fu, G., Djordjević, S., Zhang, C., and Savić, D. A.: An integrated framework for high-resolution urban flood modelling considering multiple information sources and urban features, Environmental modelling & software, 107, 85–95, 2018.

Ward, P. J., Couasnon, A., Eilander, D., Haigh, I. D., Hendry, A., Muis, S., Veldkamp, T. I., Winsemius, H. C., and Wahl, T.: Dependence between high sea-level and high river discharge increases flood hazard in global deltas and estuaries, Environmental Research Letters, 13, 084 012, 2018.

White, C. J.: The use of joint probability analysis to predict flood frequency in estuaries and tidal rivers, Ph.D. thesis, University of Southampton, 2007.

World Meteorological Organization: Urban flood risk management: a tool for integrated flood management, https://library.wmo.int/doc$_n$$um.php?expln$$um_i$$d = 7342, 2008.

Wrang, L., Katsidoniotaki, E., Nilsson, E., Rutgersson, A., Rydén, J., and Göteman, M.: Comparative analysis of environmental contour approaches to estimating extreme waves for offshore installations for the baltic sea and the north sea, Journal of Marine Science and Engineering, 9, 96, 2021.

Xie, D., Zou, Q.-P., Mignone, A., and MacRae, J. D.: Coastal flooding from wave overtopping and sea level rise adaptation in the northeastern USA, Coastal Engineering, 150, 39–58, 2019.

Xu, H., Xu, K., Lian, J., and Ma, C.: Compound effects of rainfall and storm tides on coastal flooding risk, Stochastic Environmental Research and Risk Assessment, 33, 1249–1261, 2019.

Xu, H., Tian, Z., Sun, L., Ye, Q., Ragno, E., Bricker, J., Mao, G., Tan, J., Wang, J., Ke, Q., et al.: Compound flood impact of water level and rainfall during tropical cyclone periods in a coastal city: the case of Shanghai, Natural Hazards and Earth System Sciences, 22, 2347–2358, 2022.

Xu, K., Ma, C., Lian, J., and Bin, L.: Joint probability analysis of extreme precipitation and storm tide in a coastal city under changing environment, PLoS One, 9, e109 341, 2014.

Yang, X., Wang, J., and Weng, S.: Joint Probability Study of Destructive Factors Related to the "Triad" Phenomenon during Typhoon Events in the Coastal Regions: Taking Jiangsu Province as an Example, Journal of Hydrologic Engineering, 25, 05020 038, 2020.

Yue, S.: Joint probability distribution of annual maximum storm peaks and amounts as represented by daily rainfalls, Hydrological Sciences Journal, 45, 315–326, 2000a.

Yue, S.: The Gumbel logistic model for representing a multivariate storm event, Advances in Water Resources, 24, 179–185, 2000b.

Yue, S.: A bivariate gamma distribution for use in multivariate flood frequency analysis, Hydrological Processes, 15, 1033–1045, 2001a.

Yue, S.: A bivariate extreme value distribution applied to flood frequency analysis, Hydrology Research, 32, 49–64, 2001b.

Yue, S.: The bivariate lognormal distribution for describing joint statistical properties of a multivariate storm event, Environmetrics: The official journal of the International Environmetrics Society, 13, 811–819, 2002.

Zhang, H., Wu, C., Chen, W., and Huang, G.: Assessing the impact of climate change on the waterlogging risk in coastal cities: A case study of Guangzhou, South China, Journal of Hydrometeorology, 18, 1549–1562, 2017.

Zhang, L. and Singh, V. P.: Bivariate rainfall and runoff analysis using entropy and copula theories, Entropy, 14, 1784–1812, 2012.

Zheng, F., Westra, S., Leonard, M., and Sisson, S. A.: Modeling dependence between extreme rainfall and storm surge to estimate coastal flooding risk, Water Resources Research, 50, 2050–2071, 2014.

Zhong, M., Wang, J., Jiang, T., Huang, Z., Chen, X., and Hong, Y.: Using the Apriori Algorithm and Copula Function for the Bivariate Analysis of Flash Flood Risk, Water, 12, 2223, 2020.

Zscheischler, J., Westra, S., Van Den Hurk, B. J., Seneviratne, S. I., Ward, P. J., Pitman, A., AghaKouchak, A., Bresch, D. N., Leonard, M., Wahl, T., et al.: Future climate risk from compound events, Nature Climate Change, 8, 469–477, 2018.